Design of an Atmospheric Engine Test Cell

Student Name: **Preshen Singh**

Student Number: **0411247X**

Degree Code: **ER 000 – Masters (R) Degree**

School of Mechanical, Industrial, & Aeronautical Engineering
University of the Witwatersrand
Johannesburg, South Africa.

Supervisor: **Prof. Craig Law**

A dissertation submitted to the Faculty of Engineering and the Built Environment, University of the Witwatersrand, in fulfilment of the requirements for the degree of Master of Science in Engineering.

Date: **31 Jan 2019**

Executive Summary

The objective was to design an Atmospheric Engine Test Cell to test an experimental Gas Turbine Engine (Ø = 0.35 m). It should be capable of performing all 'engine design' clearance tests. It would have to simulate the specific Design Point of Mach number = 0.7 at an Altitude Temperature = 219 K (35000 ft). The Design was split into 2 parts:

- The Wind Tunnel Design – The Tunnel had to achieve the Design Point Velocity (M_{TS} = 0.7) at the Engine Test Piece from a 'deliverable' set of Inlet conditions (P_0, T_0, and $\dot{m}$). These Inlet conditions served as the Design objectives for the 2nd part; the Mixing Chamber.
- The Mixing Chamber Design – The component had to cool the airflow supply prior to the Wind Tunnel Inlet. The objective was to deliver the Wind Tunnel Inlet conditions, and ultimately achieve the Design Point Test Section Temperature (T_{TS} = 219 K) at the Engine Test Piece.

The hypothesis for each part (Wind Tunnel and Mixing Chamber) was developed using F-Chart Engineering Equation Solver. The hypotheses were then Analytically Modelled in 3-D using Solid Edge ST6, and simulated using Numerical Methods (Meshing = ANSYS 14.5 ICEM, Solving = ANSYS 14.5 FLUENT). No scaled physical model was attempted. The Wind Tunnel was validated against the respective Analytical Model; given the simplicity of the 1-D flow path. The Mixing Chamber, which served as the research component of the Project, was validated using available published data.

The Wind Tunnel was designed as an Open Circuit Blowdown Tunnel with an Open Test Section (to house the Engine Test Piece). The Tunnel delivered the flow as a free-jet; which rammed the Test Piece. The Tunnel achieved the Velocity objective (M_{TS} = 0.7) in the most efficient way; using the least expensive Wind Tunnel Inlet specifications. The Project-specific purpose of the Wind Tunnel was to determine the Design objectives for the preceding Mixing Chamber. The Mixing Chamber was designed using the experimental mechanism of Underexpanded Supersonic Cooling. The cooling requirements (Absolute Temperature T_0 and Cooling Capacity $\dot{Q}$) was not possible using conventional methods (Vapor Cycle or Dry Ice sublimation). The Supersonic Cooling mechanism, however, was theoretically capable of dynamically cooling large amounts of airflow. The mechanism rapidly expanded air at ambient T_0 and high P_0 to achieve air at ambient P_0 and low T. The Mixing Chamber was fed by a single Low Pressure Centrifugal Fan (to deliver the Main flow P_0 and $\dot{m}$) and 6 High Pressure Rotary Compressors (to achieve the Supersonic Cooling contribution). The Cost per run (1 hour) amounted to ± R 1363.18 (dated 2013).

The Mixing Chamber exceeded the P_0 and $\dot{m}$ Wind Tunnel Inlet requirements, in order to achieve the Velocity objective (M_{TS} = 0.75 > 0.7). However, it underperformed with the Altitude Temperature objective. It only cooled the flow to T_{TS} = 222.2 K (> 219 K). This Altitude Temperature revised the Design Point capability of the Project to M0.75 at 222.2 K (32000 ft), instead of the 'ideal' M0.7 at 35000 ft. The reason for the shortcoming was the incomplete expansion of the latter Supersonic flows within the Mixing Chamber. This was due to the cumulative Main flow increasingly occupying the Mixing Chamber cross sectional area. It effectively suppressed the complete expansion of the latter Supersonic Jets. The Main flow inherited the higher P_0 of the Supersonic flow (hence higher M_{TS}), instead of extracting the respective Cooling potential (hence higher T_{TS}). It was proposed that additional Convective Devices be installed within the Mixing Chamber; to disrupt the flow streams and achieve further mixing.

Declaration

University of the Witwatersrand, Johannesburg

School of Mechanical, Industrial and Aeronautical Engineering

I, Preshen Singh (Student number: 0411247X), am a student registered for ER 000 Masters Degree (Research Dissertation) in Mechanical Engineering in the year 2018. I hereby declare the following:

- I am aware that plagiarism (the use of someone else's work without their permission and/or without acknowledging the original source) is wrong.
- I confirm that ALL the work submitted for assessment for the above course is my own unaided work except where I have explicitly indicated otherwise.
- I have followed the required conventions in referencing the thoughts and ideas of others.
- I understand that the University of the Witwatersrand may take disciplinary action against me if there is a belief that this is not my own unaided work, or that I have failed to acknowledge the source of the ideas or words in my writing.

Signature: ________________________________ Date: ________________________________

Acknowledgements

I wish to express my appreciation to the following people/entities:

- Principal Supervisor: Dr. Craig Law.
  Serving as the primary guide and director on the Project; converging the scope, and pointing me in the correct direction. Proposing the concept of Supersonic Cooling, and reasoning the investigative mechanism. Assessing the relevance of the Design (Mathematical hypothesis and CFD result); suggesting methods of refinement. Supervising the Project; both in the technical development and design engineering (cost analysis).

- External Supervisor: Glen Sneddon (CSIR).
  Serving as the Project client. Imposing the real-world implications of the Project (costs and operating conditions), and appreciating the capabilities and limitations of the Design.

- Sponsor: Department of Defence (Ballast Project)
  Financially supporting the MSc. Dissertation; as part of the Ballast Project. Dividing the development tasks (Engine Internal Mechanism, Engine External Design, Test Chamber Design – *this Design*, etc.) among several Post-Grad students; to result in a collective effort.

- Flow Research Assistance: Prof. Beric Skews
  Supplementary guidance in the development of the Mathematical Model (hypothesis); for compressible fluid flow. Thank you for lending me your *Handbook of Hydraulic Resistance*.

- CFD (Fluent) Assistance: Randall Paton
  Supplementary guidance in the development of the CFD (Fluent) simulation methods; for compressible fluid flow. In particular, defining the boundary and reference conditions.

Table of Contents

The remaining Appendices were included, in electronic format, on the Supplementary Disc (SUPDisc):

List of Figures

Main Report Figures

Appendix Figures

List of Tables

List of Equations

Main Report Equations

Appendix Equations

Nomenclature

a	- Local Speed of Sound	- m/s
α	- Angle (Contraction/Expansion)	- ° (degrees)
$\mathbb{A}$	- Cross Sectional Area	- m^2
A.R.*	- Area Ratio at Critical Point ($\frac{\mathbb{A}}{\mathbb{A}^*}$)	- dimensionless
β	- Otis [41] Indicator Variable of Thermal Choking	- dimensionless
C_P, C_V	- Specific Heat of Fluid at constant Pressure, Volume (air)	- 1005, 718 J/kg·K
C_f	- Coefficient of Skin Friction	- dimensionless
Cr	- Courant Number	- dimensionless
Ø	- Diameter	- m (mm)
ϵ	- Equivalent Roughness	- m
η_X	- Area Ratio	- dimensionless
f	- Fanning Friction Factor	- dimensionless
g	- Gravitational Acceleration	- 9.81 m/s^2
γ	- Kinematic Viscosity ($\frac{\mu}{\rho}$)	- m^2/s
k	- Specific Heat Ratio (air)	- 1.4 dimensionless
K_X	- Component Loss Coefficient	- dimensionless
L	- Characteristic length	- m (mm)

l_{TURB}	- Turbulent Length Scale	- m
M	- Mach Number	- dimensionless
$\dot{m}$	- Mass Flow Rate	- kg/s
μ	- Dynamic Viscosity	- $N \cdot s/m^2$
Pr	- Prandtl Number	- dimensionless
P	- Pressure	- Pa (bar, psi, psig)
P.R.	- Pressure Ratio used in Compressor Specifications ($\frac{P_0}{P_{Ambient}}$)	- dimensionless
P.R.*	- Pressure Ratio at Critical Point ($\frac{P_0}{P_B}$)	- dimensionless
$\bar{q}$	- Volumetric Flow Rate Ratio	- dimensionless
$\dot{Q}$, $\dot{W}$	- Heat, Work transfer in/out of system	- kJ/s
R	- Universal Gas constant	- 287 J/kg·K
Re	- Reynolds Number	- dimensionless
ρ	- Density	- kg/m^3
Su	- Sutherland Constant	- 110.56 K
T	- Temperature	- K (°C)
T.R.*	- Temperature Ratio at Critical Point ($\frac{T_0}{T_B}$)	- dimensionless
T.I.	- Turbulent Intensity (Percentage)	- dimensionless
u	- Internal Energy	- kJ/kg
V	- Velocity	- m/s
∀	- Volume	- m^3
$\dot{\forall}$	- Volumetric Flow Rate	- m^3/s
y+	- Dimensionless Wall Distance	- dimensionless

1 Introduction

The Project tasks were stated, by the Wits MIA [1] Project Brief, to address the research and design needs of a small gas turbine development programme. In order to verify the performance at altitude of a small gas turbine, a need has been identified for an altitude engine test cell. The proposed test cell should be able to perform clearance tests at a number of conditions as close as possible to actual flight conditions. These included cold soaking and starting a gas turbine at a simulated altitude of 35000ft with speed of Mach number M0.7 and maximum thrust tests across a range of altitudes and air speeds. The full range of tests was specified to meet the requirements to clear a gas turbine for flight. The quality of the Design was measured against this primary requirement. A critical aspect of the Project was the airflow cooling that was required to simulate the various altitude levels. The component responsible for this task (Mixing Chamber) was subject to detailed investigation; via comparison to published results.

1.1 Motivation

The fundamental concept of a wind tunnel was to replicate aerodynamic behaviour of a moving body through still air. This was achieved by reversing the process; i.e. moving air around a still body. By simulating this behaviour, one could understand the airflow dynamics associated with the body concerned, and facilitate optimum design qualities for the intended flight schedule. In order to fully replicate the conditions experienced, the wind tunnel must be able to provide airflow according to altitude requirements (Pressure, Temperature, Air Density, etc.). This concept, of using conditioned airflow to test capabilities along the flight schedule, also held true for aircraft engines. The conditions experienced at altitude affected the maximum thrust available at a given fuel consumption. The Project objective was to design an altitude wind tunnel to test the capabilities of an aircraft engine throughout its flight schedule. In this specific case, the aircraft engine concerned was a small gas turbine. This need arose from the Ballast Gas Turbine Skills Development Programme; detailed in Ledger [2]. The initiative identified gas turbine engines as the main driver of the Air Force operating costs. In order to address this issue directly, the Ballast initiative tasked tertiary education systems with the development of a UAV (Unmanned Aerial Vehicle) gas turbine engine. The smaller size of the UAV engine allowed for the components to be readily manufactured within the restricted budget. The UAV engine performance could then be evaluated; and extrapolated to scale as necessary. The purpose of this Project was to design a testing cell to evaluate the performance of said UAV engine.

1.2 Facility Survey

Aircraft turbine engine testing is conducted in various ways, including Engine Bench tests and Altitude Test Cells (Propulsion Wind Tunnels), as described in Rolls Royce [3]. The former (Engine Bench tests) were used to verify performance and reliability of the individual engine. It was conducted at ambient conditions; and primarily used during manufacture and overhaul. This testing method however, did not simulate the flight schedule altitude range. The Propulsion Wind Tunnel testing method was used on sample engines for design purposes. It allowed for the evaluation of the engine behaviour during a simulated flight schedule. These wind tunnels were designed specifically to meet the set testing requirements of: Mach number, simulated altitude, and engine size (cross-sectional area of Test Section). Table 1 listed a summary of the airflow conditions simulated by some of the existing Propulsion

Wind Tunnels; designed to meet the respective testing requirements. The Propulsion Wind Tunnel method was the only option capable of testing the engine in an environment with airflow of M0.7; at different Altitude Temperature conditions.

Table 1. Various available Propulsion Tunnels with capabilities, as extracted from NASA [4], AEDC [5], ONERA [6], and DERA [7]

	Glenn Research 10ft x 10ft (Supersonic)	Glenn Research 9ft x 15ft (Low Speed)	Arnold Engineering 16ft^2 (Transonic)	Onera Modane S3 0.8m x 0.76m (Blow Down)	RAE Pyestock Cell 3 6m Ø (Supersonic)
Simulated Altitude [ft]	55 000	Sea Level	150 000	38 000	70 000
Mach number Range [M]	0 – 3.5	0 – 0.23	0.06 – 1.6	0.1 – 5.5	0 – 2.2
Test Section Temperature [K]	288-633	Ambient-305	-	Ambient-530	203.15–523.15

1.3 Problem Definition

The Project Brief (Wits MIA [1]) was elaborated and refined at this point to include the engine and specific airflow condition variants:

- Small Turbojet Engine
  Engine Specifications: Ø= 0.35 m (Ø with dress = 0.4 m), Thrust = 100 kg, Flow Rate = 1 kg/s
  Airflow Specifications: 35000 ft altitude conditions, maximum Mach number of 0.7
- Engine with Propeller Blades
  Engine Specifications: Ø = 2 m (blade diameter), Engine Rating = 90 kW
  Airflow Specifications: 25000ft altitude conditions

The Design must achieve the following objectives:

- A Propulsion Wind Tunnel that was capable of simulating the altitude conditions up to 35000 ft.
- A Tunnel that could immerse the UAV gas turbine engine in a flow velocity of M0.7.
- A Tunnel test section that could accommodate the dimensions and contributions of the UAV engine.
- A Design that could accomplish the comprehensive flight testing requirements dictated by a military standard; specified from literature.

The Mixing Chamber, which was responsible for altitude replication through airflow cooling, designated the classification of the proposed Design. It classified the Design as a Propulsion Tunnel; comparable to the examples listed in Table 1. The importance of its role, and the complexity of the Temperature Mixing mechanisms within the component, justified its selection as the research aspect of the Project.

2. Needs Analysis

The analysis here served to define the objectives listed in Section 1.3. The evaluation concerned the objective-specific Tunnel components, altitude flow conditions, and flight testing requirements. The layout of the Tunnel, and the flow requirements for Engine Testing, defined the capability requirements for the Mixing Chamber airflow and cooling capacities. The analysis was used to define the Design specific Product Requirement Specifications (Section 3).

2.1 Fundamental Wind Tunnel Components

Wind tunnels, as described in Markovich [8], were built to the 2 shape classifications shown in Figure 1:

- Open Circuit (Part A) – Configuration which did not re-circulate airflow, but rather extracted new air from the environment and evacuated accordingly.
- Closed Circuit (Part B) – Configuration which re-circulated airflow within the tunnel, thus allowing for the conditioned air to be maintained within the circuit.

These Wind Tunnel classifications, as demonstrated in Figure 1, conventionally consisted of:

1. Wind Tunnel Inlet
2. Drive Fan and Motor
3. Flow Conditioners (Turning Vanes to preserve flow uniformity around corners, Honeycomb to straighten airflow, Wire Mesh to bring uniformity to airflow velocity)
4. Heat Exchangers (Heat or cool the airflow)
5. Nozzle (Contraction prior to Test Section to increase flow Velocity and decrease Static Pressure)
6. Testing Section (Cross Sectional Area proportional to the specimen concerned)
7. Diffuser (Expansion aft of Test Section to decrease Velocity and recover flow Static Pressure)

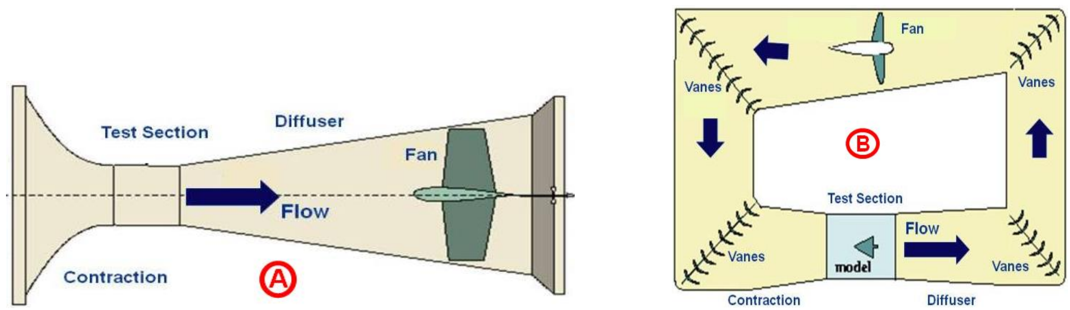

Figure 1. Typical wind tunnel configurations. Part A) Open Circuit design, Part B) Closed Circuit design, modified from NASA [9]

For the purposes of a Propulsion Test, it was more appropriate to use an Open Circuit shape due to the exhaust gases emitted by the Test Piece Engine. It was imperative that no exhaust products be re-ingested by the engine during testing. The alternative, reconditioning the existing air, would prove to be resource intensive (given the scale of the Design objective). Following the shape classification, the airflow dynamic was described in Markovich [8] to be appropriated from either:

- Blow Down – using a fan upstream of the Engine; in conjunction with a high Pressure inlet to discharge to Atmosphere at the outlet.
- Draw Down – using a fan downstream of the Engine; in conjunction with a low Pressure outlet to extract Atmospheric air from the inlet.

For the purposes of this Design, equipment effectiveness (and preservation) necessitated a Blow Down airflow dynamic. This dynamic avoided the potential draw-down redundancy of the Test Piece Engine. The Test Piece drew airflow into the Engine inlet upstream, and emitted the high Temperature exhaust products downstream. This would override/diminish the airflow dynamic capacity of a Draw Down mechanism. The upstream positioning of the Device also avoided heated gases and Engine exhaust products from damaging sensitive equipment (Supply Mechanisms).

Focusing on the Test Section segment of the Propulsion Wind Tunnel, its design and implementation could be varied according to Engine size, cost, and development stage. The sizing and configuration of this component directly affected the Tunnel Inlet flow requirements; a larger Test Section diameter meant a larger Tunnel Inlet flow rate. This relationship increased the demand placed on the Mixing Chamber; with regards to the proportional airflow cooling requirements. The Test Section options were depicted in Figure 2, and described in Davis [10], including:

- Direct Connect (Part A) – the tunnel connected directly to the Engine inlet to feed it the conditioned airflow, and continued from the Engine outlet to extract exhaust airflow. This was a cost efficient method of evaluating conventional (civil airliner) turbine engines, but did not take into account the flow around the nacelle and other engine dress. Whilst this method minimized wind tunnel inlet supply requirements, it did not offer the ability to assess Ram effects on the Engine frontal area.

- Free Jet (Part B) – the segment consisted of a discontinuation of tunnel structure at the Test Section. The conditioned air was projected into the Engine inlet. This allowed for change in Angle of Attack (AoA) of both airflow and Engine. The tunnel structure continued aft of the Test Section; to extract the exhaust emissions. This configuration presented an issue of airflow instability and would only prove beneficial if the airflow AoA was pertinent to the Design objective. The objectives of this Project however, were focused on feeding and Ramming the Engine inlet with conditioned flow in the most economic method. Flow distortion was considered secondary to these objectives.

- Self-contained (Part C) – the Test Piece Engine was contained within the wind tunnel and the airflow passed through and around it. The configuration allowed for the analysis of Engine performance and Engine dress characteristics (inlet icing). This method was mostly applicable to smaller engines (missiles); due to the tunnel cross section size constraints. It would be the ideal testing scenario, but highly inefficient in airflow supply mechanism utilization. The supply mechanisms would have to provide altitude conditions across the entire Test Section Chamber diameter in order to produce adjacent free streams; and would not suit the cost effective ambitions of this Project.

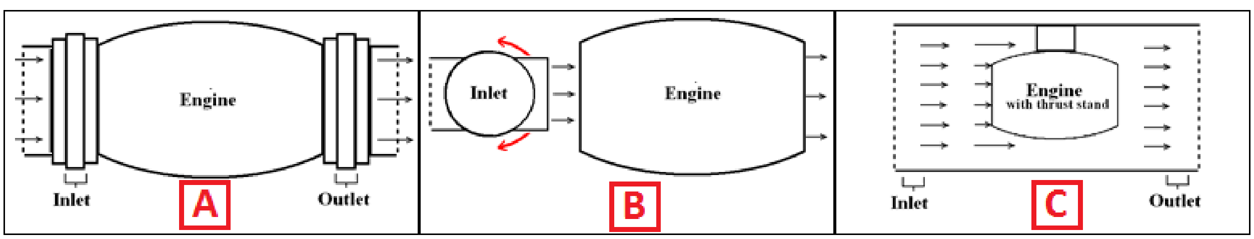

Figure 2. Wind Tunnel Test Section options. Part A) Direct Connect method - airflow was fed directly into the engine inlet, similar to Pyestock Cell 3 of DERA [7]. Part B) Free Jet method - airflow was directed towards the engine inlet area, similar to Pyestock Cell 1 of DERA [11]. Part C) Self-contained method - airflow was passed through and around the engine, similar to PWT of AEDC [5]

Given the size of the engines to be tested, it was appropriate to create an interchangeable Test Section that could supply conditioned airflow to both the Primary Objective Gas Turbine Engine and the Secondary Objective Propeller Engine. This was a compromise between the Free-Jet and Self-contained Test Section designs. It comprised of an Open Test Section that was fed by either a Nozzle (for the Gas Turbine Engine) or a Diffuser (for the Propeller Engine). The configuration best suited to this Design was summarised as an Open Circuit Blow-Down Wind Tunnel with a Free-Jet Open Test Section.

2.2 Flight Simulation Conditions

For the purposes of Engine testing, priority was placed on the similitude of Mach number (Temperature) rather than Reynolds Number (Viscosity). This decision was affirmed by The RAND Corporation [12]; when attempting to simulate altitude conditions. The Design objectives lay in the ability to change Temperature, Pressure, and humidity levels to match that of the intended altitude. These parameters (Temperature and Pressure) affected the mass flow rate of the airflow, and thus the Engine Thrust. An increase in altitude resulted in a decrease in both Pressure and Temperature, as described in Rolls Royce [3]. But these properties affected mass flow rate, and effectively Engine thrust, very differently. The decrease in Temperature resulted in an increase in Air Density, whereas the decrease in Pressure resulted in a decrease in Air Density. The distinction between the effects of these 2 properties on Air Density was in the mathematical scale described by Halpern [13]. As Temperature increased, the Volume (inverse to density) increased linearly. As Pressure increased, the Volume decreased exponentially. The Pressure - Volume relationship (exponential) outweighed that of Temperature - Volume relationship (linear), and resulted in overall decrease in Thrust with increasing altitude.

The Design Point altitude conditions for the Gas Turbine Engine (35000 ft) were quoted from the Standard Atmosphere Table as: Air Density Ratio = 0.3099, Temperature = -54.34 °C, Pressure = 23.84 kPa, and Speed of Sound = 576.4 Knots. In keeping with the Mach number similitude objective of The RAND Corporation [12], the Test Section objective was the replication of M0.7 at 35000 ft. This required the Wind Tunnel Design to achieve:

- Test Section Static Temperature: 218.8 K
- Test Section Air Velocity: 207.7 m/s

The relationship between the Static Pressure and Air Density Ratio, in response to altitude change, was not the Primary Test Section Design objective. Instead, the Design was focused on the Temperature and Air Velocity required for Mach number similitude. This flow property repurposing was distinct from typical Wind Tunnel applications where the aerodynamic qualities of Lift and Drag were analysed from boundary layer flow; in which Reynolds Number was the key parameter.

2.3 Rules and Regulations pertaining to Engine Testing

In pursuit of the Propulsion Tunnel design, as opposed to an Engine Bench Test design, only the relevant testing criteria were adhered to. Testing rules proposed by the Federal Aviation Authority FARS and Advisory Circular handbooks [14] were not considered; as these pertain to Engine Bench Tests. Instead, focus was placed on the relevant material found in the US Department of Defense MIL-SPEC and JSSG handbooks [15] summarized in the following subsections:

Military Specification MIL – E – 5007D

The specifications listed in the MIL-SPEC subsections (from MIL-E-5007D [15]) provided information that concerned the operation/analysis of the Test Piece Engine. In saying that, it described the required capabilities of the Wind Tunnel in meeting these analyses. The directly quoted specifications were included in Appx. F.1, which included:

- The tunnel must be able to test altitudes in an incremental capacity ranging Sea Level (0 ft) to the Design Point (35000 ft). This required the Supply Devices be capable of modular contribution.

- The tunnel must be designed as independent of the contribution of the Test Piece Engine. It must not rely on the Engine performance to provide/assist the Wind Tunnel flow path. This allowed the tunnel to immerse an inactive Engine (Hot/ Cold Start) in existing altitude specific airflow. This requirement necessitated an Open Test Section as opposed to a Direct Connect method.
- It was stated in the MIL-E-5007D that these test procedures should be conducted within a duration long enough to stabilize the engine and establish characteristics. The explicitly stated minimum time for stability verification was 5 minutes at each power setting.

Joint Service Specification Guide JSSG – 2007 A2
The directly quoted specifications were included in Appx. F.1, which included:

- The tunnel must be able to achieve 10 incremental altitudes between Sea Level and the Design Altitude. This required the Wind Tunnel Supply Devices to have modularity in function.
- The maximum achievable simulated altitude of the tunnel must exceed the 14764 ft required for testing starting limits. This served as the minimum capability limit of the Cooling Devices.
- The tunnel must allow for the post-design modular insertion of distortion patterns prior to the Test Section Inlet. The distortion pattern testing would evaluate the effects of swirl (and asymmetric air supply) on the Engine inlet ingestion. This required the Wind Tunnel configuration to include an intermediate length of constant diameter prior to the Test Section; to accommodate the device.

These specifications (MIL-SPEC and JSSG) defined the Tunnel operation requirements in meeting the military standard flight testing requirements for the UAV. The Tunnel design layout and performance would have to achieve the altitude levels and testing times specified.

2.4 Test Specimen Approximation

Using the engine specifications provided with the Design Brief (Section1.3), the geometric dimensions were approximated from existing miniature liquid-fuelled turbojet engines listed in Chiang [16] and AMT [17]. The patent design in Chiang [16] listed the characteristics, and scaled illustrations, of specific available engines. The particular AMT [17] Nike EVP gas turbine served as a larger model; to provide comparative scaling. Using the average engine length to diameter ratio ($\frac{l}{\emptyset}$), the cubic dimensions were approximated and listed in Table 2.

Table 2. Engine characteristics from Chiang [16], AMT [17], and the resultant Test Piece Engine size approximation

Engine	JPX T-240 (French)	FD 3/64 (German)	J450 (Japan)	Patent (Taiwan)	Nike EVP (Netherlands)	**TEST PIECE ENGINE**
Diameter [mm]	116	110	116	116	201	**400**
Length [mm]	335	265	335	305	524	**1080**
Thrust [N]	45	30	56	56	784	**981**

The geometric profile of the Test Piece Engine (for physical representation within the Test Section) was approximated from the illustrations included in Appx. F.2. The diameters of the various engines were measured at key points so as to generate an averaged volumetric 'bluff body'. This bluff body would hypothetically be situated within the Test Section. It would replicate the effect of the physical obstruction on the Wind Tunnel flow path. The Engine Test Piece bluff body did not include any inlet or exhaust contribution to the Wind Tunnel flow properties.

The Needs Analysis of this section defined the requirements to meet the objectives in Section 1.3. It provided the testing requirements (testing time and airflow specifications), and Tunnel layout (component configuration and Engine sizing) from which the Mixing Chamber demands could be established. These requirements were used to generate the Product Requirement Specification; from which the measures of Design quality were determined.

3 Performance Requirement Specifications

The objective list from Section 1.3 was detailed using the Needs Analysis (Section 2); to produce this set of Product Requirement Specifications. The Propulsion Wind Tunnel had to replicate conditions equivalent to M0.7 at 35000 ft (Design Point). The flow path of the Propulsion Wind Tunnel Design (depicted in Figure 3) included: Open Circuit tunnel, Blow-down pressure gradient (upstream High Pressure source), Free-jet Nozzle into Test Section, Open Test Section (housing Engine Test Piece), and Exit to Atmosphere ($P_{ISA\ (JHB)}$ = 83000 Pa). The Open Test Section design must accommodate the geometry of the Test Piece Engine (L = 1080 mm, Ø = 400 mm, thrust = 100 kg, and mass flow rate = 1 kg/s) under Design Point flow conditions. The Engine Testing Rules and Regulations provided the basis from which the Primary and Secondary Performance Requirements were formed.

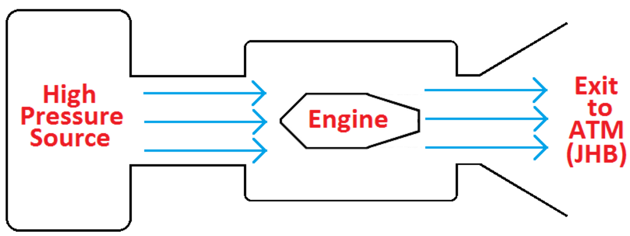

Figure 3. Preliminary Flow Path (from Wind Tunnel Inlet to Exit)

3.1 Primary Requirements

The Primary Requirements set were derived from the Rules and Regulations for Engine Testing (Section 2.3). This set focused on the Wind Tunnel Design in satisfying the Gas Turbine testing requirements. These requirements dictated the Tunnel Air Supply and fluid dynamic requirements.

- Simulate at least 10 altitude conditions at the Test Section (with emphasis on Mach number, as opposed to Reynolds Number) up to and including 35000 ft (M = 0.7, T = 218.8 ≈ 219 K).
- Air supply capable of performing engine tests including Hot Soak, Cold Soak, Windmilling, Spooldown, and Starting Limits (Take-off altitude).
- Primary equipment (Air Supply and Air Conditioning) capable of simulating the altitude conditions for a testing time of at least (≥) 5 minutes.

3.2 Secondary Requirements

The Secondary Requirements pertained to Propeller Engine Testing; as it was specifically addressed as a secondary requirement in Wits MIA [1]. Also included in this subsection, with a higher significance to Design quality, were the Rules and Regulations that did not directly affect the Tunnel Air Supply and fluid dynamic requirements. These regulations concerned the analysis of the Test Piece Engine itself, and did not necessarily influence the Tunnel flow path.

- High Significance: Inlet Distortion testing (> 4 different distortion pattern frames placed upstream of the Test Section; to alter the flow profile).
- High Significance: Transient Engine Operation at 10 altitude settings.
- Low Significance: Variable Test Section Inlet (Free-Jet Diffuser to facilitate optimum airflow to the Propeller Engine diameter).
- Low Significance: Open Test Section that could accommodate the Propeller Engine (Blade Ø = 2000 mm, Engine Power = 90 kW).

3.3 Constraints

The Constraints of the Project presented the physical and financial limits of the Design envelope. It concerned the Tunnel Air Supply mechanisms, Wind Tunnel physical geometry, and the operational requirements of the Design.

- The testing time was limited by equipment costs and functionality. The supply capacity had to be addressed using readily available market options; ie. avoiding purpose-made equipment.
- The efficiency of airflow supply (mass flow rate) had to be optimized; since the Power required was proportional to Velocity cubed (V^3).
- The airflow had to exit the Tunnel to atmosphere without excessive Static Pressure difference; to avoid over/under expansion at the Tunnel exit plane.
- The Tunnel had to include a design component that allowed engine exhaust products to be drawn out in event of hazard.
- The Tunnel had a designated purpose of academic research. This heavily weighted the prioritization of cost reduction (components and machinery). But, it also made the issues of equipment downtime (between runs), and ‘industrial utilization schedules’, relatively insignificant.

3.4 Measures of Compliance

The quality of the Design was based on the Fluid and Thermal Dynamics modelling of the intended flow path; at no point was Structural modelling featured in this Project. The acceptability of the solution was judged on the ability to achieve the required flow conditions, given the specific purposes of its implementation. The Design quality was measured through the following parameters:

- The ability to achieve the Design Point altitude condition (35000 ft); through the effectiveness of the Cooling mechanism.
- The ability to achieve the Design Point airflow velocity (M0.7); through the effectiveness of the Air Supply mechanism.
- The validity of the Wind Tunnel design modelling; to confirm the intended flow path from the designated Supply Devices.
- The efficiency of the Open Circuit Wind Tunnel flow path in achieving Design Point conditions; reducing excessive Pressure Energy wastage.
- The cost effectiveness of the Supply Device utilization in achieving the Design Point conditions; in keeping with the designated academic purposes.
- The modularity of the Supply Device capability; to achieve the incremental altitude replication.
- The modularity of the Wind Tunnel Open Test Section (and preceding components) in achieving the Secondary Objectives (Propeller Testing and Inlet Distortion Pattern Testing).

4 Investigation Method

The focus of the Design Study was placed on the fluid flow path. It required the aerodynamic design of the Wind Tunnel to: make use of readily available machinery, achieve the end goal of the Design Point Test Section requirements, and then vent to atmosphere with the engine exhaust products. The design process was broken down into 2 distinct parts. The 1st part was the Preliminary Design of the Wind Tunnel (comprising of the Wind Tunnel Inlet, Test Section, and Exit to atmosphere) in order to specify the Design objectives for the Mixing Chamber. The Preliminary Wind Tunnel flow path established the Inlet conditions ($P_{0\ WT\text{-}IN}$ and $T_{0\ WT\text{-}IN}$) required to achieve the Design Point at the Test Section (M0.7 at T = 219 K). The 2nd part was the Detailed Design of the Mixing Chamber (comprising the main airflow supplies, the cooling mechanism, the flow conditioners, and the Wind Tunnel Inlet conditions). The Detailed Design identified the most effective and economic Supply Devices (readily available machinery) necessary to achieve the Wind Tunnel Inlet conditions. The design approaches for each of these 2 distinct parts were detailed in the next sections; demonstrating the literature analysis, analytical modelling, numerical modelling, and economic validity that resulted in the finished product.

4.1 Wind Tunnel Design Study

The Wind Tunnel Design Process, illustrated in Figure 4, began with the detailed literature survey of the Fluid Dynamics encountered with the intended flow path. The Analysis included the development of a base model with the respective Wind Tunnel components necessary to achieve the Test Section conditions (M0.7 at T = 219 K) from the Inlet conditions. This base model was subject to parameter optimization (Test Section and Tunnel Outlet dimensions) to minimize the airflow cooling demands of the Mixing Chamber. These base model components (complete with respective energy losses) compiled to form the Analytical Model; which estimated the flow path from theoretical expectations. The Wind Tunnel Analytical Model results were triangulated using Numerical Methods (CFD), to determine the Mixing Chamber Design objectives ($P_{0\ WT\text{-}IN}$, $\dot{m}$, and $T_{0\ WT\text{-}IN}$).

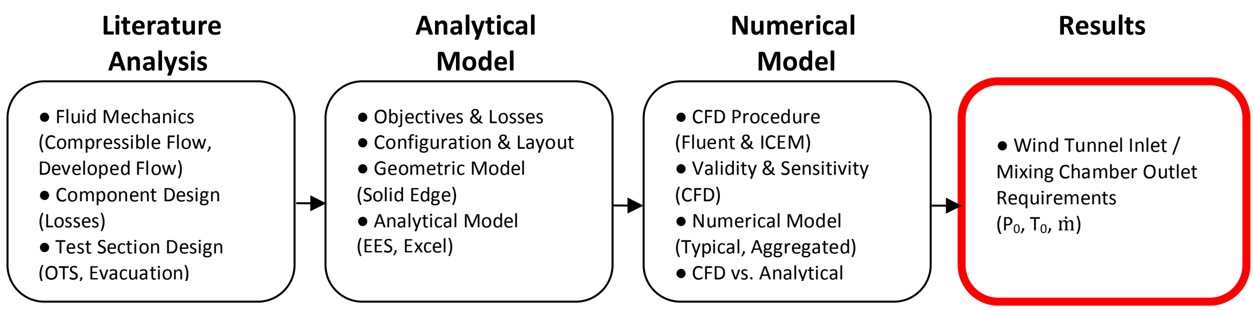

Figure 4. Flowchart demonstrating the Wind Tunnel Design Approach

4.2 Mixing Chamber Design Study

The Mixing Chamber Design Process, illustrated in Figure 5, began with the assessment of the Supply Device requirements in order to achieve the Airflow (P_0 and $\dot{m}$) and Cooling (T_0) demands. Once the best options were selected for the respective delivery requirements, the Design proceeded with an investigation of the Fluid and Thermal Dynamics concerned with the Cooling Mechanism. These parameters formed the basis of the Analytical Model. The solution estimated the Supply Devices and

Mixing Chamber layout required to achieve the Design Point Wind Tunnel Inlet conditions ($P_{0\ WT\text{-}IN}$, $\dot{m}$, and $T_{0\ WT\text{-}IN}$). This Model was then translated (via geometry) to produce a Numerical Model; for result triangulation. The Complete Propulsion Wind Tunnel (Mixing Chamber and Wind Tunnel) was then specified; with performance, cost, and capabilities. The Mixing Chamber Numerical Model demonstrated the effectiveness of the Temperature Mixing mechanism in replicating the required altitude conditions. These mixing processes, which were not readily quantifiable using analytical methods, formed the research aspect of the Project (as outlined in Section 1.3). The approach to the Mixing Chamber cooling analysis was described in the next section.

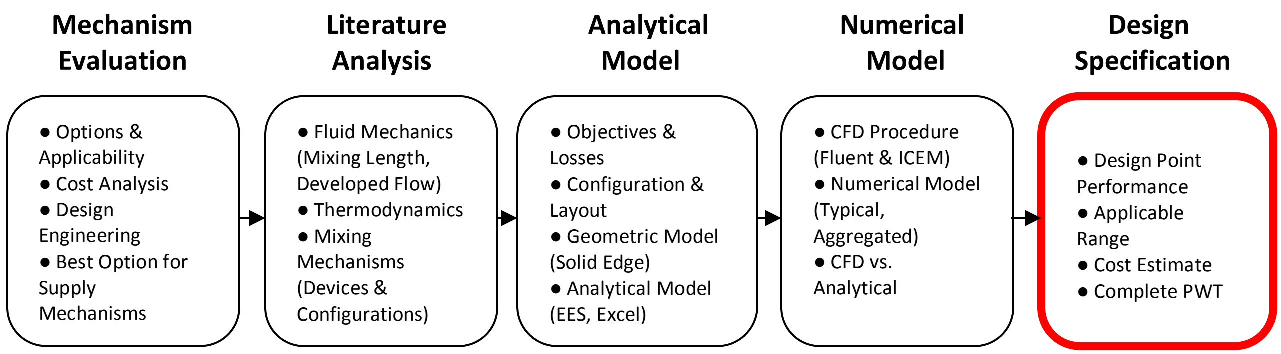

Figure 5. Flowchart demonstrating the Mixing Chamber Design Approach

4.3 Numerical Modelling Approach

The Design was modelled using Analytical and Numerical methods. The Analytical solution, which was derived from theoretical relationships, served to validate the Numerical solution by triangulation. The models were developed as 1-dimensional flow paths to determine the relationships between the Test Section objectives and the Tunnel Inlet conditions. These 1-D models focused on the bulk flow objectives of the Tunnel potential core, rather than the near-wall flow behaviour. This process was followed for both the Wind Tunnel and Mixing Chamber. The Numerical Models were developed for the geometry of the respective completed assemblies (Wind Tunnel and Mixing Chamber). The Models were generated using a coarse mesh; to improve the turn-around time in testing the numerous model sets. This coarse mesh was compared to external sources; to determine the respective resolution capabilities and simulation objectives. The objective of the simulation was to confirm the flow parameters required in order to achieve the flow path specified in Section 3, rather than to investigate the characteristic performance of each component. As such, the mesh was focused on the potential core, rather the capturing the viscous boundary layer.

The Numerical Model of the Wind Tunnel was validated by the respective Analytical Model. It achieved a triangulated solution for the 1-D flow path, and produced the Mixing Chamber Design Point objectives. The Numerical Model of the Mixing Chamber, on the other hand, was focused on interpreting the Temperature Mixing beyond the capabilities of the respective Analytical Model. Even though the Mixing Chamber Design quality was determined by the airflow conditions at the Wind Tunnel Inlet, the assessment and validation of the Numerical Model was performed on the basis of the Temperature Mixing mechanisms. The near-field and far-field cooling concepts implemented within the Mixing Chamber were validated using data published by the respective referenced sources.

5 Wind Tunnel (WT) Literature Review

This section details the relationships used to develop a model that represented the Wind Tunnel flow path (from Section 3). The model was developed using isentropic fluid dynamics to establish relationships between the Test Section, Outlet (Exit to atmosphere), and Inlet (Wind Tunnel Inlet). The isentropic model could then be implemented with the relevant component losses, and produce the Wind Tunnel (WT) Analytical Model.

5.1 Fluid Dynamics (Ideal Gas)

It was beneficial to start the Design with 'limiting' assumptions; to illustrate the fundamental relationships in the fluid flow within the Tunnel. This allowed properties of the intended flow path to be estimated using an isentropic model. As the design process progressed, certain assumptions were replaced with relationships to provide a more realistic performance estimate. These non-isentropic implementations were clearly stated upon the respective inclusion. The assumptions, as identified from Oosthuizen [18] and detailed in Munson [19], included:

- The gas was treated as a continuous medium, ignoring behavior at the molecular level.
- There were no changes to the chemical composition within the flow field.
- Gravitational effects were negligible, given that the gas concerned was air and the fluid motion was primarily horizontal movement.
- Magnetic and Electric effects were negligible; ignoring gas ionization.
- No work energy was extracted from or added to the flow system. There was no contribution to the flow path energy profile, other than the specified inlets.
- The gas behaved as an Ideal Gas, which enabled the use of the charts/tables pertaining to: Perfect Gas Law, Calorifically Perfect values (Specific Heats), and ISA conditions.
- The fluid flow was regarded as Isentropic, along all surfaces and interfaces: Frictionless flow, Lossless components (expansions and contractions), Adiabatic walls (no heat transfer).

The Fluid Dynamic relationships were outlined in 2 categories; Universal relationships and Compressible relationships. Universal relationships encompassed the basics of fluid mechanics that concerned air as an ideal gas. Compressible relationships contained the information that was specific to high speed fluid flow; a primary concern of this Design given the WT Test Section M0.7 requirement.

5.1.1 Universal Fluid Dynamic Relationships

Figure 6 showed an isentropic control volume. This figure, and associated points of interest, was used in the next subsections to demonstrate the relevant transport properties of each isentropic relationship. There were 3 points of interest from which the relationships were demonstrated: Point 0 (Storage Tank with stagnant fluid), Point 1 (entry into control volume), and Point 2 (exit to larger cross sectional area). There were fluid properties attached to each point (with the respective subscript). The flow properties included: P = Static Pressure [Pa], ρ = Density [kg/m^3], T = Static Temperature [K], Ø = diameter of a circular duct [m], $\mathbb{A}$= cross –sectional area of duct [m^2], and V = Velocity [m/s].

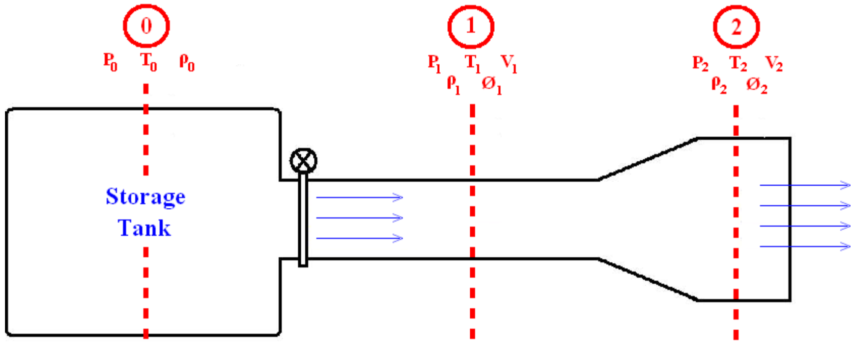

Figure 6. Storage Tank emptying (via. faucet) into Typical Isentropic Control Volume with demarcated areas and respective variables

Equation of State (Ideal Gas Law)

Following the Ideal Gas Law described in Munson [19]:

$$\frac{P_1}{\rho_1 \cdot R \cdot T_1} = \frac{P_2}{\rho_2 \cdot R \cdot T_2} \quad \text{... (1)}$$

Where R = universal gas constant [air = 287 J/kg·K]

Continuity Equation (Conservation of Mass)

According to Oosthuizen [18], assuming no gas left/entered through any permeable surface:

$$\dot{m}_{IN} = \dot{m}_{OUT} \quad \text{... (2)}$$

$$\rho_1 \cdot V_1 \cdot \varnothing_1^{\ 2} = \rho_2 \cdot V_2 \cdot \varnothing_2^{\ 2}$$

Where $\dot{m}$ = mass flow rate [kg/s]

Energy Equation (1st Law of Thermodynamics)

Munson [19] described the one dimensional energy equation for steady flow as:

$$\dot{m} \cdot \left(u_{OUT} - u_{IN} + \frac{P_{OUT}}{\rho_{OUT}} - \frac{P_{IN}}{\rho_{IN}} + \frac{V_{OUT}^{\ 2} - V_{IN}^{\ 2}}{2} + g \cdot [Z_{OUT} - Z_{IN}] \right) = \dot{Q}_{NET} + \dot{W}_{SHAFT} \quad \text{... (3)}$$

Where u = internal energy [kJ/kg], g = gravity [9.81 m/s^2], Z = height [m], $\dot{Q}$ = heat transfer in/out of system [kJ/s], $\dot{W}$ = work transfer in/out of system [kJ/s].

Using the Enthalpy equation, the internal energy (u) variables can be expressed in terms of Static Temperature (T) and Specific Heat (C_P). Utilizing the assumptions of no heat nor work transfer, and ignoring gravitational effects, the Energy equation for the control volume in Figure 6 was:

$$C_P \cdot T_1 + \frac{V_1^{\ 2}}{2} = C_P \cdot T_2 + \frac{V_2^{\ 2}}{2} \quad \text{... (4)}$$

5.1.2 Fluid Compressibility

When dealing with high Velocity flow involving gases, as was the case with the Test Section requirement, it was necessary to take into consideration the compressibility effects imposed on the fluid. The gas Density changed according to changes in Static Pressure. The validity of this 'variable density' model was determined by the dimensionless value of Mach number (M).

Isentropic Implications of Compressibility

Prior to detailing the compressible specific Mach number equation, it was important to state the associated relationships involving the Ideal Gas Law. Oosthuizen [18] described these relationships as:

- $C_P = 1005$ → Specific Heat at a constant Pressure [J/kg·K]
- $C_V = 718$ → Specific Heat at a constant Volume [J/kg·K]
- $R = C_P – C_V = 287$ → Gas constant [J/kg·K]
- $k = (C_P/C_V) = 1.4$ → Specific Heat ratio
- $P/(\rho^k) = CONST$ → Pressure-Density relationship [constant value]

The constant value Pressure-Density relationship was of particular interest. When used in conjunction with the Equation of State (eqn. 1), one can determine the fluid properties at a certain point (Point 2 in Figure 6) with respect to the other points (Point 1 in Figure 6):

$$\frac{T_2}{T_1} = \left(\frac{\rho_2}{\rho_1}\right)^{k-1} = \left(\frac{P_2}{P_1}\right)^{\frac{k-1}{k}} \quad \text{… (5)}$$

Mach number (M)

Mach number, described in Munson [19], was the ratio of fluid velocity to local speed of sound (a):

$$\mathbf{M} = \frac{V}{a} = \frac{V}{\sqrt{k \cdot R \cdot T}} \quad \text{… (6)}$$

There was clearly an inverse relationship between M and T. That is to say: if Velocity was held constant and Static Temperature was decreased, such as the case with an increase in altitude, the result would be a higher Mach number. The value of the Mach number determined the compressibility regime of the fluid flow under question. The primary Mach number regimes, as described by Munson [19], were: $M < 0.3$ (Incompressible Subsonic flow), $0.3 < M < 1$ (Compressible Subsonic flow) and $M > 1$ (Compressible Supersonic flow). According to the Design Point objective (M 0.7), the most applicable regime to the WT Test Section was the Compressible Subsonic flow regime. So, whilst Supersonic flow mechanisms (involving Mach disks and choking) did not feature as part of the WT design, consideration was still given to the compressible nature of the fluid flow.

Reynolds Number (Re)

Even though Reynolds number wasn’t a design priority in the Test Section (with regards to similitude), it was still pertinent to the flow behaviour within the WT. In that sense, Reynolds Number was not a result that was measured for Design Quality, but a ‘tool’ used to develop the flow to achieve a ‘successful’ Mach number. It provided a basis from which a fully developed flow path (consistent profile) was achieved; following flow disturbances. Reynolds Number was defined in Munson [19] as the ratio of Inertial Forces to Viscous Forces:

$$\mathbf{Re} = \frac{\rho \cdot V \cdot \emptyset}{\mu} \quad \text{… (7)}$$

Where μ = dynamic viscosity [N·s/m^2]

The Dynamic Viscosity (μ) was scaled with the fluid Static Temperature. This was accomplished using the 3-coefficient Sutherland Formula, described in ANSYS [20] as:

$$\mu = \mu_{ISA} \cdot \left(\frac{T}{T_{ISA}}\right)^{\frac{3}{2}} \cdot \left(\frac{T_{ISA} + Su}{T + Su}\right) \quad \text{… (8)}$$

Where Su = Sutherland Constant (110.56 K)

There were times when a Turbulent flow was preferable; these included flow mixing and heat exchange. But for flow integrity approaching a Test Section, Turbulence needs to be at a minimum in order to achieve valuable results. This was achieved through the use and manipulation of Reynolds Number.

Straight Duct Flow Behaviour

Reynolds Number aided in determining the starting length of a duct; to achieve a stabilized velocity profile. This length calculation and associated flow result was specific to the Re category concerned i.e. Laminar or Turbulent. For this Design, the Test Section required a potential core of inviscid flow. The Reynolds Number starting length provided the limit length for ducts prior to the Test Section. This length ensured that the Tunnel developed a potential core, and did not achieve fully developed flow. Idelchik [21] stated starting length (L_{ST}) in a circular cross section duct for the Turbulent Re category as:

$$\frac{\mathbf{L_{ST}}}{\emptyset} = \mathbf{7.88 \cdot \log Re - 4.35} \qquad \text{... (9)}$$

This starting length also provided an isentropic estimate of how long a duct should be aft of a geometry change, before stabilized flow could be achieved. It served as the starting point when calculating the required ‘intermediate lengths’ (components of constant diameter) between each ‘complex geometry component’ (components consisting of geometry changes).

5.1.3 Compressible Fluid Dynamic Relationships

Whilst the Universal Fluid Mechanic equations listed previously were still relevant, attention was put on the variable density mechanic ($\rho_1 \neq \rho_2$) and its consequent effect on all other fluid properties. To demonstrate these compressible relationships, the storage tank depicted in Figure 6 (Point 0) was utilized in this subsection as the Stagnation Point.

Euler’s Equation of Motion

The compressible nature of the flow meant that the Bernoulli equation could not be directly used. Instead, Munson [19] described the application of Euler’s equations; integrated along a streamline of steady flow. The Euler equation set was reduced to:

$$\int \frac{dP}{\rho} + \frac{V^2}{2} + g \cdot Z = \text{CONST} \qquad \text{... (10)}$$

Manipulating the integral in this equation to include the isentropic Pressure-Density relationship from eqn. 5 ($P/(\rho^k)$ = CONST), removing the contribution of gravity (due horizontal flow profile), and integrating the equation over point 1 and point 2 in Figure 6, resulted in:

$$\mathbf{\left(\frac{k}{k-1}\right) \cdot \frac{P_1}{\rho_1} + \frac{{V_1}^2}{2} = \left(\frac{k}{k-1}\right) \cdot \frac{P_2}{\rho_2} + \frac{{V_2}^2}{2}} \qquad \text{... (11)}$$

Stagnation Conditions (P_0, T_0, ρ_0)

Stagnation condition was equivalent to bringing the flow to rest (without integrity loss). This allowed the measure of total energy for Temperature and Pressure at any point. This theoretical value system was best explained with the airflow conditions inside the Storage Tank (point 0) of Figure 6. Comparing the Pressure in the tank (point 0) with the Pressure at either point 1 or 2 revealed that P_0 was higher than either of these positions (P_1 and P_2); due to the energy requirements for the respective Velocity components. It was apparent that the Stagnation Conditions were equal to the sum of mechanical energy at any point. Utilizing equation 11 with the Mach number equation (eqn. 6) produced the Stagnation Condition for Temperature (T_0). This was described in Oosthuizen [18] for any position as:

$$\frac{T_0}{T} = 1 + \frac{k-1}{2} \cdot M^2 \quad \text{... (12)}$$

This equation was used with the isentropic relationship equation (eqn. 5) to produce the Stagnation Conditions for Pressure and Density in terms of Mach number. These Stagnation Condition equations allowed for the calculation of flow conditions at any point, as long as the flow was continuous.

$$\frac{P_0}{P} = \left(1 + \frac{k-1}{2} \cdot M^2\right)^{\frac{k}{k-1}}, \qquad \frac{\rho_0}{\rho} = \left(1 + \frac{k-1}{2} \cdot M^2\right)^{\frac{1}{k-1}} \quad \text{... (13)}$$

5.1.4 Modelling Test Section Similitude (Dimensionless Variables)

There were 2 dimensionless variables that featured prominently in the design of the WT; Reynolds Number and Mach number. These variables allowed for the capture of scalable data that best replicated the ‘real-world’ flow conditions in a controlled representative manner; i.e. Similitude. The Reynolds Number usually holds universal relevance when discussing fluid mechanics but, as previously mentioned in Section 2.2, the emphasis was placed on Mach number. This was the proposition when testing engines in a Propulsion Wind Tunnel; in terms of Test Section requirements. With the explanation of Mach number and its implications presented up to this point, this proposition can now be substantiated by showing how compressibility has an effect on Test Section similitude (irrespective of whether its engine testing or aerodynamic testing).

Reynolds Number VS. Mach number in Similitude

According to Munson [19], complete Kinematic Similarity between model and prototype required both Geometric and Dynamic Similarity. When dealing with high Velocity flows (M > 0.3), one also had to include Mach Similarity as an additional requirement to achieve complete Kinematic Similarity. Combining the Mach Similarity equation with the Dynamic Similarity equation, both from Munson [19]:

$$\frac{a_r}{a_m} = \frac{\gamma_r}{\gamma_m} \cdot \frac{L_m}{L_r} \quad \text{... (14)}$$

Where γ = kinematic viscosity (μ/ ρ) [m^2/s], L = characteristic length [m]
Subscripts ‘m’, and ’r’ pertain to the Scaled Model and Real Prototype respectively.

This equation showed that if one was looking to maintain Mach ($a_r = a_m$) and Reynolds ($\gamma_r = \gamma_m$) similarity, the length scale ($\frac{L_m}{L_r}$) must be = 1. This in effect defeated the fundamental purpose of a wind tunnel; to test geometrically scaled models. In such cases, where the flow was high speed compressible air, Munson [19] suggested the preferred use of a ‘Distorted Model’. This was where Mach Similarity was maintained at the expense of a distorted Dynamic Similarity. This was seen as an acceptable compromise in high speed aerodynamics. It should be noted though that in this particular Design, an actual sized Engine prototype ($\frac{L_m}{L_r}$ = 1) was tested; as opposed to a scaled specimen. The ‘Distorted Model’ argument served as supplementary substantiation to the primary argument of ‘Mach number relevance when testing engines’ from Section 2.2. It was necessary then for the Design to replicate the airflow Velocity and altitude Temperature at Design Point in order to maintain Mach Similarity.

5.2 Non-Isentropic Flow (Pressure Losses)

In this section, certain previously made assumptions were replaced with suitably realistic models. These replacements mainly concerned the isentropic flow assumptions; to include factors such as friction and Pressure losses associated with geometry changes. The WT walls were still assumed adiabatic.

5.2.1 Friction Losses (Fanno Flow)

Fanno flow, as described by Oosthuizen [18], involved the effects of friction along surfaces that were regarded as adiabatic. The implications of friction on compressible subsonic flow included: increasing Mach number and Velocity, whilst decreasing Pressure and Temperature. Figure 7, showing a constant diameter duct flow between 2 points, was used to demonstrate the Fanno flow equation.

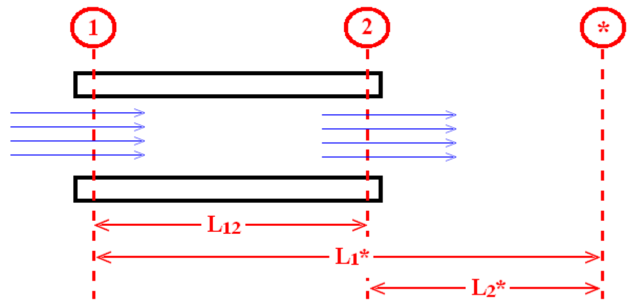

Figure 7. Air flow through an adiabatic duct (constant Ø) between points 1 and 2 before exiting to the theoretical Fanno choke location (*), also showing the corresponding lengths

The Fanno flow equation, between points 1 and 2 in Figure 7, was stated in Miller [22] as:

$$\frac{4 \cdot f \cdot L_{12}}{\emptyset} = \frac{1}{k} \cdot \left(\frac{1}{{M_1}^2} - \frac{1}{{M_2}^2}\right) + \frac{k+1}{2k} \ln \frac{{M_1}^2\left(1+\frac{k-1}{2} \cdot {M_2}^2\right)}{{M_2}^2\left(1+\frac{k-1}{2} \cdot {M_1}^2\right)} \quad \text{... (15)}$$

Where f = friction factor using Colebrook-White relation for turbulent flow ($\frac{0.0625}{[\log(\frac{\epsilon}{3.7 \cdot \emptyset} + \frac{5.74}{Re^{0.9}})]^2}$)

L_{12} = length between point 1 and 2 [m], Є = equivalent roughness [m]

The equivalent roughness (Є) was specific to the material and its respective machining process. The WT could hypothetically be composed of multiple materials according to the associated stress at specific locations along the length; in an effort to minimize material cost. In this Design, a common surface roughness was utilized throughout. This value was selected as:

Є = 0.05 x 10^{-03} m (Design Equivalent Roughness) ... (16)

A practical way to use the Fanno flow equation, described by Miller [22], was by utilizing a hypothetical choke point further downstream. At this hypothetical point, the high speed subsonic flow became sonic; due to the increase in Mach number caused by the friction. This was illustrated in Figure 7 by the point (*) aft of the duct. The occurrence of a sonic transition identified the Mach number at the hypothetical point to be unity (M* = 1). Using the Fanno flow equation (15) at this point (*) in relation to any other hypothetical point (1, 2, or any point in-between) resulted in:

$$\frac{4 \cdot f \cdot L_*}{\emptyset} = \frac{1 - M^2}{k \cdot M^2} + \frac{k+1}{2k} \ln \frac{(k+1)\, M^2}{2\left(1+\frac{k-1}{2} M^2\right)} \quad \text{... (17)}$$

Where L_* = length between hypothetical point and choke point (*)

Using eqn. 17 for the distances L_{1*} and L_{2*}, the intermediate length L_{12} (i.e. the original Fanno equation) can be determined from subtraction: $L_{12} = L_{1*} - L_{2*}$. This choke point relationship presented a convenient method to determine the flow properties (P, T, ρ) at any hypothetical point, stated in Miller [22] as:

$$\frac{T}{T_*} = \frac{\frac{k+1}{2}}{1+\frac{(k-1)M^2}{2}}, \qquad \frac{P}{P_*} = \frac{1}{M}\sqrt{\frac{\frac{k+1}{2}}{1+\frac{(k-1)M^2}{2}}}, \qquad \frac{\rho}{\rho_*} = \frac{1}{M}\sqrt{\frac{1+\frac{(k-1)M^2}{2}}{\frac{k+1}{2}}} \qquad \text{... (18)}$$

5.2.2 Generic Component Losses

Component losses concerned the Stagnation Pressure (P_0) reduction over contractions, expansions, and obstructions of the flow field. The implementation of these losses into the fluid mechanic equations involved an estimated loss coefficient (K_X). The K_X value implied the dissipative effect over the geometric feature concerned (i.e. $P_{02} < P_{01}$). The K_X values for Compressible Flow were described in Miller [22] as:

Compressible Contraction: $$K_C = \frac{P_{01} - P_{02}}{P_{02} - P_2} \qquad \text{... (19a)}$$

Compressible Expansion: $$K_E = \frac{P_{01} - P_{02}}{P_{01} - P_1} \qquad \text{... (19b)}$$

The actual value of the loss coefficient was dependent on the geometry and the flow velocity (Re) involved. The analysis that follows elaborated the loss coefficient values associated with: sudden geometry changes, gradual geometry changes, and ancillary devices (WT specific).

Sudden Geometry Changes

Sudden geometry changes included massive and immediate contractions and expansions in the flow stream. The losses associated were estimated using the equations presented by Idelchik [21] as:

Sudden Expansion (Figure 8 Part A): $$K_{SE} = \left(1 - \frac{\mathbb{A}_1}{\mathbb{A}_2}\right)^2 \qquad \text{... (20a)}$$

Sudden Contraction (Figure 8 Part B): $$K_{SC} = \frac{1}{2}\left(1 - \frac{\mathbb{A}_2}{\mathbb{A}_1}\right) \qquad \text{... (20b)}$$

By examining the limits of these Sudden Geometry Change equations (20a, 20b), the Maximum Expansion Loss ($\mathbb{A}_2 \rightarrow \infty$) was $K_{SE} = 1$, whereas the Maximum Contraction Loss ($\mathbb{A}_2 \rightarrow 0$) was $K_{SC} = 0.5$. These limits served as the preliminary K_X bounds when estimating the basic flow path.

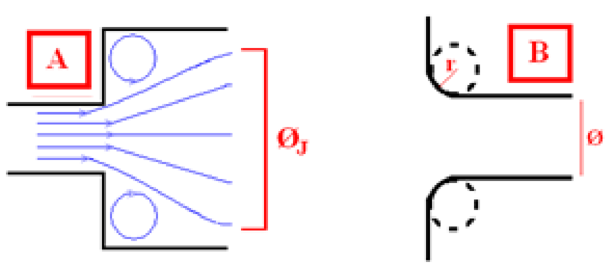

Figure 8. Sudden Geometry Changes, Part A) Sudden Expansion showing flow seperation, Part B) Sudden Contraction showing inclusion of rounded inlet

It was important to note that when expanding airflow into larger areas, flow separation occurred. This separation prevented the Maximum loss of $K_{SE} = 1$ from ever being reached. This was demonstrated in Figure 8 Part A: the maximum flow expansion formed a separated flow $Ø_J$, surrounded by recirculation.

The Sudden Contraction loss (K_{SC}), on the other hand, could be reduced by implementing a relatively minor geometry change at the small duct inlet. This was demonstrated in Figure 8 Part B with the edge being rounded (via. radius 'r'). This modification could reduce K_{SC} by > 75%; using Idelchik [21] tables.

Gradual Geometry Changes

Gradual geometry change allowed the flow to adjust to the contraction or expansion at a controlled rate. This endeavour minimized Pressure loss at the expense of added component length. In the case of subsonic flow, the contraction was referred to as a Nozzle, and the expansion as a Diffuser. For these loss coefficients, the analysis did not rely on generic equations but was instead treated on a case-by-case basis. There were fixed limit conditions though, that were placed on the general implementation of nozzles and diffusers. These limits were addressed before any consideration to the specific applications.

Focusing on a Conical Nozzle, shown in Figure 9 Part A, Idelchik [21] recommended: the area ratio ($\eta_{AR} = \frac{\mathbb{A}_2}{\mathbb{A}_1}$) was > 0.3, and the angle of expansion (α) was > 10°. This ensured that wall separation did not occur.

In the ideal case ($\eta_{AR} > 0.3$, and $10° < \alpha < 40°$): $\mathbf{K_{NOZ} = 0.045}$ ($Re > 10^6$) ... (21)

Nozzle performance was further improved by implementing compound geometry changes. This allowed for larger contraction angles ($\alpha > 40°$) and more effective area ratios ($\eta_{AR} < 0.3$) at a relatively lower K_{NOZ}.

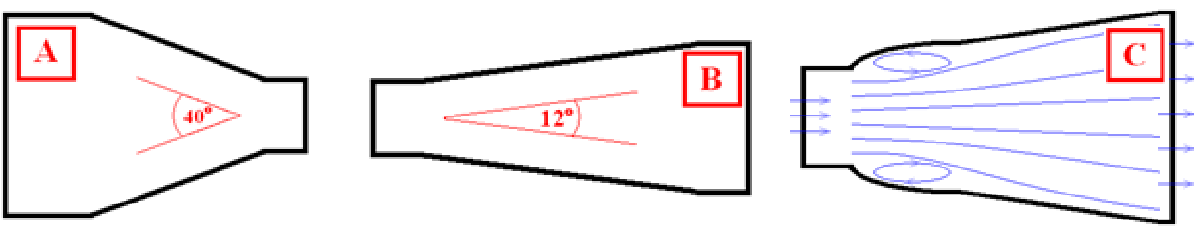

Figure 9. Gradual Geometry Changes, Part A) Conical Contraction (Nozzle) with α = 40°, Part B) Conical Expansion (Diffuser) with α = 12°, Part C) Diffuser with concave entry [NOT TO SCALE]

Diffuser design was considerably more complex than Nozzle design due to the presence of recirculation. Reynolds [23] stated that in an attempt to aspire to isentropic expansion in a diffuser, the $\Delta\mathbb{A}$ should be gradual enough to avoid recirculation. The implication of this, having a very long diffuser, would be the increasingly present wall friction dissipation. This friction loss would reach a point of overriding the expansion loss saving. The balance of recirculation vs. friction put forward the acceptable compromise of incurring inefficient diffusion in order to avoid overbearing friction loss. When using a Conical Diffuser, shown in Figure 9 Part B, Idelchik [21] limited maximum expansion at $\eta_{AR} = \frac{\mathbb{A}_2}{\mathbb{A}_1} < 8$, and $\alpha < 40°$.

In the ideal case ($\eta_{AR} < 5$, and $\alpha < 30°$): $\mathbf{K_{EXP} = 0.08}$ ($Re > 10^6$) ... (22)

Diffuser performance could be further improved by implementing compound geometry changes. These changes focused on increasing the expansion angle (reducing diffuser length) at the expense of increasing the K_{EXP} loss. It was stated explicitly here that the actual Diffuser loss coefficient (K_{DIFF}) was the summation of the expansion loss coefficient (K_{EXP}) and the frictional loss component (K_{FRIC}), i.e.:

$$\mathbf{K_{DIFF} = K_{EXP} + K_{FRIC} = K_{EXP} + \frac{4 \cdot f \cdot L}{\emptyset}} \quad \text{... (23)}$$

This K_{DIFF} equation implied that decreasing the diffuser length, effectively reducing K_{FRIC}, may make an increased K_{EXP} viable. It was possible to expand at a greater angle but the focus of this Design was to achieve a consistent flow to and from the Test Section; rather than optimize for the shortest possible length. In optimizing the Design to meet the current expansion objectives, Nordwall [24] suggested destabilizing the flow earlier in the diffuser length and incurring the loss beforehand via 'Early Onset Recirculation'. This allowed the flow to overcome severe recirculation before the diffuser design point, rather than letting it propagate and eventually grow to complete and irrecoverable boundary layer detachment. The option which was most effectively incorporated into the currently available diffuser variants was that of a concave entry conical diffuser; seen in Figure 9 Part C. The sizing of the concave surface was estimated on the height ratio of the 2-D expansion ($\frac{h_{Concave}}{h_{Expansion}}$). For the implementation in this Design, the minimum concave height was established through prelim CFD.

Ancillary Devices

This category included typical wind tunnel features such as flow straighteners and screens. The actual construction was not of great concern, but rather the impact on the flow via the loss coefficient (K_{LOSS}). There were 2 possible devices that were suitable to this Design: Thick Grid Lath (placed upstream of the Test Section to correct unevenness of flow), and Mesh Screen (placed at the WT exit to prevent foreign object entry). It was recommended in Idelchik [21] that these devices be positioned where the flow velocity was relatively lower in comparison to the Test Section conditions; i.e. large $\mathbb{A}_{C\text{-}S}$ segments. This placement ensured that excessive losses were not incurred. The implementation of these loss coefficients used the Compressible Contraction equation (eqn. 19a).

The K_{GRID} loss coefficient for the Mesh Screen was extracted from Idelchik [21] as:

$\mathbf{K_{MESH}}$ **= 0.14** (for M = 0.15, η_{GRID} = 0.9) … (24a)

The K_{GRID} loss coefficient for the Thick Grid Lath was extracted from Idelchik [21] as:

$\mathbf{K_{LATH}}$ **= 0.24** (for M = 0.15, η_{GRID} = 0.9, L = 0.05m, $\emptyset_0$ = 0.01, f = 0.02) … (24b)

Ideally when implementing these ancillary devices, the η_{GRID} ratio should be as high as possible. The value chosen to estimate the loss coefficients was mentioned to be η_{GRID} = 0.9. Observing the data trends in Idelchik [21], K_{LATH} and K_{MESH} increased exponentially with η_{GRID} reduction. These losses (K_{MESH} and K_{LATH}) become considerable when compared to geometry and friction losses, and may well render such devices impractical. If stabilized flow (uniform flow profile) could be achieved through duct length extension alone, it would be preferable to remove flow straighteners altogether.

5.2.3 Specialized Component Losses

In fulfilling the Performance Specifications of this Design, the WT had to include an Open Test Section (OTS) and be able to evacuate the engine by-products (in event of hazard). The analysis to follow entailed the compilation, constraints, and losses associated with: an OTS, and an Eductor device.

Open Test Section (OTS)

The design of this OTS had to adhere to the measures prescribed by literature for hypothetical 'open working sections', but also had fit the Design specific objective of testing a Gas Turbine Engine. These Engine-specific concerns included: the specific dimensions, operating profile, and points of interest (inlet and outlet) of the Test Piece Engine. Pankhurst [25] described the Static Pressure (P) across the free stream jet in an OTS to be that of the surrounding chamber, as shown in Figure 10. The OTS model included the following sizing estimates:

- Test section length (L_{TS}) to Entry diameter ($\emptyset_{IN}$) ratio: $\frac{L_{TS}}{\emptyset_{IN}} > 3$ … (25a)

This allowed for the airflow jet to develop into a stable expanded stream.

- Entry area ($\mathbb{A}_{IN}$) to Collector area ($\mathbb{A}_{COLL}$) ratio: $\frac{\mathbb{A}_{COLL}}{\mathbb{A}_{IN}} > 1.1$ … (25b)

This allowed for the efficient capture of the resultant expanded flow.

Pankhurst [25] recommended the inclusion of vents downstream of the Collector; also shown in Figure 10. These vents not only reduced the effects of pulsations (intermittent vibrations associated with an OTS), but it was also beneficial to Engine testing. It allowed for supplementary cooling air to be drawn into the WT, and prevented the accumulation of combustion products aft of the OTS.

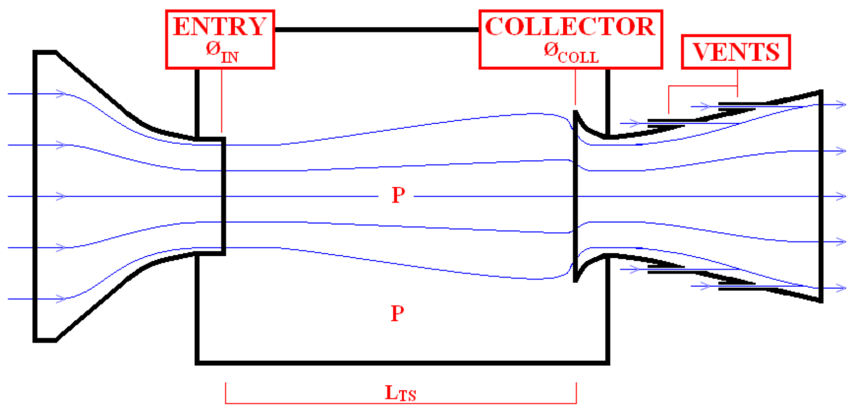

Figure 10. Open Test Section (OTS) showing incoming flow through Entry, expanding in the Test Section, before exiting through Collector, to be supplemented by Vent flow [NOT TO SCALE]

The estimates of L_{TS} and $\mathbb{A}_{COLL}$ were further refined when presented with the restrictions suggested by Rennie [26]. The article put forward the concern of pressure fluctuations associated with an OTS wind tunnel. These fluctuations resulted from the Static Pressure equivalence between the free jet stream and surrounding OTS chamber air. Solutions to the unwanted fluctuations included:

- Decreasing L_{TS} (below the eqn. 25a minimum: $\frac{L_{TS}}{\emptyset_{IN}} > 3$)

This reduced the amount of shear layer thickness growth (between jet stream and OTS free air); thereby reducing turbulent energy (vortices).

- Increasing $\mathbb{A}_{COLL}$ (considerably beyond the eqn. 25b minimum: $\frac{\mathbb{A}_{COLL}}{\mathbb{A}_{IN}} >> 1.1$)

This reduced the reflective capability of the Collector; restraining more of the vortex.

- Implementing a 'breather gap' at the base of the Collector; to reduce disturbance strength.

The loss associated with the OTS was divided into 3 components (visible in Figure 10): the Entry ($\emptyset_{IN}$), the working section (L_{TS}), and the Collector ($\emptyset_{COLL}$). The Entry and Collector loss coefficients followed the Nozzle (K_{NOZ}) procedure, whereas the working section required a separate coefficient (K_{OTS}). The K_{OTS} value, as described by Idelchik [21], was independent of flow Velocity (Re) and relied solely on $\frac{L_{TS}}{\emptyset_{IN}}$:

$\mathbf{K_{OTS}} = \mathbf{0.29}$ (for $\frac{L_{TS}}{\emptyset_{IN}} = 4.3$) … (26)

Eductor Device

As mentioned in the development of the OTS, the vents downstream of the Collector aided in the reduction of pulsations. For the purposes of this Design, these vents needed to address the respective OTS issues and also draw out the Engine exhaust products. This required the device to create a minor vacuum effect downstream of the Test Section. Utilizing an Eductor device at this point would accomplish the goal. The device had to balance the purposes of both an Ejector and a Blower.

Green [27] detailed the Ejector concept of using a high Pressure stream to boost the energy of a low Pressure source. It effectively entrained the secondary (low Pressure) flow with a primary (high Pressure) flow. The objective of this device was to boost the energy of the resultant mixed flow. It was not the most efficient method of accomplishing this task, but it was a simple mechanism without any moving parts. The assumption was that the high Pressure flow was readily available to achieve up to an equal contribution in flow rate ($\frac{\dot{m}_{PRI}}{\dot{m}_{SEC}} = 0.9$); corresponding to the highest ejector efficiency. When implementing this concept into the current Design, one had to keep in mind the specific objective of creating an entrainment of Test Section flow (as opposed to boosting the resultant energy profile). It meant that the supplementary flow requirement would be much lower than that of a typical Ejector.

The Blower device, as depicted in Figure 11, was the inclusion of a supplementary flow stream into the diffuser expansion of a primary flow stream; as described in Idelchik [21]. The primary objective of this mechanism was to reduce diffuser expansion loss (> 200%). The revised loss coefficient (K_{DIFF}) was dependent on 2 factors: the ratio of 'Blower Area' to 'Diffuser Entry Area' (η_{BLOW}), and the ratio of 'Blower Flow Rate' to 'Total Flow Rate' ($\bar{q}$). These values were interpreted from Figure 11 as:

- $\eta_{BLOW} = \frac{\mathbb{A}_{BLOWER}}{\mathbb{A}_{DIFFSUER\ IN}} = \frac{\mathbb{A}_B}{\mathbb{A}_1}$ $(0.03 < \eta_{BLOW} < 0.1)$ … (27a)
- $\bar{q} = \frac{\dot{\forall}_B}{\dot{\forall}_1 + \dot{\forall}_B}$ $(0.04 < \bar{q} < 0.12)$ … (27b)

The Blower device achieved the loss reduction benefit by pushing the primary flow boundary layer away from the walls. In doing this though, the supplementary flow was at the same Static Pressure as the primary flow; in order to maintain the mechanical energy stream path.

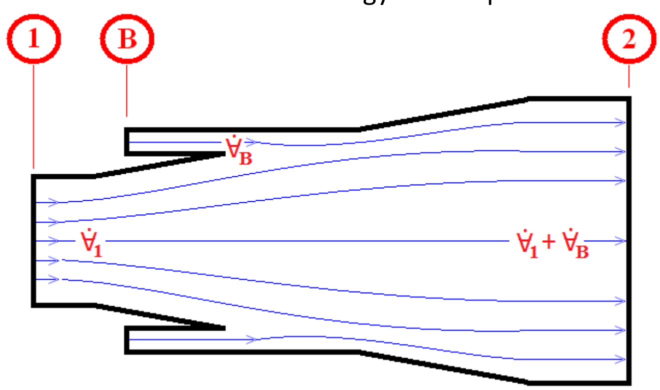

Figure 11. Blower Device (B) implemented in a Diffuser showing primary and supplemented flows

The Eductor device implemented in this Design was a balance between the operations of both the Ejector and Blower, but not necessarily the intended respective benefits. There was no intention to achieve optimum flow energy boosting, nor was any 'supplementary flow benefit' included into the Diffuser loss (i.e. no K_{DIFF} reduction). The purpose was to entrain the Test Section flow, as opposed to improving diffuser performance. It was designed with a relatively high Pressure flow, emitted from the vents within the Diffuser. It was sized according to the conventional Blower dimension limits (η_{BLOW}, $\bar{q}$). The optimization of this Eductor device was left for Further Work (Appx Q.3.2). For the purposes of this Project, the Eductor served as a placeholder that provided the higher Pressure flow at the suggested flow rate. There was no attempt to assess the effectiveness of evacuating the Test Section chamber; only the confirmation of the expected flow behaviour. This evacuation effectiveness would only prove representative if the Test Piece Engine was tested in active state.

With the fluid dynamics relationships detailed in Section 5.1, the isentropic model for the WT flow path could be developed in the next section (Section 6). The model could then be implemented with the respective losses from Section 5.2, to produce the WT Analytical Model.

6 Wind Tunnel (WT) Analytical Modelling

The WT Analytical Model was used to predict the intended flow path using the components (and associated losses) outlined in Section 5. The Analytical Model was built in 3 stages:

1) Isentropic Sizing – optimizing the Test Section Inlet and Tunnel Exit diameters using the Design Point requirements and Atmospheric Exit conditions.
2) Component Sizing – optimizing the various WT component lengths and diameters in achieving the intended flow path.
3) Complete Analytical Model – compiling the various components and intermediate lengths that form the WT structure; to determine the required WT Inlet conditions at Design Point. The Analytical Model would serve as the means of validation for the WT Numerical Model.

6.1 Isentropic Sizing (WT IN/OUT)

The flow conditions within the WT were determined with respect to the Test Section requirements (Design Point), and the Tunnel Exit to Atmosphere (JHB ISA). The key flow properties pertaining to these 2 locations were presented in Figure 12. These properties formed the basis of the flow expansion.

- **Test Section**: Static Temperature (T_{TS}) = 219 K, Mach number (M_{TS}) = 0.7
- **Outlet:** Static Pressure (P_{EXIT}) = 83000 Pa (> 81980 Pa Johannesburg ISA at 5751 ft)

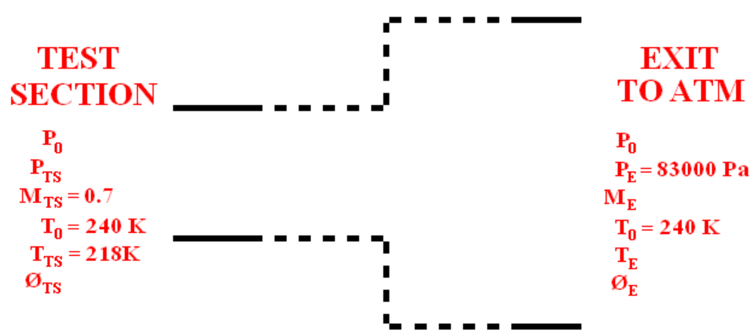

Figure 12. Isentropic relationship between the Test Section and Exit to Atmosphere

The priority of the Test Section design was to supply the frontal area of the engine ($\mathbb{A}_{FRONTAL\ ENG}$), including inlet and dress, with conditioned high speed airflow. This allowed for the analysis of engine performance subjected to rammed altitude air. To replicate the concept of a 'true OTS', the Test Piece would have to be immersed in a diameter of flow ($\mathbb{A}_{TS\ INLET}$) that minimized blockage ratio ($\frac{\mathbb{A}_{FRONTAL\ ENG}}{\mathbb{A}_{TS\ INLET}}$). It had to ensure that the boundary layer of the free jet was undisturbed by the Test Piece. This 'true OTS' concept was contextually over-specified for the purposes of this Design; as aerodynamic properties along the Test Piece were not as important as directly feeding the Engine. It also presented significant economical hurdles concerning the increased $\dot{m}$ ($f_X\{\mathbb{A}_{TS\ INLET}\}$) including: Increased Supply Device capability (Higher Tier Centrifugal Fans), Increased Electrical Power demand (Power $\alpha\ V^3$), and Increased Cooling capacity ($\dot{Q}\ \alpha\ \dot{m}$). Instead, the OTS was designed to supply the airflow directly proportional to $\mathbb{A}_{FRONTAL\ ENG}$. This flow encompassed and rammed the Engine inlet and dress; providing the most economical method of achieving the objective. The method implied that $Ø_{TS}$ ($\mathbb{A}_{TS\ INLET}$) was sized to expand the flow to $Ø_{ENGINE}$ ($\mathbb{A}_{FRONTAL\ ENG}$) within the OTS.

The optimization process of $Ø_{TS}$ (involving the balance between immersing $\mathbb{A}_{FRONTAL\ ENG}$ and minimizing $\dot{m}$) was included in Appx. A.1. $Ø_{TS}$ in this Design was set to 0.35 m; which was smaller than the $Ø_{ENGINE}$ = 0.4 m. It actually required the potential core of $Ø_{TS}$ to be retained (upon entering the OTS), and the boundary layer of the free jet had to expand within the OTS (prior to Engine frontal area). The sizing of the Outlet was calculated using an isentropic model based on the flow properties from Figure 12, and $Ø_{TS}$ = 0.35 m. The optimization of $Ø_E$ (involving the balance between minimizing P_{TS} and minimizing $Ø_E$) was included in Appx.A.2. The $Ø_E$ in this Design was set to 1.25 m. The complete list of flow properties from the relationships in Figure 12 was listed in Table 3. The table provided the initial isentropic estimate of P_0, T_0, and $\dot{m}$ required to achieve M_{TS} and T_{TS}.

Table 3. Isentropic Flow Properties of Test Section and Exit

	Test Section	Exit
Ø [m]	0.35	1.25
P_0 [Pa]	83100	83100
P [Pa]	59909	83000
T_0 [K]	240	240
T [K]	219	240
M	0.70	0.04
$\dot{m}$ [kg/s]	19.05	19.05

6.2 Component Sizing and Associated Losses

The layout of the WT (seen in Figure 13) consisted, in respective order, of:

1. Large diameter Plenum Chamber (between the Mixing Chamber and Wind Tunnel) –to reduce the flow Velocity, stabilize the flow, and achieve a 1-D flow path.
2. Nozzle to Test Section diameter – to contract and accelerate the Inlet flow to Design Point.
3. Open Test Section (including Collector and Test Piece Engine body).
4. Eductor device –to supplement the WT flow and aid in OTS evacuation.
5. Diffuser segment – to expand the flow to Outlet size.
6. Outlet to Atmosphere with Mesh Screen – to prevent foreign object from entering.

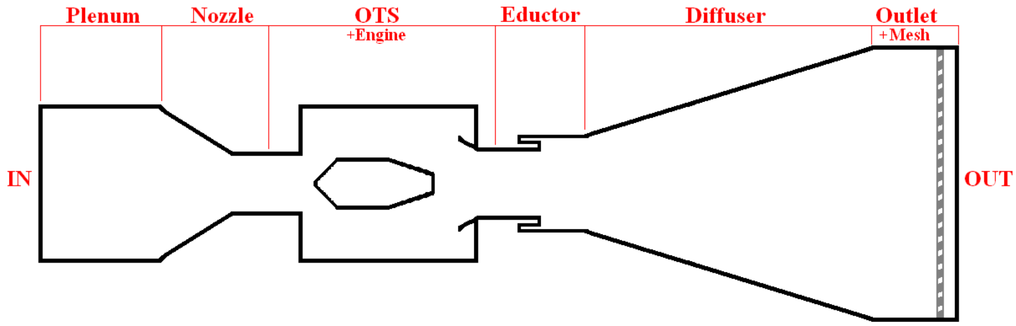

Figure 13. Wind Tunnel layout with components in respective order (NOT TO SCALE)

The sizing, geometry details, and associated losses of the individual components were included in Appx. H.1. The geometry profile was kept simple in an attempt to keep machining procedures economical. Straight lines along the WT profile were used as much as possible, with curvatures limited to only the immediate area of effect. The complete WT (assimilation of components) was presented in Figure 14, including a numbering format (1-16, and 9ed) corresponding to the flow conditions at Key Point locations along the WT length. These points were of importance when developing the Analytical Model (Section 6.3). These Key Points (and associated losses) included:

- **1.** WT Inlet (aft of Mixing Chamber)
- **2.** Start Thick Grid Lathe Ghost Plane ($\mathbf{K_{LATHE} = 0.24}$)
- **3.** End of Thick Grid Lathe Ghost Plane
- **4.** Start of Nozzle ($\mathbf{K_{NOZ} = 0.05}$)
- **5.** End of Nozzle
- **6.** Start of Open Test Section ($\mathbf{K_{OTS} = K_{OTS\ STD} + K_{ENG\ LOSS} = 0.29 + 0.11 = 0.4}$)
- **7.** End of Open Test Section / Start of Collector ($\mathbf{K_{COLL} = 0.05}$)
- **8.** End of Collector
- **9.** Main flow immediately prior to mixing with Eductor flow ($\mathbf{K_{EDUCT} = 0.047}$)
- **9ed.** Eductor Inlet (irrespective of annular Eductor duct length)
- **10.** Joining of Main flow and Eductor flow upon the expansion
- **11.** Start of 1st Diffuser ($\mathbf{K_{DIFF1} = 0.08}$)
- **12.** End of 1st Diffuser
- **13.** Start of 2nd Diffuser ($\mathbf{K_{DIFF2} = 0.08}$)
- **14.** End of 2nd Diffuser
- **15.** Start of Mesh Screen ($\mathbf{K_{MESH} = 0.14}$)
- **16.** End of Mesh Screen / WT Outlet (to Atmosphere)

Certain components of the WT required additional design considerations:

- The Plenum Chamber was initially outfitted with a Thick Grid Lathe flow straightening device. The development of the preceding Mixing Chamber (Section 12) proved this device to be redundant, and it was subsequently removed from the Final Plenum Chamber design.
- The OTS component included the geometry of the Test Piece Engine, and associated loss ($\mathbf{K_{ENG\ LOSS} = 0.11}$). This $K_{ENG\ LOSS}$ value was estimated using CFD, and was included in Appx. I.1.
- The loss associated with the Eductor component was due to the Sudden Expansion of the Main flow upon the inclusion of the annular Eductor; no supplementary flow benefit was included.
- In order for the Diffuser to conform to maximum expansion parameters from Section 5.2.2, it had to be divided into 2 separate components (with an intermediate length in between). The 1st and 2nd Diffusers shared the total geometric expansion via 1/3 and 2/3 respectively.

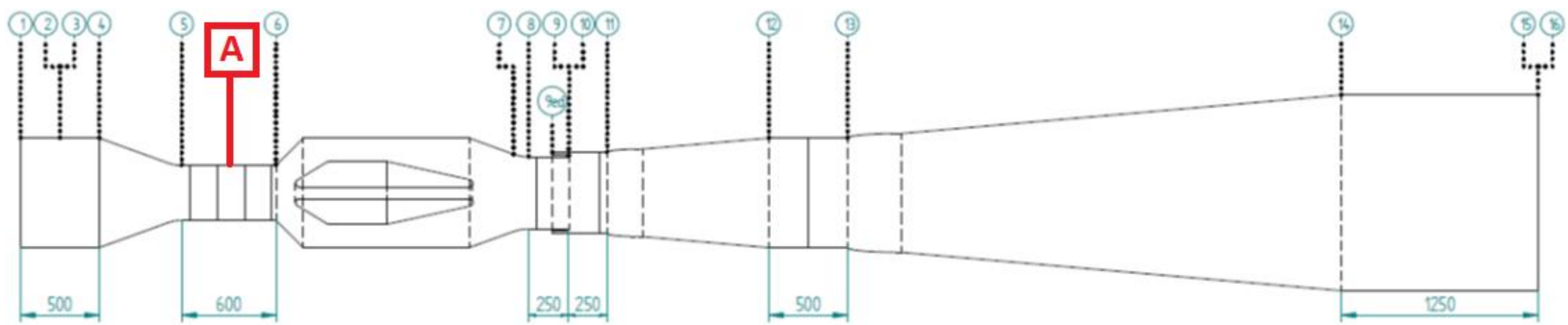

Figure 14. Complete Wind Tunnel (including intermediate lengths and Key Point numbering), with Point A indicating the extended intermediate length prior to the OTS Inlet

It was noted here that there were intermediate lengths (subject to friction losses) between the complex geometry components (Tunnel $\mathbb{A}_{C\text{-}S}$ changes). These lengths allowed for intermediate stabilization of the flow profile before further geometry manipulation. The lengths were sized to approximate the diameter at the respective point (i.e. L ≈ Ø), with the only exception being the length prior to the Test Section. This Test Section intermediate length (Point A in Figure 14) was sized > 1.5×$Ø_{TS}$; to ensure a developed potential flow core prior to the OTS. This extended length also allowed room for component modularity; in pursuit of the Secondary PRS Requirement of Propeller Engine Testing (Section 3.2). This intermediate length (and upstream components: Plenum Chamber and Nozzle) were designed as an interchangeable collective for a single Diffuser. The replacement Diffuser would expand the flow from Ø = 0.7 m (Plenum Chamber) to Ø ≈ 2 m (Propeller Blades). This was described as Further Work (Appx. Q.1.2).

6.3 WT Analytical Model

The Analytical Model was created using EES software (Engineering Equation Solver© Academic Commercial V9.704 by F-Chart). The program used to develop the model was a specialized Thermodynamic application; designed to solve non-linear equations simultaneously. The mathematics of the Analytical Model was verified using the methods presented by Sargent [28]. The model was developed with a structured walkthrough, by developing analytical models for each component in isolation. These isolated component models were compared to the theoretical expectation, before the complete assembly was modelled as the Analytical Solution. The results from the Analytical Model provided the WT Inlet conditions (P_0, T_0, $\dot{m}$) required to satisfy the Test Section (M_{TS}) and Outlet (P_{EXIT}) requirements. Sample calculations were provided for common procedures (Friction, Contraction, and Expansion) in Appx. G.2. The important flow properties from the Analytical Model were presented in Table 4; in correspondence with the Key Points along the WT length. These flow properties included: Distance along WT length (X), Stagnation Pressure (P_0), Static Pressure (P), Mach number (M), Static Temperature (T), and Mass Flow Rate ($\dot{m}$). Table 4 displayed the Design objectives in boxed cells. The Analytical Model was varied to achieve the PRS objectives: M_{TS} = 0.70 (Objective = 0.7), T_{TS} = 218.2 K (Objective = 219 K), and P_{EXIT} = 83030 Pa (Objective = 83000 Pa).

The results of the calculations allowed for the various Inlet conditions (Main Flow and Eductor Flow) and Outlet conditions to be determined. The WT Inlet requirements included the Airflow Delivery capacity ($\dot{m}$ = 22.16 kg/s at 98400 Pa), and the Cooling Mechanism capability (T_0 = 240 K). The Eductor Inlet requirements served as a placeholder. It fulfilled the intended purposes of entraining the Main flow with a higher Mach number (M_{EDUCT} 0.51 > M_{MAIN} 0.38), whilst maintaining the mechanical energy stream path ($P_{MAIN} = P_{EDUCT}$ = 76744 Pa). The WT Outlet T_0 was well below ambient ($T_{0\ 16}$ = 249.4 K << $T_{0\ ATM\ (JHB\ ISA)}$ ≈ 288 K).This significant Temperature difference presented a ‘real-world’ issue when implementing a scaled physical WT model; such as icing at the backend. This concern however falls outside of the scope of this Project. It was also important to note that no Engine contribution had been included in the Design; the potential exhaust gas Temperature (EGT) would play a significant role in increasing the thermal energy downstream of the Test Section. The WT Outlet P (P_{16} = 83000 Pa) was a conservative over-prediction of JHB Atmospheric Pressure. This Static Pressure was actually set as the higher bound of ISA 5751 ft and, as such, represented the lower bound of the Design performance.

Table 4. Selected Results from Wind Tunnel Analytical Model (Objectives Boxed)

Point Number	X [mm]	P_0 [Pa]	P [Pa]	Mach	T [K]	$\dot{m}$ [kg/s]
(Main In) 1	0.0	98400	97225	0.13	239.2	22.16
2	250.0	98395	97220	0.13	239.2	22.16
3	250.0	98112	96933	0.13	239.2	22.16
4	500.0	98107	96928	0.13	239.2	22.16
5	1025.0	96765	69924	0.69	218.7	22.16
(Test Section) 6	1625.0	96140	68862	0.70	218.2	22.16
7	3136.5	85229	79699	0.31	235.4	22.16
8	3233.5	84827	76797	0.38	233.3	22.16
9	3488.5	84780	76744	0.38	233.3	22.16
(Eductor In) 9ed	3383.5	91500	76744	0.51	275.8	5.14
(Join) 10	3488.5	84402	76626	0.37	242.6	27.30
11	3733.5	84353	76571	0.37	242.6	27.30
12	4762.2	83559	81340	0.20	247.5	27.30
13	5262.2	83540	81320	0.20	247.5	27.30
14	8405.5	83276	83063	0.06	249.2	27.30
15	9655.5	83274	83060	0.06	249.2	27.30
(Outlet) 16	9655.5	83244	83030	0.06	249.2	27.30

Interpreting the P_0 decline in Table 4 along the WT length, the combined OTS segment accounted for 74.6% of the total P_0 loss (shared by the OTS expansion, Engine obstruction, and Collector). The friction losses within the various intermediate lengths were far less significant when compared to the complex geometry components (contractions and expansions). The only significant friction loss occurred prior to the Test Section (Point 5 to Point 6); where the Velocity (Re) was considerably higher. The low influence of these losses were due to the surface roughness employed in the Analytical Model ($\epsilon = 0.05 \times 10^{-03}$ m).

With the Analytical Model (and corresponding geometry) in place, the concept was modelled using CFD (Section 7). This allowed for the confirmation of the flow path prediction, and provided relevant estimates of the loss coefficients (K_{LOSS}) implemented in the Analytical Model. The impacts of these various losses, predicted by the Analytical Model, shaped the focus of the Numerical Model. Friction losses only played a significant role in the intermediate length prior to the OTS. Complex geometry component losses played a significant role throughout the flow profile (especially across the OTS). The focus of the Numerical Model was then shifted to the bulk flow fluid dynamics (1-D fluid core performance), instead of near-wall behaviour (with the exception of the length preceding the OTS). This decision focused on the core flow profile development from the WT Inlet to the OTS free shear jet, and finally exiting at the WT Outlet. It directed the simulation efforts toward resolving the OTS Inlet objectives (M_{TS} and T_{TS}), in satisfying the PRS, rather than the performance optimization (reduced P_0 loss) of the various WT components. The WT Inlet conditions, that produced these PRS objectives (M_{TS} and T_{TS}), were then used to define the Design objectives for the preceding Mixing Chamber.

7 Wind Tunnel (WT) Numerical Modelling

The Numerical Model was developed to determine the WT Inlet conditions. These conditions would serve as the Design requirements for the Mixing Chamber. The Numerical Model was compared to the Analytical Model to validate the Entrance/Exit conditions (Main Flow Inlet, Eductor Flow Inlet, and Outlet), and determine the flow properties along the WT length (16 key point locations). Whilst there were no certain Numerical Model rules to adhere to, when achieving results from CFD simulation, there were guidelines provided by Roache [29]. These guidelines provided a checklist from which CFD results could be considered reliable. Selected guidelines included:

- Provide a precise description of the Numerical Methods used. Including the assessment of truncation error introduced by the governing equations (diffusive, convective, etc.).
- The Numerical Methods should be ≥ 2nd order accuracy; any blending/mixing or artificial 2nd order method will be relegated to 1st order accuracy.
- Produce a range of solutions across multiple (significantly different) mesh grids; so as to demonstrate grid independence and 'ideal solution' convergence.
- The stopping criteria (if not converged) must be precisely explained with convergence error.

Certain guidelines were omitted due to the particular design processes of this Project, including:

- Transient phase error evaluation and minimization

The Project only entailed a steady state solution; no transient analysis was performed. The solution required a still frame that represented the intended flow path over the 5 minute test duration.

- Comparison to appropriate analytical benchmark solutions

The complete WT assembly, as opposed to an individual test piece, limited the available benchmark Numerical Solutions for comparison. No physical scaled model was attempted either, due to time and financial constraints, and was left as Further Work (Appx. Q.1.4). Instead, the Numerical Model was compared to the 1-d flow path of the Analytical Model.

With the absence of a scaled physical model (to provide experimental results), or directly comparable Numerical Model results (from published sources), the CFD validation was performed in a piece-wise manner. Jauregui [30] listed the possible forms of CFD validation including:

- Validation using Analytical Solutions

If the theory was known, and the case was relatively simple, an Analytical Model could be used to validate the Numerical Model.

- Validation using Solution Convergence

If the Numerical Model achieved a converged solution, a comparison of the 'pattern' could be made. Whilst this method was not recommended as a final validation, it did serve to confirm the relevance of the Solution. This method was commonly used for coarse meshes.

The simplicity of the 1-D WT flow path and the Design focus of core flow properties (as opposed to near-wall behaviour) made the method of validation through Analytical Solution a feasible option. This validation type was bolstered by the utilization of the Re-specific Idelchik [21] K_{LOSS} coefficients in the Analytical Model. The Numerical Solution was also run until residual convergence, before being refined further to achieve a stricter mass flow balance across the control volume. This method provided validation through Convergence by achieving a comparable 'pattern'.

A number of publications presented Numerical Solutions to wind tunnel flow; allowing for comparisons to experimental data. However, these publications were largely based on low-speed flows that focused exclusively on Test Section Inlet performance (including: Calautit [31] and Moonen [32]). There were significant design differences between these publications and the current Design:

- Reynolds Number – The publications used low speed incompressible flow.
- Wind Tunnel shape classification – The publications were Closed Loop tunnels.
- Wind Tunnel purpose – The publications were designed as Boundary Layer tunnels.

The Numerical Model data of these publications could not directly be used to validate the performance of the various components within the current Design. However, these sources (Calautit [31] and Moonen [32]) provided a basis for the meshing procedures of completely rendered wind tunnel geometries. The sources provided the geometric volume and associated cell count for each component in the respective geometries. These cell-to-volume ratios were used, in conjunction with the relative processing capabilities available to each model, to estimate the mesh cell count for this Design.

7.1 Meshing (ICEM)

The program chosen for the Meshing Procedure was the ANSYS® 14.5 ICEM CFD™. The meshing program was set to operate in Multiple Processing mode (as opposed to Serial Processor) with 2 processors (Intel Core 2 Duo) available on the ICEM Operating Computer. The maximum number of tetrahedral cells available to render the mesh = 1 500 000 cells.

7.1.1 Mesh Cell Size Estimation

The mesh used in the current WT Design contained 466215 cells. This amount was far less than the upper limit capabilities of the meshing computer, but the decision was made to reserve enough cells for the eventual inclusion of the Mixing Chamber mesh. The amount of cells used in the WT mesh, although appearing to be sparse, was comparable to the mesh counts of the published sources (Calautit [31] and Moonen [32]). These cell-to-volume ratios were presented in Table 5.

The Moonen [32] wind tunnel was significantly larger than the current Design, with the Test Section dimensions alone including $L \times W \times H = 25 \times 10 \times 7$ m^3. Put into perspective, the length and maximum diameter of the current Design was L = 9.665 m and $Ø_{MAX}$ =1.25 m. The comparison was made between the complete mesh of the current Design and isolated Test Section mesh of the Moonen [32] tunnel; as the Test Section had the strictest mesh setting. The Calautit [31] wind tunnel was more comparable in dimension to the current Design, with Test Section dimensions including $L \times W \times H = 1 \times 0.5 \times 0.5$ m^3. The Calautit [31] mesh data listed in Table 5 excluded the Diffuser and Turning Corner portions. It instead focused exclusively on the Test Section, Contraction, and constant Ø ducts. This decision was due to the Calautit [31] focus on its design-specific variable geometry of Diffusers and Turning Corners.

Table 5. Comparison of Cell sizes for selected components from Moonen [32] and Calautit [31]

	Cell Count	Approx. Volume [m^3]	Average Cells/m^3
Moonen [32] Test Section only	371586	1750	212
Calautit [31] Selected Geometry (excl. Turning Corners and Diffuser)	1738195	4.405	394596
Current Design Archetype (x2, symmetry)	932430	5.296	176063

The Calautit [31] mesh had more than twice the cell density of the current Design. The Moonen [32] mesh however, was considerably less populated with cells than either the current Design or the Calautit [31] mesh. If the Calautit [31] mesh was used as the benchmark, the current Design (45% Cells/m^3) far outperformed the Moonen [32] mesh resolution (0.05% Cells/m^3). The reason for the Moonen [32] sparse mesh, which could also be extended to the explanation for the current Design mesh, was the total cell count available due to the meshing computer capacity. The Moonen [32] geometry was meshed using a single processor computer (3 GHz Pentium 4) with 440 MB RAM. The Calautit [31] wind tunnel, on the other hand, was meshed with a parallel processor computer (2.1 GHz Xeon) with 16 GB DDR2 RAM. The Calautit [31] computing capacity allowed for a finer mesh to be utilized.

Although the Moonen [32] mesh had a considerably lower cell concentration, it still rendered the required 1st layer cell size in order to achieve y+ = 250. The lower Velocity (lower Re) of the Moonen [32] flow allowed for a much larger cell size for the 1st layer (Δy). This was not the case with current Design, as the Velocity (Re) was too large for the 1st layer cell sizes to conform to y+ requirements. This analysis of WT 1st Layer Cell Size, with regards to y+ conformance, was included in Appx. J.1. Leap [33] addressed this particular scenario, large applications with high Re (eg. a ship hull), resulting in y+ > 10000. In these instances, it was impractical to resolve the boundary layer. Focus was instead placed on the inflation layers; in this case the 'Tunnel wall flow' to 'Tunnel core flow' cell size inflation. The focus of the Design mesh cells was shifted from boundary layer flow (near- wall) to shear stresses (potential core). The Turbulence Model followed respectively; a robust option that handled y+ non-conformance.

7.1.2 WT Mesh

The mesh was generated for the symmetrically cut 3-D model of the WT, as depicted in Figure 15. The surfaces of the model were defined (labelled in Figure 15), and meshed with cell sizes corresponding to 3 size classifications (viz. Half Size, Archetype, and Double Size). These 3 cell size classes served as the variants for the Mesh Sensitivity Analysis (Section 7.3.1); with the Archetype cell size determined to be the best fit. The mesh was generated with Unstructured Tetra/Mixed cells using the Robust (Octree) Method. The surface mesh specifications for the WT, including the cell sizes for all 3 Mesh Sensitivity Analysis variants, were included in Appx. K.1.

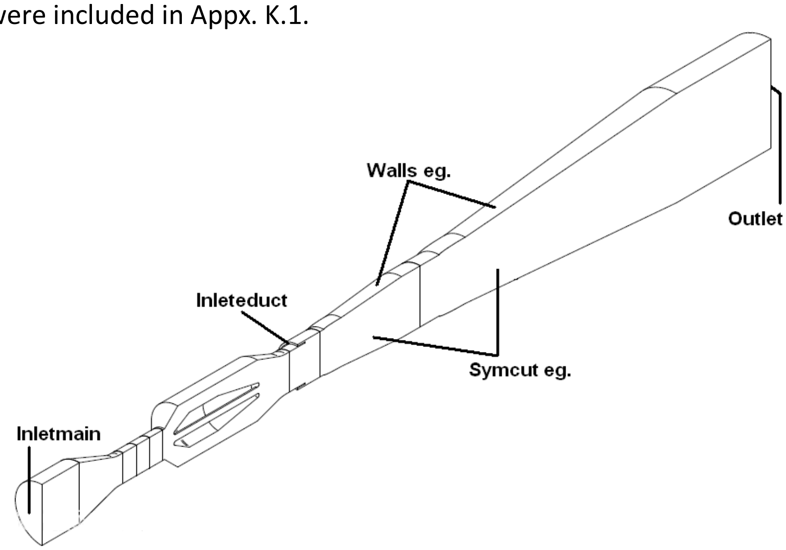

Figure 15. Isometric View of Wind Tunnel (symmetrical cut), including labels

7.2 Solution (Fluent)

The program chosen for the Solving Procedure was ANSYS® 14.5 FLUENT ®. The solver was set to operate in Parallel Processing mode with 4 processors available on the Fluent operating computer (Intel Core i7 8GB RAM). The Solver computer had a larger processing capacity than the Meshing Computer.

7.2.1 Solver Settings

The Fluent Solver was specified to best represent the flow scenario within the WT. It had to allow for consistent compressible flow throughout the required run time = 5 min. The Main Inlet conditions (P_0 and T_0) were varied to obtain the Test Section objectives (M0.7 and T = 219 K); using the mass flow rate calculated in the Analytical Model ($\dot{m}$ = 22.16 kg/s). The Solver Settings (Solver Parameters, Convergence Criteria, and Turbulence Modelling) were briefly listed in this section. The definitions of, and reasoning behind, the setting selections were included in Appx. L.1.

- Solver Parameters

Density based, Coupled (with rudimentary Under-Relaxation factors and Artificial Time Step), Steady State (Pseudo Steady Defined by Courant Number), Implicit Solver (Cr ≤ 5). Compressible Boundary Types (Pressure Inlet and Pressure Outlet) with Operating Pressure = 0 Pa.

- Convergence Criteria

The quantitative relevance of the Numerical Solution was based on the ability to achieve the Analytical Model $\dot{m}$ balance (monitored as $\dot{m}_{WT\text{-}IN} + \dot{m}_{EDUCT} = \dot{m}_{OUT}$). The quality of the solution was assessed by the RMS residuals of the flow property equations (RMS Residuals = 0.001).

- Turbulence Modelling

The WT flow had a high Re, was compressible at points (prior to OTS), and recirculation was expected to occur within the OTS and Diffusers. It was due to these combined effects that the Realizable k_{TKE} - ε_{TDR} Turbulence Model (defined by T.I. and $Ø_H$) was included in the simulation.

7.2.2 Solving Outline

The mesh was read into the Fluent Solver; with the previously defined surfaces. The simulation was performed in 2 parts: 1st Order, followed by 2nd Order Solution Methods. The 1st Order Solution was performed until residual convergence (Qualitative convergence). However, the Global mass flow balance ($\dot{m}_{IN} = \dot{m}_{OUT}$) at this point was not accurate enough; producing an imbalance of $\Delta\dot{m}$ = 0.65 kg/s. This was due to the 1st Order Methods exaggerating the effects of the Turbulence Model at the expense of $\dot{m}$ tracking. The RMS converged 1st Order solution was then refined using 2nd Order Methods until the Global $\dot{m}$ balance converged to within 3 orders of magnitude (Quantitative convergence). The 2nd Order Solution did not converge to residual requirements, but was stopped after 15000 iterations.

The Mass Flow Rate Balance at the end point of 2nd Order iterations was calculated as:

$\dot{m}_{MAIN}$ + $\dot{m}_{EDUCT}$ = $\dot{m}_{OUT}$

11.01 + 2.55 = 13.52 → imbalance ($\Delta\dot{m}$) = 0.04 kg/s Inflow

This presented the desired quantitative imbalance of ≤ 3 orders of magnitude ($\frac{\Delta\dot{m}}{\dot{m}_{OUT}} = \frac{0.04}{13.52}$ ≈ 0.003).

The values of the various RMS residuals at 2nd Order 'economic' convergence were:

Continuity = 1.674 x10^{-02} Energy = 1.818 x10^{-02}

X- Velocity = 1.544 x10^{-03} Y- Velocity = 1.045 x10^{-03} Z- Velocity = 8.037 x10^{-04}

k (TKE) = 3.850 x10^{-05} ε (TDR) = 4.798 x10^{-05}

The RMS errors for velocity (x, y, z) and turbulent components (k, ε) did approximate the convergence criteria (0.001, i.e. 1x 10^{-03}), but the Continuity and Energy RMS errors remained comparatively large. This was due to the refined 2nd Order interpretation of compressible flow at the OTS and Diffusers. The resolution of the recirculation was attempted with stricter standards with regards to the $\dot{m}$ and energy balances. The confirmation of a suitable solution was limited to the Quantitative measure. The detailed solving procedure, including the convergence criteria analysis, was included in Appx. L.2. Before the 2nd Order Solution was analysed, a Sensitivity Analysis of the Mesh Sizes and Convergence Criteria was performed in the next section (to substantiate the decision on the Archetype Mesh and Criteria).

7.3 Sensitivity Analysis

A Sensitivity Analysis was performed in 2 parts: Mesh variants, and Convergence Criteria variants. These parts identified the respective influence of the Meshing Procedure steps and Solving Procedure steps on the final Numerical Model result. There were 3 Mesh variants created and tested; by scaling the cell count in accordance with the Archetype Mesh. There were also 3 Convergence Criteria variants tested on the Archetype Mesh; by scaling the Continuity and Energy residual values. The plan layout of the Sensitivity Analysis was illustrated in Figure 16.

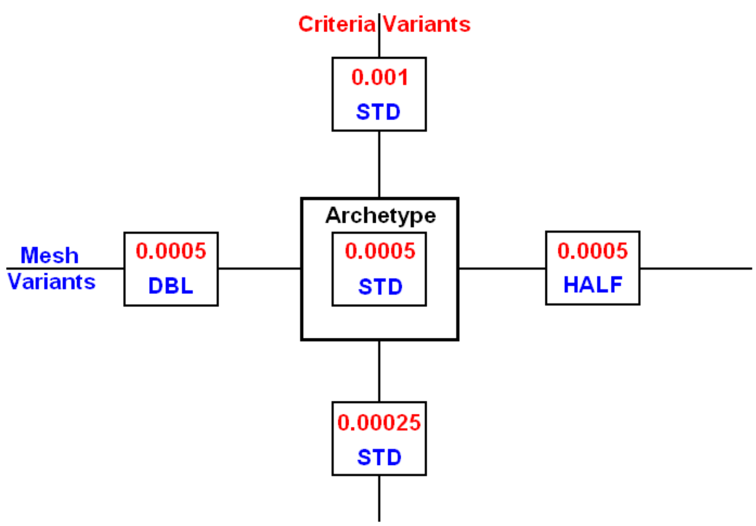

Figure 16. Layout of Sensitivity Analysis; Mesh Types (BLUE) on X-axis, Criteria Types (RED) on Y-axis

The Sensitivity Analysis variants stemmed from the Archetype Model. The analysis evaluated the impact of changing: the mesh cell size (X-axis in Figure 16: Double, Standard, and Half), and the RMS criteria (Y-axis in Figure 16: 0.00025, 0.0005, and 0.001). All variant simulations were accomplished using 1st Order Solution Methods; due to guaranteed RMS convergence. Having an RMS converged 1st Order Solution under the same governing inputs provided a more reliable datum than an 'economically' converged 2nd Order Solution. The results were accessed through Mass-Weighted Averages (MWA) taken across 'Ghost planes' at the 16 Key Point locations (corresponding to the Analytical Model). The Sensitivity Analysis was performed by plotting the Stagnation Pressure (P_0) and Mass flow Rate ($\dot{m}$) for each variant, along the WT length. The detailed analyses, including the plots and discussions, were included in Appx. M.2 and Appx. M.3. The important findings from the analyses were listed in this section.

7.3.1 Mesh Sensitivity Analysis (Appx. M.2)

- The MWA (Mass-Weighted Average) results summated the complete flow through each plane; including perpendicular Velocity components, recirculation, and the unresolved near-wall flow. It prevented asymptotic behaviour between the variants. Mesh Independence could not be attained.
- There was a discernible $\dot{m}$ inconsistency in all the variants at the OTS. This was due to the retentive nature of the large OTS chamber, and it was expected to have an effect on the Global $\dot{m}$ balance.
- The Archetype Mesh, in comparison to the other variants, adequately captured the complex geometry components. It correctly interpreted the P_0 variation along the Tunnel (including the influence of the Eductor on the Main Flow), and provided more accurate $\dot{m}$ tracking of the flow.

The Sensitivity Analysis was not interpreted in terms of an ideal asymptotic result (Richardson Extrapolation) and the respective deviation (Grid Convergence Index); as recommended by NASA [34]. The analysis was instead a trend confirmation of expected macro behaviour ($\dot{m}$ tracking and P_0 losses) across the mesh variants. The recourse included in the WT Numerical Model was the continuous (Dynamic) Gradient Adaptation of the Mesh. This decision utilized the advantages of the Archetype Mesh, whilst refining the cells within the problematic segments. Carpenter [52] described the Grid Adaptation technique as an improvement to Solution accuracy in coarse meshes; as was the case in this Model. The mechanism ensured equidistributional error over the grid points, and rendered the mesh independent (i.e. an asymptotic Sensitivity Analysis was moot). The Archetype Mesh (+ Grid Adaptation) was capable of resolving the flow and provided an acceptable grid for the WT Numerical Model.

7.3.2 Convergence Sensitivity Analysis (Appx. M.3)

This Convergence Criteria analysis was performed to demonstrate the error in simulating at the Archetype RMS criteria specifications. The Numerical Model refined the Energy and Continuity residuals further than the 0.001 requirement suggested by Fluent [35].

- The analysis was performed on a consistent mesh with increasing levels of RMS accuracy. The MWA shortcomings that affected the Mesh Sensitivity Analysis did not affect the Convergence Criteria Sensitivity Analysis; which displayed asymptotic behaviour.
- The OTS resulted in a discernible $\dot{m}$ inconsistency for all variants (as it did for the Mesh Sensitivity variants). This location signalled the subsequent abandonment of asymptotic behaviour.
- The most prominent observation from the analysis was the diminishing return in refining the RMS criteria beyond the Archetype value. The Archetype RMS produced a maximum P_0 error, compared to the strictest RMS variant, of < 3 orders of magnitude.

The Convergence Criteria Sensitivity Analysis justified the selection of the 0.0005 RMS value (Archetype Criteria). This selection was based solely on the accuracy of the P_0 assessment, and not necessarily $\dot{m}$ tracking. The $\dot{m}$ imbalances were addressed by refining the simulation with 2nd Order Solution Methods. The Archetype Residual produced an adequate prediction of the WT 1-D flow path.

7.4 Solution Analysis

The 2nd Order 'economically converged' Solution of the Archetype was assessed by taking the Mass Weighted Average (MWA) values of selected fluid properties at the 16 Key Point locations (from Figure 14). The results of the Numerical Model could then be compared to the respective values of the Analytical Model; to achieve a triangulated solution for the WT Inlet requirements. The 2nd Order Solution was, as described in Section 7.2.2, an 'economically' converged solution. The Solution did not converge to the RMS criteria set, but was stopped at 15000 2nd Order iterations (beyond 1st Order RMS convergence). The Design-specific geometry features (OTS, Eductor, and consecutive Diffusers), when simulated with high speed compressible subsonic flow, produced conditions that were difficult to fully resolve in a cell-to-cell analysis (RMS convergence). These flow conditions (and irregularities) had to be tolerated as part of the 'economic' convergence. The solution was assessed on the Global $\dot{m}$ balance ($\sum\dot{m}_{IN} = \dot{m}_{OUT}$) accuracy, to assess Bulk Convergence, as opposed to cell-to-cell $\dot{m}$ balance.

Fluid properties at the 16 Key Point locations were listed in Table 6, with parameters including: Distance along the Tunnel length (X), Stagnation Pressure (P_0), Static Pressure (P), Mach number (M), Static Temperature (T), and Mass Flow Rate ($\dot{m}$). The $\dot{m}$ values in Table 6 were doubled to account for the symmetric surface (Symcut); this allowed for direct comparison to the Analytical Model values (Table 4). The 2nd Order Solution resulted in a set of WT inlet/outlet requirements that correlated well with the Analytical Model. It was important to note here that, due to geometrical considerations put into effect for the benefit of the Numerical Model, the Eductor P_0 was inflated to $P_{0\ EDUCT}$ = 92000 Pa (to overcome the nominal intermediate length not included in the Analytical Model). Table 6 displayed the Design objectives in boxed cells. The Inlet conditions were specified to achieve the PRS objectives: M_{TS} = 0.70 (Objective = 0.7), T_{TS} = 218.5 (Objective = 219 K), and P_{EXIT} = 83000 Pa (Objective = 83000 Pa).

Table 6. Selected Results from Wind Tunnel Numerical Model (Objectives Boxed)

Point Number	X [mm]	P_0 [Pa]	P [Pa]	Mach	T [K]	$\dot{m}$(x2)[kg/s]
(Main In) 1	0.0	98500	97199	0.14	239.1	22.02
2	250.0	98464	97287	0.13	239.2	22.01
3	250.0	98464	97287	0.13	239.2	22.01
4	500.0	98453	97161	0.14	239.1	22.02
5	1025.0	97943	72180	0.68	220.0	21.99
(Test Section) 6	1625.0	96555	69448	0.70	218.5	21.99
7	3136.5	84316	77969	0.33	234.7	21.95
8	3233.5	84018	75818	0.39	233.1	21.98
9	3488.5	83839	75708	0.38	233.1	21.99
(Eductor In)9ed	3383.5	92000	74932	0.54	273.4	5.09
(Join) 10	3488.5	84315	76084	0.38	242.1	27.09
11	3733.5	83910	76302	0.37	242.6	27.10
12	4762.5	83630	81261	0.20	247.4	27.09
13	5262.5	83566	81340	0.20	247.5	27.10
14	8405.5	83353	82923	0.08	249.0	27.10
15	9655.5	83303	83000	0.07	249.1	27.05
(Outlet) 16	9655.5	83303	83000	0.07	249.1	27.05

The $\dot{m}$ column in Table 6 allowed for the monitoring of fluid continuity at each of the 16 Key Point locations. The Maximum error in $\dot{m}$ consistency (measured as percentage deviation from Main Inlet, i.e. $\frac{\|\dot{m}_1-\dot{m}_x\|}{\dot{m}_1}\times 100$, and subsequently adjusted from the Eductor onwards) occurred at the Collector lip, aft of the Test Section (Key Point 7). This Maximum $\dot{m}$ error was 0.33%; which was relatively insignificant considering the recirculation and inherent holding capacity of the OTS. This substantiated the Bulk

Convergence accuracy of the 2nd Order Solution in attaining a sustainable Steady solution (a 'still' frame). Interpreting the P_0 decline along the Tunnel length, the bulk of the loss occurred across the OTS. The component accounted for 80.53% of Total P_0 loss. This was the expected behaviour; as per the Analytical Model. Even though the frictional losses (along the intermediate lengths) were typically not as significant as the complex geometry component losses, the particular intermediate length between the Nozzle (Key Point 5) and OTS Inlet (Key Point 6) presented a noticeable P_0 loss. This segment contributed to 9.14% of the Total P_0 loss. Throughout this length, the flow reached the Maximum Velocity within the WT; MWA of ±M0.7. At this Velocity, the frictional loss ($f_X\{M\}$) was at its peak. The purpose of this length, apart from Test Section modularity, was to develop a potential core profile prior to entering the OTS. This intermediate length (and the unique associated loss) was indispensable.

The complete analyses of the Numerical Model results, and the comparisons with the Analytical Model, were included in Appx. N.1 and Appx. N.3 respectively. The analyses also included the Contour Plot investigation of the P_0 and M variation along the Tunnel length (Appx. N.2). With the express purpose of the Numerical Model being the triangulation of the WT Inlet conditions (for the development of the Mixing Chamber), the remainder of the analysis in this section focused solely on the Design Point objective comparisons. Table 7 listed the objective conditions from the Analytical Model (Table 4) and Numerical Model (Table 6); revealing the corresponding deviation percentages ($\frac{X_{MATH} - X_{CFD}}{X_{MATH}} \times 100$). The percentage deviation was presented with the negative/positive sign convention; this implied the respective over/underestimation of the Numerical Solution from the Analytical Model 'ideal'.

Table 7. Comparison of Results from Analytical Model and Numerical Model

	Analytical Model	Numerical Model	% Deviation
	Test Section Conditions		
M	0.70	0.70	0.85
V [m/s]	209.3	207.7	0.78
T [K]	218.2	218.5	-0.14
	Main Inlet Requirements		
P_0 [Pa]	98400	98500	-0.10
$\dot{m}$ [kg/s]	22.16	22.02	0.61
T_0 [K]	240.0	240.0	0
	Eductor Inlet Requirements		
P_0 [Pa]	91500	92000	-0.55
$\dot{m}$ [kg/s]	5.15	5.09	1.11
T_0 [K]	290.0	290.0	0
	Outlet Conditions		
P [Pa]	83030	83000	0.04
$\dot{m}$ [kg/s]	27.30	27.05	0.93
T_0 [K]	249.4	249.4	0.01

- **Test Section**

The results revealed that T replicated the Analytical Model and met the Design objective (≤ 219 K). The 0.14 % deviation represented ΔT = 0.3 K. The only relatively significant deviation in the Test Section conditions arose from M; presenting a 0.85 % deviation (ΔM = 0.006) between the Numerical and

Analytical results. This was due to the slight over-specification of the Analytical Model; where the model was developed by varying $P_{0\ MAIN}$ in pragmatic increments to achieve $M_{TS} \geq 0.7$. The Numerical Model provided a more accurate account, where the Velocity was much closer to the objective (207.7 m/s).

- **Main Inlet**

The results showed that despite the Numerical Model requiring a slightly higher P_0 (+100 Pa), there was a lower $\dot{m}$ required in the Tunnel (-0.14 kg/s). It implied that there was a higher P_0 loss interpreted within the Tunnel than what was budgeted for in the Analytical Model. The increased $P_{0\ MAIN}$ was due to the Analytical Model underestimating the losses associated with the OTS and the intermediate length prior to the OTS.

- **Eductor**

According to Table 7, the largest errors in both P_0 and $\dot{m}$ arose in the Eductor specification. This was expected from the outset, as the Eductor served as a placeholder for Further Work (Appx. Q.3.2). The Eductor was only provided with a diameter in the Analytical Model. The Numerical Model required a preceding intermediate length; to allow this secondary flow to develop a 1-D profile. To achieve the corresponding $\dot{m}_{EDUCT}$ of the Analytical Model, the Numerical Model had to be specified with a higher $P_{0\ EDUCT}$. This was necessary to overcome the friction loss of the respective nominal intermediate length.

With the exception of the Eductor, and its subsequent contribution to the Outlet flow, the results of the Numerical Model conformed to the expectations of the Analytical Model. The largest WT model comparison error only registered 1.11 % ($\dot{m}_{EDUCT}$ in Table 7). The Numerical Model results could be used to specify the Design requirements for the Mixing Chamber. The comparison also validated the Numerical Modelling approach of the WT. The Solver Settings, Archetype Mesh, and Convergence Criteria produced a solution that held validity with regards to the bulk flow objectives.

7.5 WT Numerical Model Conclusions

The conclusions of the WT Design were based on the Numerical Model results; the Analytical Model served as the validation for the flow behaviour. Proceeding to the design of the Mixing Chamber, the WT Model was used to provide the respective Design objectives (since the Wind Tunnel Inlet = Mixing Chamber Outlet). The Design Point WT Inlet requirements were triangulated with high confidence as:

$Ø_{WT\text{-}IN}$ = 0.7 m, P_0 = 98500 Pa, T_0 = 240 K, $\dot{m}$ = 22 kg/s.

The major findings of the WT modelling approach, which played a role in the Mixing Chamber Numerical Model (Section 13), were summarized as:

- The Archetype Mesh cell sizing, in conjunction with Dynamic Gradient Mesh Adaptation, provided an adequate solution. The Archetype Residual (0.0005) provided the best return when compared to the computational cost of further residual refinement.
- The 1st Order Turbulence Model emphasized the turbulent and diffusive flow behaviour, at the expense of accurately tracking $\dot{m}$ and maintaining continuity. This occurrence necessitated the refinement to 2nd Order methods in order to reduce Global $\dot{m}$ imbalance. This particular behaviour was noted, and leveraged as a tool in the development of the Mixing Chamber (Section 13.2.1).

8 Air Supply Mechanism Design Study

The Mixing Chamber had to achieve the WT Inlet conditions from a specified set of Supply Devices. The role of the Mixing Chamber was described by 2 distinct mechanisms: The Air Supply mechanism to deliver the flow rate ($\dot{m}$ = 22kg/s at P_0 = 98500 Pa), and the Cooling Mechanism to achieve the Altitude Temperature (T_0 = 240 K). The process of mechanism selection involved assessing the readily available options (avoiding custom manufacture) against the Design needs, equipment costs, and practicality of implementation. It was important to note that in the evaluation of Mechanism options, the associated processes (for Air Supply and Cooling) were assumed to be Isentropic. This provided a common frame of reference for the varying implementations. Upon selection of the Mechanisms, the development proceeded with a 'realistic' loss inclusive model.

8.1 Air Supply Mechanism Evaluation

The Air Supply Mechanism evaluation process entailed:

- Design Point Optimization – Determining the relationship between P_0 and $\dot{m}$ of the Supply Mechanism; and identifying the optimum delivery range.
- Available Air Supply Options – Listing the readily available (not purpose-made) options capable of meeting the Supply Mechanism requirements.
- Best Fit Cost Analysis – Estimating the costs of the options.

Design Point Optimization

As stated in Section 7.5, the Design Point requirement was to deliver $\dot{m}$ = 22kg/s of air at P_0 = 98500 Pa to the WT Inlet. If this Design Point were to be compromised, by the choice of Air Supply Mechanism, the Test Section Mach number would be reduced (directly affecting Design quality). This parameter optimization (P_0, $\dot{m}$ vs. Mach) was attached in Appx. B.1, with the major findings presented here. The optimization revealed that reduction of the Test Section Mach number from M0.7 to M0.5 resulted in a saving of P_0 = 7250 Pa and $\dot{m}$ = 4.75 kg/s. The $\dot{m}$ reduction was readily identified as ± 22%. The P_0 reduction, when interpreted as the respective Pressure increase from ambient (i.e. $P_{JUMP} = P_0 - 83000$ Pa), was identified as ±47%. This represented a significant reduction in overall Supply Mechanism requirements; more so with respect to P_{JUMP} than $\dot{m}$. The $\dot{m}$ capability did not present an immediate concern; as multiple Mechanisms could be connected in parallel to deliver a combined effort. The P_0 capability, however, presented a considerable hurdle in Mechanism applicability.

The Mechanism types had a limited range of applicable Pressure Ratio; as demonstrated in the compressor maps of Harmadipedia [36]. The typical sequence, with increasing P_0 capability (and decreasing $\dot{m}$ capability), was suggested as: Axial → Centrifugal → Rotary → Reciprocating. It was possible that, by reducing the P_{JUMP}, an entirely different type of Mechanism could be implemented (Axial instead of Centrifugal). This could have a significant impact on the cost and operating concerns. It should be pointed out however, that lowering Mach number (from M0.7 to M0.5) at the Design Point Altitude (T_{TS} = 219 K) required additional Cooling ($T_{0\ IN}$ = 230.5 K instead of 240 K). Whilst this was not an immediate concern in the Air Supply Mechanism evaluation, it did present a considerable consequence on the Cooling Mechanism evaluation. It was shown in Section 10 that the 'Costs vs. Capability balance' of the Cooling Mechanism far outweighed that of the Air Supply Mechanism.

It was in the best interest of an economically viable Design to increase $T_{0\ IN}$ as much as possible, and that implied a higher Test Section Mach number. The Design Point was retained at M_{TS} = 0.7 at $T_{0\ IN}$ = 240 K; requiring the Air Supply Mechanism to deliver $\dot{m}$ = 22kg/s at P_0 = 98500 Pa.

Air Supply Mechanism Options

The applicable options for Air Supply Mechanism were weighed against the following requirements:

- Pressure (98500 Pa) → P_{JUMP} = 15500 Pa = 2.25 psi
  → Pressure Ratio (P.R.) = $\frac{P_0}{P_{Ambient}} = \frac{98500}{83000}$ = 1.19
- $\dot{m}$ (22kg/s) → Flow Rate ($\dot{\forall}$) = $\frac{\dot{m}}{\rho_1} = \frac{22}{1.418}$ = 15.52 m^3/s = 32874.42 CFM
- Flow Integrity → Continuous = 5 Minutes

Multiple units of dimensions were listed; so as to readily identify and compare available machinery. This evaluation served to identify 2 possible solutions (Investigative and Back-Up). These 2 solutions were then compared through an encompassing cost analysis to produce the best option for implementation. The applicable Air Supply Mechanism options were briefly listed here, with the detailed descriptions of the Mechanism options included in Appx. O.1.1.

1. Axial Fan - ≥ 2x required $\dot{\forall}$, ≤ 1/10 required P_{JUMP}
2. Centrifugal Fan - matched required $\dot{\forall}$, ≥ 10x required P_{JUMP}
3. Reciprocating Compressor - incomparably low $\dot{\forall}$, ≥ 77x required P_{JUMP}
4. Rotary Compressor - ≤ 13x required $\dot{\forall}$, ≥ 55x required P_{JUMP}
5. High Pressure Air Cylinder - modular delivery, capable of meeting requirements

The options were compared using a House of Quality weighted assessment. The assessment parameters and performance characteristics of the Mechanism options were included in Appx. O.1.2. The House of Quality was presented in Figure 17; with the Key symbol (√) allocating weight to the rating.

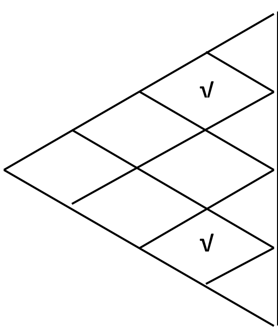

Key √ = ½	Rating [/5]	Axial Fan	Centrifugal Fan	Reciprocating Compressor	Rotary Screw Compressor	Air Cylinder (Bottled Gas)
Flow Rate	3	√√	√√	0	√	√√
Pressure	5	0	√√	√√	√√	√√
Continuous	4	√√	√√	0	√	√√
Practicality	3	√	√√	0	√	√
	15	8.5	**15**	5	10	**13.5**

Figure 17. House of Quality to determine the best 2 fits for Air Supply Mechanism (Key √ = ½ POINT) identifying the Centrifugal and Air Cylinder as best options

Best Fit Cost Analysis

The 2 best fits were identified in Figure 17 as: the Centrifugal Fan (rating of 15/15) and the High Pressure Air Cylinder (rating of 13.5/15). These options were then assessed according to the cost requirements to determine the order of preference (Investigative and Back-Up). The detailed cost breakdown and assessment were included in Appx. O.1.3; with the major findings listed here.

- Centrifugal Fan Cost per run (1 hr) = R 141.77
  The largest component of the test run cost was the Electricity Cost (≈ 89% of total cost).
- Air Cylinder Cost per run (13.6 min) = R 288.46
  The largest cost component of the test run cost was the Refill Cost (98% of total cost).

Comparing the 'cost per run' of the 2 best fits, the importance of cost effectiveness in this Design (as it pertained to the PRS) necessitated the choice of the Centrifugal Fan.

Air Supply Mechanism: **Centrifugal Fan, Howden Donkin, Series HBC-M Size 1250(E) 1.0**

Despite the added complications of holding and operating the machinery (compressor), the running cost advantage made this prospect much more attractive. There were 2 cost parameters that could possibly reverse the choice: Electricity Cost (R 126.14/hr) and Air Refill Cost (R 12.63/Lt). If these costs changed significantly enough (relative to each other) from the 2013 quotes, the responsibility (and complications thereof) of holding and operating the Centrifugal Fan might justify opting for the Air Cylinder. In the next subsection (Section 8.2), the second component of the Mixing Chamber was addressed; cooling the dynamic Air Supply to the required Design Point T_0.

8.2 Cooling Mechanism Evaluation

The Cooling Mechanism evaluation process entailed:

- Cooling Mechanism Requirements – Identifying the Temperature range needed to perform 10 altitudes (up to 35000 ft), and identifying the Heat Transfer Rate needed in the Mixing Chamber.
- Cooling Mechanism Options – Listing the readily available options capable of meeting the Cooling requirements.
- Best Fit Cost Analysis – Estimating the costs of the options.

Cooling Mechanism Requirements

A Primary Requirement (Section 3.1) was the ability to test the Engine at ≥ 10 altitudes; up to the Design Point Altitude. The applicable Test Section T range was [218.8 K $_{\text{(Design Point 35000 ft)}}$ – 276.96 K $_{\text{(JHB ISA 5751 ft)}}$]. At Design Point, the Cooling Mechanism had to cool the Air Supply to $T_{0\ IN}$ = 240K. It effectively had to reduce the combined Temperatures of the JHB ISA Atmospheric air (5 °C) and the heat from the Centrifugal Fan (20°C from Appx. O.1.3); ultimately cooling from 298.15K to 240K (ΔT = 58.15K). This cooling was described by the 'Rate of Heat Transfer' ($\dot{Q}$) equation, defined in Reynolds [23] as:

$$\dot{Q} = \dot{m} \cdot C_P \cdot (\Delta T) \quad \text{… (28)}$$

$$= 22 \cdot 1007 \cdot (58.15) \quad = 1288.26 \text{ kW}$$

With these basic requirements ($T_{0\ MIN}$ = 240K, ΔT = 58.15K and $\dot{Q}$ = 1288.26 kW), a preliminary analysis of the possible Cooling Mechanism options was attempted.

Cooling Mechanism Options

The applicable options for Cooling were weighed against the following requirements:

- Absolute Temperature → T = 240K = -33.15 °C
- Cooling Capacity → $\dot{Q}$ = 1288.26 kW

The applicable Cooling Mechanism options were briefly listed here, with the detailed descriptions of the mechanism options included in Appx. O.2.1.

1. Once-off Sublimation (Dry Ice) - capable of T, incapable of $\dot{Q}$, changed air composition
2. Vapor Cycle - incapable of T (only -7 °C), capable of $\dot{Q}$
3. Supersonic Expansion - experimental concept capable of meeting requirements

The options were compared using a House of Quality weighted assessment, presented in Figure 18; the details of which were included in Appx. O.2.2. The performance characteristics of the Experimental Supersonic Expansion option were based on the outcome of the investigation in Section 9.2. The 2 best fits were identified in Figure 18 as: Supersonic Expansion (rating of 10.5/15) and Vapor Cycle (rating of 9.5/15). It was noted here that the Vapor Cycle did not accomplish the required Absolute Temperature (cooling only to 265.15 K). It served only as a contingency (Back-Up) to the preferred Supersonic Expansion Concept (Investigative). The remainder of the Cooling Mechanism evaluation was continued in Section 10; upon the development of the Supersonic Expansion Cooling Concept.

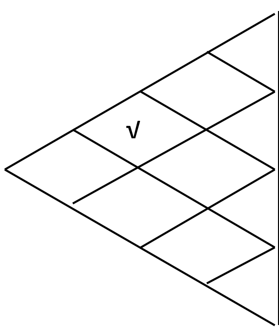

Key √ = ½	Rating [/5]	Once-off Sublimation	Vapor Cycle	Supersonic Expansion (Experimental)
Absolute Temperature	4	√√	0	√√
Dissipation Rate	3	0	√√	√
Air Quality	5	0	√√	√√
Practicality	3	√√	√	0
	15	7	**9.5**	**10.5**

Figure 18. House of Quality to determine the best 2 fits for Cooling Mechanism (Key √ = ½ POINT) identifying Supersonic Expansion (Experimental) and Vapor Cycle as best options

9 Supersonic Expansion Cooling (SSEC) Concept

The Investigative solution of Supersonic Expansion Cooling (SSEC) provided the best approach to achieving the required Altitude Temperature, whilst preserving the representative performance of the Test Piece Engine. This SSEC concept represented the research aspect of the Project. The concept was adapted from the large scale application of the Dera [7] Pyestock Cell 3 Supersonic Facility; the Altitude Temperature simulation was accomplished using a large cold air expansion turbine.

In its simplest approach, air at ambient Stagnation Temperature and high Stagnation Pressure was rapidly expanded to achieve ambient Stagnation Pressure air at low Static Temperature. This expanded air was then mixed with the WT Air Supply to achieve the Design Point Inlet flow (P_0, $\dot{m}$, and T_0).

9.1 SSEC Concept Literature Review

The preliminary literature analysis in this section highlighted the fundamental mechanisms used to develop the isentropic SSEC model, including:

- The rudimentary Thermodynamic balance involved in the heat exchange mechanism.
- Identification of the best Supersonic regime, upon expansion, for cooling purposes.

Thermodynamics (Ideal Gas)

The typical mechanism of the Vapor Cycle involved the conduction heat exchange between segregated flow streams. The method proposed for the SSEC concept enabled the direct contact, and inevitable mixing, of the 'Hot' and 'Cold' streams. The 'Cold' Supersonic stream mixed with the 'Hot' Air Supply flow; to produce a resultant air stream of combined flow at an intermediate Temperature. Figure 19 showed the Mixing Chamber with a closer resemblance to the scale and orientation of the SSEC concept. The figure showed the injection of the secondary Supersonic stream (Flow 2) into the primary Centrifugal moving stream (Flow 1); to produce the Resultant stream (Flow 3). The Isentropic Heat Exchange for the flow balance depicted in Figure 19 was calculated using the Energy Equation (eqn. 4):

$$\dot{m}_1\left(C_P T_1 + \frac{V_1{}^2}{2}\right) + \dot{m}_2\left(C_P T_2 + \frac{V_2{}^2}{2}\right) = \dot{m}_3\left(C_P T_3 + \frac{V_3{}^2}{2}\right) \quad \ldots (29)$$

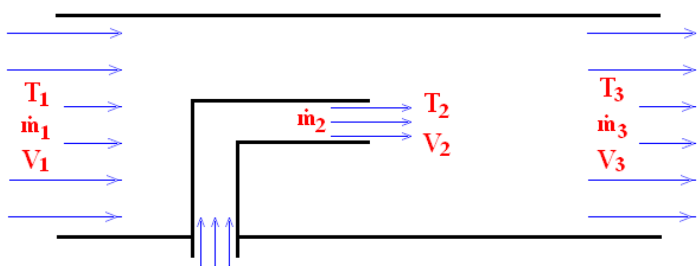

Figure 19. Direct Contact mixing of Primary flow (Centrifugal supply) and Secondary flow (Supersonic supply) to produce the Resultant flow ($V_3 = V_1$, $\dot{m}_3 = \dot{m}_1 + \dot{m}_2$)

The Energy Equation (eqn. 4) was previously only used for isentropic models. Even in the development of the WT Analytical Model, the Energy Equation was excluded from the calculation set due to the P_0 losses along the Tunnel length. The various Key Point locations along the WT length were related to each other using the Continuity Equation (eqn. 2) and the Stagnation Temperature Equation (eqn. 12); with the assumption of constant T_0 = 240 K. The only exception to this calculation set was the Eductor Device which, in its preliminary implementation, did not necessarily affect the WT Design Point objectives. For the development of the SSEC Concept in Figure 19, the assumption of constant T_0 was not valid in the Mixing mechanism segment of the flow field. Instead, the Key Point locations associated with the flow balance had to be related to each other using the Energy Equation (in conjunction with the Continuity Equation). Equation 29 however, could no longer be used in its isentropic form; due to the P_0 loss associated with the sudden expansion of the Supersonic stream (Flow 2).

This particular scenario of sudden expansion loss, flow emitting as a jet into a large tank, was described in Munson [19] to dissipate the entire Kinetic Energy of the exiting flow ($K_{SE} = 1$). The Velocity component of the jet was dissipated through viscous effects. This head loss revised eqn. 29 to:

$$\dot{m}_1\left(C_P T_1 + \frac{{V_1}^2}{2}\right) + \dot{m}_2(C_P T_2) = \dot{m}_3\left(C_P T_3 + \frac{{V_3}^2}{2}\right)$$

$$\mathbf{\dot{m}_1(T_{01}) + \dot{m}_2(T_2) = (\dot{m}_3)(T_{03})} \quad \text{… (30)}$$

The head loss of the secondary Supersonic Flow, due to the sudden expansion, resulted in the elimination of its Velocity component (V_2). The Supersonic Flow only conveyed its Thermal component (T_2) to the Energy balance. This assumption, of complete Jet Kinetic Energy loss ($K_{SE} = 1$), was retained for the development of the SSEC Concept. It was shown in Section 12.1 that the sudden expansion loss could be optimized (by varying the respective sizes of $\mathbb{A}_1$ and $\mathbb{A}_2$), but the principal value was still large enough ($K_{SE} = 0.9$) to retain the assumption for the Energy balance. The SSEC concept, according to eqn. 30, concerned the Stagnation Temperature of the primary Centrifugal Flow (T_{01}) and the significantly lower Static Temperature of the secondary Supersonic Flow (T_2). The Resultant mixed stream (Flow 3) retained the bulk Velocity of Flow 1 (i.e. $V_3 \approx V_1$), but with a Static Temperature between that of Flow 1 and Flow 2 (i.e. $T_1 > T_3 > T_2$); proportional to the respective $\dot{m}$ contributions.

Best Supersonic (SS) Flow Regime

Supersonic (SS) Flow was identified by the Mach number being increased to, and beyond, 1 (i.e. $M \geq 1$). The SS regime displayed different flow property behaviours depending on: SS Tunnel geometry, and respective Inlet Stagnation Pressure. If the Stagnation Pressure ($P_{0\,SS}$) of a hypothetical SS Tunnel was continually increased, given a constant Back Pressure ($P_E = P_B$), M at the Tunnel Throat (narrowest diameter) would eventually reach unity ($M_T = 1$). This would result in a Normal Shock Wave at the Tunnel Throat; choking the SS Tunnel mass flow rate ($\dot{m}_{SS}$). Miller [22] described the Normal Shock to imply P_0 loss, M reduction, and (most significant to the Cooling Mechanism) T increase. The implications of this regime did not favour the outcomes desired for the Design. According to Skew [37], if the P_0 were to be increased further still, the Shock would move out of the Tunnel Throat and further downstream along the SS Tunnel length. The Shock would become increasingly stronger as it moved further and, consequently, the scale of the effects on the flow properties (in particular: P_0 loss and T increase). This relationship would continue until the Shock reached the Exit of the SS Tunnel. At this point, hence forth referred to as the 'Exit Plane Shock Condition', the Shock wave existed as its strongest form (most P_0 loss and T increase). The flow behaviour from this point was of utmost relevance to the SSEC concept, including the regimes of: Ideal Expansion, Overexpansion, and Underexpansion.

If the $P_{0\,SS}$ were to be increased further (from Exit Plane Shock Condition), to where the Exit Plane Static Pressure = Back Pressure (i.e. $P_E = P_B$), then the flow would exit the SS Tunnel in an Isentropic fashion. It would avoid Shocks altogether, and retain all Supersonic characteristics dictated by the Supply conditions (i.e. $M > 1$, High P_0, low T, $P_E = P_B$). This scenario was depicted in Figure 20 Part A. This was the desired regime (Ideal Expansion) for the SSEC concept. This Ideal Expansion Condition though, was very situational. The condition was dictated by the Pressure Ratio of Stagnation Pressure and Back Pressure (i.e. $P.R.^* = \frac{P_{0\,SS}}{P_B}$). Fluctuating the $P_{0\,SS}$ Supply below or above this P.R.* ratio would forgo Ideal Expansion, and result in either Overexpansion or Underexpansion of the flow respectively.

If the P.R.* was lower than the Ideal Expansion Condition requirement, such that the $P_E < P_B$, the resultant flow would undergo Oblique Shocks. These Shocks occurred at the SS Tunnel Exit edges; so as to contract the exiting flow stream, as seen in Figure 20 Part B. These Oblique Shocks had the same impact on flow properties as Normal Shocks (P_0 loss and T increase), just to a lesser extent. This condition was referred to as Overexpanded Flow. If the P.R.* was higher than the Ideal Expansion Condition, such that the $P_E > P_B$, the resultant flow would undergo Expansion Waves. These Waves occurred at the SS Tunnel Exit edge so as to expand the exiting flow stream; as seen in Figure 20 Part C. The Expansion Waves (Prandtl-Meyer fans) reduced P_E to the point of reaching P_B. In doing so, it produced a continuous flow (i.e. no Shocks) with smooth isentropic adjustments to flow conditions. During the flow passage through the Expansion Waves, the Mach number increased (due to the reduction in Pressure), and all Static Properties decreased (P, T, and ρ). This particular condition, Underexpanded Flow, was a viable option for the Cooling Mechanism.

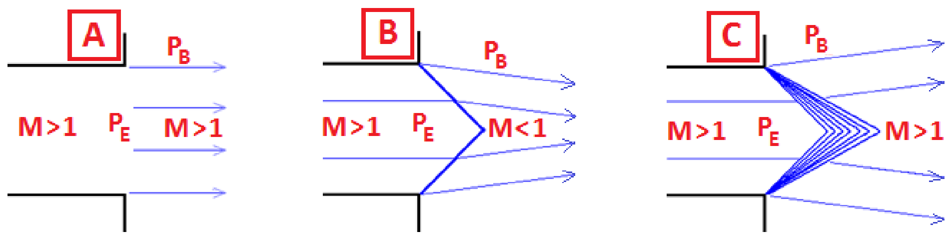

Figure 20. SS Tunnel Exits excluding choked Throat, Part A) Ideal Expansion - flow exited without Shocks ($P_E = P_B$), Part B) Overexpanded Flow - Oblique Shocks at exit edge ($P_E < P_B$), Part C) Underexpanded Flow - Prandtl-Meyer expansion fans at exit edge ($P_E > P_B$)

Exceeding the required P.R.* excessively (i.e. Severely Underexpanded Flow) resulted in P_E not being reduced to P_B within a single set of Prantl-Meyer expansion fans. The flow stream path (including Expansion Waves) was then reflected back into itself by the free stream. The reflection of the Expansion Waves formed Oblique Shocks within the SS Tunnel Exit jet. This pattern of expansion (Prandtl-Meyer fans) and relative compression (Oblique Shocks) repeated until the $P_E = P_B$; resulting in the formation of 'Shock Diamonds'. This situation should be avoided, and the P.R.* would have to approximate Ideal Expansion Condition as close as possible (erring on the side of Underexpanded Flow). This 'Robust' range required a flow delivery that met/exceeded the required P.R.*, but not overly exceed it.

i.e. Ideal Expansion Condition with $P_E \geq P_B$

In achieving Isentropic Supersonic flow at the SS Tunnel Exit, the Exit Mach number had to be in excess of $M_E = 1$. Using the Isentropic Stagnation Condition equations (eqns. 12 and 13), the proposed Minimum limits ($M_E > 1$) of Temperature Ratio (T.R.*) and Pressure Ratio (P.R.*) were calculated as:

T.R.* > $\frac{T_0}{T_E} > (1 + \frac{k-1}{2} \cdot {M_E}^2) = 1 + \frac{1.4-1}{2} \cdot 1^2 \quad > \mathbf{1.2}$

P.R.* > $\frac{P_0}{P_E} > (1 + \frac{k-1}{2} \cdot {M_E}^2)^{\frac{k}{k-1}} = (1 + \frac{1.4-1}{2} \cdot 1^2)^{\frac{1.4}{1.4-1}} \quad > \mathbf{1.8929}$

At this Minimum limit, $M_E = 1$, it implied that the SS Tunnel Exit diameter ($\mathbb{A}_E$) equalled the Tunnel Throat diameter ($\mathbb{A}_T$). This was because the Choke ($M_T = 1 = M_E$) occurred at the narrowest segment ($\mathbb{A}^* = \mathbb{A}_T = \mathbb{A}_E$). These diameters were related using the Area Ratio (A.R.*), defined in Oosthuizen [18], as:

$$\frac{\mathbb{A}}{\mathbb{A}^*} = \frac{1}{M} \left(\frac{1+\frac{k-1}{2} \cdot M^2}{\frac{k+1}{2}}\right)^{\frac{k+1}{2(k-1)}} \quad \text{... (31)}$$

Suffice to say, at the Minimum limit of $M_E > 1$, eqn. 31 became:

$$\textbf{A.R.*} \quad > \qquad \frac{\mathbb{A}_E}{\mathbb{A}^*} = \frac{1}{M_E}\left(\frac{1+\frac{k-1}{2}\cdot 1 M_E{}^2}{\frac{k+1}{2}}\right)^{\frac{k+1}{2(k-1)}} = \frac{1}{1}\left(\frac{1+\frac{1.4-1}{2}\cdot 1^2}{\frac{1.4+1}{2}}\right)^{\frac{1.4+1}{2(1.4-1)}} \qquad > \mathbf{1}$$

Using the 3 Critical Point ratios (T.R.*, P.R.*, and A.R.*) with a variable Mach number (M_E), revealed the following relationships between the SS Tunnel Exit Static Temperature (T_E, i.e. Cooling Mechanism objective) and the SS Tunnel Inlet Stagnation Pressure ($P_{0\,SS}$, i.e. Supply Device capability):

Increase M_E	→	Increase T.R.*	→	Decrease T_E	(since T_0 given)
	→	Increase P.R.*	→	Increase $P_{0\,SS}$	(since P_E given)

The $P_{0\,SS}$ increase could easily be achieved with higher specification Supply Devices, but the contribution of T_E was ultimately limited by the $\dot{m}$ capacity defined by A.R.*. The A.R.* dictated the SS Tunnel Throat diameter ($\mathbb{A}_T$) and, since the flow through the Tunnel Throat was limited by $M_T = 1$, also dictated the $\dot{m}$. The flow conditions required to achieve the Ideal Expansion Condition were then not attributed to a single SS Tunnel Design Point, but rather an optimization balance between the $P_{0\,SS}$ (Supply Device Capability) and $\dot{m}_{SS}$ (Tunnel Throat Diameter). The isentropic model for the SSEC Concept was developed in the next subsection, and identified the best (most practical) approach to the P_0 and $\mathbb{A}_T$ balance.

9.2 SSEC Concept Isentropic Model

In the Isentropic SSEC Model, seen in Figure 21, there was no consideration given to heat contributions of the SS Supply device ($T_{0\,SS} = T_{0\,ATM} = 278.15$ K), nor to the P_0 losses incurred during expansion. The simplifications were a far stretch from the actual implementation (Section 12.1). In reality, the heat generated during the compression to achieve $P_{0\,SS}$ was significant enough to warrant a Compressor Intercooler (Appx. O.2.5). The Sudden Expansion loss, from the SS Tunnel Exit to the Mixing Chamber diameter, dwarfed all other component loss coefficients (K_{LOSS}). This over-simplified Isentropic Model served to identify the theoretical optimum capability and contribution parameters of the SSEC concept. The calculation procedure consisted of:

1. The Thermodynamic Contribution – to identify the balance between the Static Temperature (T_{SS}) and Mass Flow Rate ($\dot{m}_{SS}$) required; in order to achieve $T_{0\,OUT}$.
2. Design Point optimization - $\dot{m}_{SS}$ and $P_{0\,SS}$ plotted as a function of $T_{0\,OUT}$ to determine the most economical Supply balance.

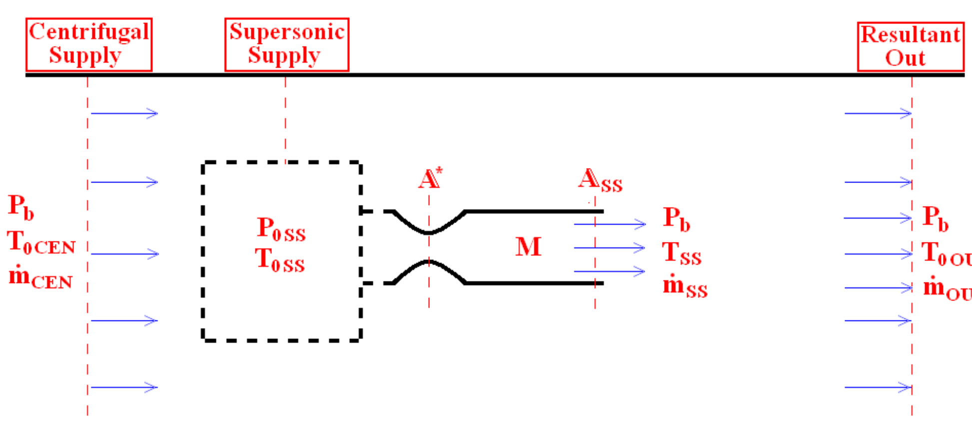

Figure 21. Ideal Expansion Condition Supersonic flow implemented in Direct Contact Mixing with Centrifugal air supply to produce the Resultant cooled flow for the Wind Tunnel

Thermodynamic Contributions

Applying the Modified Mixing Chamber Energy Equation (eqn. 30) to the flow conditions in Figure 21:

$\dot{m}_{CEN}(T_{0\,CEN}) + \dot{m}_{SS}(T_{SS}) = \dot{m}_{OUT}(T_{0\,OUT})$

From the Selected Air Supply Mechanism (Appx. O.1.3), the respective T_0 contribution was $T_{0\,CEN}$ = 298.15 K. Assuming continuity (eqn. 2) within the Control Volume, and given the required $\dot{m}$ for the WT Inlet ($\dot{m}_{MC\,OUT}$ = $\dot{m}_{CEN}$ + $\dot{m}_{SS}$ = 22kg/s), eqn. 30 was reduced to f_X {$\dot{m}_{SS}$, $T_{0\,OUT}$, T_{SS}}:

$$\dot{\mathbf{m}}_{\mathbf{SS}} = \mathbf{22} \cdot \frac{(\mathbf{T_{0\,OUT}} - \mathbf{298.15})}{(\mathbf{T_{SS}} - \mathbf{298.15})} \quad \text{... (32)}$$

The $T_{0\,OUT}$ was left variable, even though the WT Design Point objective was $T_{0\,OUT}$ = 240K. This allowed for $\dot{m}_{SS}$ contributions to be monitored at various Altitude levels (T_0 at 5751- 35000 ft). The Isentropic Model (Figure 21) was developed specific to the current Design application; $P_B = P_{WT\text{-}IN}$ = 97225 Pa ≠ $P_{JHB(ISA)}$ = 83000 Pa. The Model was calculated with a variable SS Tunnel Exit Mach number (M_{SS}). The Critical Point ratios (T.R.*, P.R.*, and A.R.*) were used, for each respective M_{SS}, to determine the SS Inlet requirements ($\dot{m}_{SS}$ and $P_{0\,SS}$) and SS Tunnel geometry ($Ø_T$ and $Ø_{SS}$). The sample calculation for the Model was included in Appx. G.3, with the major findings described here.

The sample calculation, using M_{SS} = 1.72, produced SS Inlet requirements of: $\dot{m}_{SS}$ = 10.37 kg/s and $P_{0\,SS}$ = 494620 Pa. These hypothetical Supply Device requirements were already very demanding; Flow Rate akin to Centrifugal Fans, and Stagnation Pressure akin to Reciprocating Compressors. There were 2 mutually exclusive extremes for the Supply Device options that were interpreted from this balance:

- A Device that supplied high $\dot{m}_{SS}$ (higher weighted influence on $T_{0\,OUT}$) at a low $P_{0\,SS}$ (ineffective T_{SS}).
- A Device that supplied high $P_{0\,SS}$ (effective T_{SS}) at a low $\dot{m}_{SS}$ (lower weighted influence on $T_{0\,OUT}$).

The SS Tunnel geometry ($Ø_T$ = 104.88 mm and $Ø_{SS}$ = 122.16 mm) was defined for the Ideal Expansion Condition at M_{SS} = 1.72. If this exact geometry was used at a higher M (i.e. increase $P_{0\,SS}$), the flow regime would then be Underexpanded (further reducing T_{SS} and increasing $\dot{m}_{SS}$). It was preferable then to design the fixed SS Tunnel dimensions for the Ideal Expansion Condition at a set M_{SS}, and then select a Supply Device capable of exceeding the required $P_{0\,SS}$. This method would induce Underexpanded Flow without actively altering the SS Tunnel geometry.

Design Point Optimization

The parameter optimization of $P_{0\,SS}$ and $\dot{m}_{SS}$, in achieving $T_{0\,OUT}$, was included in Appx. B.2. The analysis presented a range of P.R.* ($\frac{P_{0\,SS}}{P_b} = \frac{P_{0\,SS}}{97225}$) from 2.5 to 15. Each setting was used to determine the corresponding $\dot{m}_{SS}$ required to achieve the objective $T_{0\,OUT}$. The applicable P.R.* range for Ideal Expansion Condition across the entire Altitude spectrum was determined to be [5 - 10]. The optimum selection was defined by Supply Device capabilities, but ultimately: P_{JUMP} range = [403675 – 890351 Pa] with corresponding $\dot{m}_{SS}$ range = [10.44 – 8.30 kg/s].

The optimization process was then focused at Design Point ($T_{0\,OUT}$ = 240K), to determine the optimum SS Tunnel Inlet conditions for the Isentropic Model. The SS Supply Device was dictated by 2 factors: $P_{0\,SS}$ (ability to deliver P_{JUMP}), and $\dot{m}_{SS}$ (ability to deliver volumetric flow rate at the set P_{JUMP}). Figure 22 showed the $P_{0\,SS}$ - $\dot{m}_{SS}$ relationship in achieving $T_{0\,OUT}$ = 240 K. Addressing the asymptotic behaviour of the curve, the Maximum $\dot{m}_{SS}$ was limited by the total summation of $\dot{m}_{SS} + \dot{m}_{CENT}$ = 22kg/s, i.e. $\dot{m}_{SS}$ ≤ 22 kg/s. The Minimum $\dot{m}_{SS}$ was limited by the P.R.* relationship with T_{SS}; T_{SS} must be ≥ 1 K.

At this Static Temperature limit (T_{SS}>1), the P.R.* value (3.6 x 10^{08}) resulted in $\dot{m}_{SS} \geq 4.31$ kg/s. For clarity of scale, the Minimum and Maximum asymptotes were excluded from Figure 22. The axes limits focused instead on the Practical Optimization Range achievable with readily available machinery; i.e. $\dot{m}_{SS}$ = [6.8 - 16.4 kg/s] with corresponding $P_{0\,SS}$ = [2502484 – 221190 Pa].

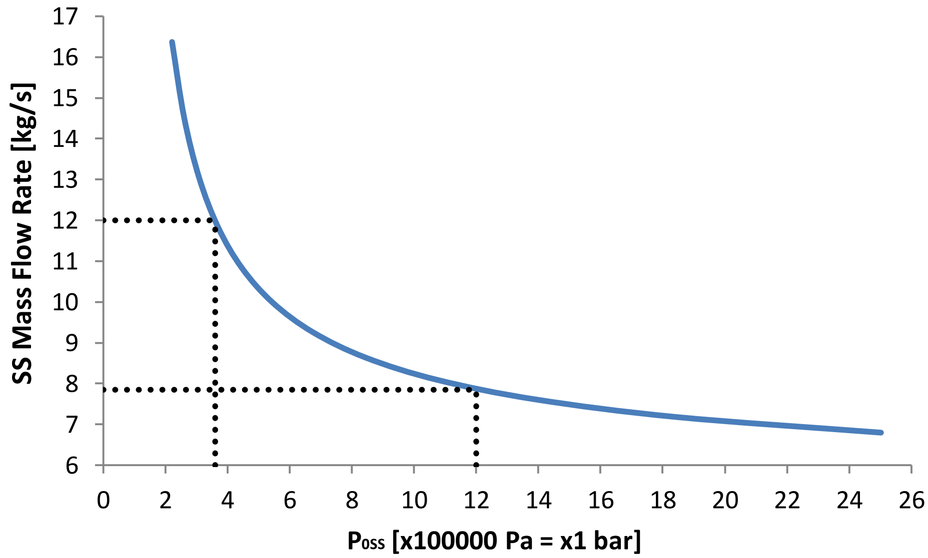

Figure 22. Supersonic Supply Mechanism requirements (P_{0SS} and $\dot{m}_{SS}$) in achieving Design Point altitude Temperature ($T_{0\,OUT}$ = 240 K)

The entire range of $\dot{m}_{SS}$ could theoretically be achieved; with the means of simultaneous Supply Devices. The corresponding $P_{0\,SS}$ range, on the other hand, was limited by the capability of each individual Supply Device. Even at Minimum $P_{0\,SS}$ (221190 Pa), the value was well out of range of Centrifugal Fans. This Mechanism limitation ($P_{0\,SS}$ capability) rendered the argument of 'increasing $\dot{m}_{SS}$ to decrease the P_{0SS} requirement' irrelevant. The goal was then to find a solution that prioritized higher P_{0SS}; via High Pressure Compressors. Figure 22 also included 2 $P_{0\,SS}$ comparison markings; to identify the most responsive change in $\dot{m}_{SS}$ with regards to $P_{0\,SS}$. It depicted markings at Minimum $P_{0\,SS}$ = 3.6 bar ($\dot{m}_{SS}$ = 12 kg/s) and Maximum P_{0SS} = 12 bar ($\dot{m}_{SS}$ = 7.85 kg/s); thereby reducing the field of parameter balance to these optimum positions. The Minimum $P_{0\,SS}$ marking defined the point where reducing further was only achievable through simultaneous Supply Devices. The Maximum $P_{0\,SS}$ marking defined the point where increasing beyond resulted in severely diminishing returns on $\dot{m}_{SS}$ saving. This range was identified as the requirement balance for prospective SS Supply Devices.

i.e. **3.6 bar < $P_{0\,SS}$ < 12 bar** (with corresponding flow rates 12 kg/s > $\dot{m}_{SS}$ > 7.85 kg/s)

The Cooling Mechanism evaluation was previously postponed in Section 8.2; to briefly explain the Experimental SSEC Concept. The results of the Concept were summarized as follows:

- Achieve Ideal Expansion Flow (err on the side of Underexpanded Flow).
- Do not over-exceed the Underexpanded regime; so as to avoid Shock Diamond formation.
- Supply Device requirements: 3.6 bar < P_0 < 12 bar with corresponding 12 kg/s > $\dot{m}_{SS}$ > 7.85 kg/s.

The Supply Device requirements formed the basis for the remainder of the Cooling Mechanism evaluation; continued in the next section (Section 10).

10 Cooling Mechanism Design Study

As previously weighed in the Cooling Mechanism House of Quality (Figure 18), the 2 best options were identified to be the Vapor Cycle and SSEC. In this Section, the Cooling Mechanism evaluation was performed only on the Investigative SSEC concept. The Vapor Cycle served as a fall-back concept. The mechanism was developed using the SSEC Isentropic Model (Section 9.2); to determine the best options for the SS Supply Device. The procedure followed the same method as the Air Supply Mechanism evaluation (Section 8.1); since the requirement for the SSEC concept was a Supply Device that was capable of delivering an airflow capacity, albeit at a much higher Pressure.

Supersonic Supply Mechanism Options

The options for the SS Supply Device were weighed against the following requirements:

- Pressure Range → 2.77 bar (40.18 psi) $\leq P_{JUMP} \leq$ 11.17 bar (162 psi)
- Corresponding $\dot{m}_{SS}$ → Flow Rate $(\dot{V}) = \frac{\dot{m}_{SS}}{\rho_{Throat}}$ with $\dot{m}_{SS}$ and ρ_{Throat} corresponding to P_{JUMP}
  → 4.19 m^3/s (8878.11 CFM) > $\dot{V}$ > 0.83 m^3/s (1758.67 CFM)
- Flow Integrity → Continuous = 5 minutes

Using the same range of devices listed for the Air Supply Mechanism, the Pressure requirement for this application (> 40.18 psi) immediately disqualified the Fan options. The remaining 3 applicable options (with revised examples; to better match the requirements) were briefly listed here. The detailed descriptions of the Mechanism options were included in Appx. O.2.3

1. Reciprocating Compressor - < 5 % of required $\dot{\forall}$, matched upper P_{JUMP} limit (162 psi)
2. Rotary Compressor - matched required $\dot{\forall}$, achieved high P_{JUMP} brackets (125 psi)
3. High Pressure Air Cylinder - modular delivery, capable of meeting requirements

The House of Quality weighted assessment was presented in Figure 23. The assessment parameters and performance characteristics of the Mechanism options were included in Appx. O.2.4.

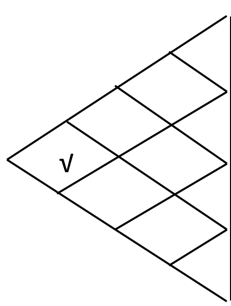

Key √ = ½	Rating [/5]	Reciprocating Compressor	Rotary Screw Compressor	Air Cylinder (Bottled Gas)
Pressure Range	5	√√	√√	√√
Corresponding Flow Rate	3	0	√√	√√
Continuous	3	0	√	√√
Practicality	4	0	√√	0
	15	5	**13.5**	**11**

Figure 23. House of Quality to determine the best 2 fits for Supersonic Supply Mechanism (Key √ = ½ POINT) identifying the Rotary Screw Compressor and Air Cylinder as best options

Best Fit Cost Analysis

The 2 best fits were identified in Figure 23 as: the Rotary Screw Compressor (rating of 13.5/15) and the High Pressure Air Cylinder (rating of 11/15). These options were then assessed according to the cost requirements to determine the order of preference (Investigative and Back-Up). The detailed cost breakdown and assessment were included in Appx. O.2.5; with the major findings listed here.

- Rotary Screw Compressor Cost per run (1 hr) = R 407.24
  The largest component of the test run cost was the Electricity Cost (≈ 80% of total cost).
- Air Cylinder Cost per run (13.6 min) = R 1145.04
  The largest cost component of the test run cost was the Refill Cost (99% of total cost).

Comparing the 'cost per run' of the 2 best fits, the importance of cost effectiveness in this Design (as it pertained to the PRS) necessitated the choice of the Rotary Screw Compressor.

SS Supply Mechanism: **Rotary Screw Compressor, CompAir, Series L200 RS**
Support Equipment: **Air Receiver, BOGE, Vertical Galvanized 5000L 11bar**

Despite the need for additional components (Air Receivers) with the associated risk mitigation factors, the cost benefit of holding the machinery far outweighed the inconvenience. The 2 major cost contributors, respectively pertaining to the Rotary Compressor and Air Cylinder, were the Electricity Costs (R 327.64/run) and Air Refill Costs (R 1136.26/run). Unlike the Air Supply Mechanism though, comparative variation in these prices (from 2013) would not likely reach a point so as to necessitate a switch in preference. The high Pressure required in delivering SS airflow emptied the Air Cylinders at an incredible rate; and rendered the 'Bottled Gas' Mechanism unfeasible.

Consequences of SSEC Concept

It was important to state here that the SSEC Concept involved pressurizing ambient air to a very high level ($P_{0\,SS} > 10\,P_{ATM}$). This compression process presented the major consequence of icing within the low Temperature Supersonic Jet plume; due to the water vapour within the ambient air feed. This concern was addressed using a preliminary evaluation of readily available Air Dryers; included in Appx. O.3. These devices would reduce the moisture content within the airflow prior to the SSEC mechanism. The comprehensive analysis of the Air Dryer mechanism (costs and implementation) was relegated to Further Work (Appx. Q.3.3). The Project only considered the Stagnation Pressure (P_0) and Volumetric Flow Rate ($\dot{\forall}$) of the Supply Devices. It focused on the fundamental Fluid and Thermal dynamics in achieving the PRS objectives, and ignored the real-world implementation of support systems (i.e. filtration, moisture handling, and safety release valves). This concern was only brought up here due to the considerable compression and the very low Temperature uniquely inherent of the SSEC Concept. If the SSEC Concept were to be tested using a scaled Physical Model (described as Further Work in Appx. Q.1.4), this moisture content would present a significant hurdle to the successful implementation of the Cooling mechanism. At which point, the Air Dryer evaluation would have to be performed in earnest.

In the next section (Section 11), the Mixing Chamber design proceeded with the actual fluid and thermal Mixing Mechanisms necessary for the process. The mechanisms converted the Airflow Supply Device conditions ($P_{0\,CENT}$, $\dot{m}_{CENT}$) and the SSEC concept Supply Device conditions ($P_{0\,SS}$, $\dot{m}_{SS}$) into the required WT Inlet conditions ($P_{0\,WT\text{-}IN}$, $T_{0\,WT\text{-}IN}$, and $\dot{m}$).

11 Mixing Chamber (MC) Literature Review

The Mixing Chamber (MC) Analytical Model was developed using the same Fluid Dynamic relationships described for the Wind Tunnel (Section 5). The modelling in this section, however, focused on 'Classical Thermodynamics' – using macroscopic flow properties (P, V, T). It looked at the fundamental mechanisms, and different implementations involved, in the mixing of the 2 streams: Cold (Supersonic) flow and Hot Main (Centrifugal) flow. The literature analyses were divided into 2 subsections:

- Temperature Mixing Theory – To analyse the impact of the mixing mechanism on the Resultant flow stream properties.
- Temperature Mixing Mechanisms – To identify the impacts of the physical geometry in the MC that facilitated the mixing.

These literature analyses formed the basis of the MC concept generation. It provided the minimum lengths and spatial orientations required for each possible MC configuration. The analysis was used to generate the MC geometry such that the Velocity profiles for the respective Inlet flows (SS and Main) were developed prior to any mixing. Upon the respective individual flow developments, the SS and Main flows were mixed (using eqn. 30) to achieve the Design Point Resultant flow at the WT Inlet.

11.1 Temperature Mixing Theory

The design process of the MC was divided into 2 parts: the fluid mechanics of the separate streams (Main and SS flow), and the parameters governing the Resultant homogenous stream. There was no inclusion of mechanical devices in the mixing process. This approach followed the mixing classification described by Sweeney [38], where the 3 mechanisms of mixing were listed as: Diffusion, Convection, and Bulk Movement. From the descriptions, it was concluded that the different mixing mechanisms were specific to the respective Viscosities and relative Velocities of the concerned fluids. In this Design, the process mixed 2 airstreams of vastly different Velocities (Supersonic and Subsonic). The fluids were of the same constituency and both had relatively low Viscosity (gases). These flow properties made the Diffusion mechanism the appropriate choice; utilizing the relative Velocities of the flows to entrain and mix through Turbulent Diffusion. The Temperature Mixing focused on conduction through macroscopic particle transport, due to turbulence, rather than the thermal conduction between isolated streams.

11.1.1 Dimensionless Variable Definitions

Reynolds Number (Re)

The Re No. eqn. (eqn. 7) was reinterpreted by characteristic length (L), described in Munson [19], as:

$$\mathbf{Re} = \frac{\textbf{Inertial Force}}{\textbf{Viscous Force}} = \frac{\boldsymbol{\rho \cdot V \cdot L}}{\boldsymbol{\mu}} \qquad \text{… (33)}$$

Re No. was the measure by which friction forces affected the fluid mixing. Turbulence encouraged mixing, whereas Advection (conserved bulk transport) promoted segregation of the fluids. Turbulent flow (high Re) was a necessary objective for this Design.

Prandtl Number (Pr)

As described in Shires [39], Pr was the ratio of 'Momentum Diffusion' to 'Heat Diffusion':

$$\mathbf{Pr} = \frac{\textbf{Momentum Diffusion}}{\textbf{Thermal Diffusion}} = \frac{\boldsymbol{\gamma}}{\boldsymbol{\zeta}} = \frac{\boldsymbol{C_P \cdot \mu}}{\mathbf{k}} \qquad \text{… (34)}$$

Where γ = Kinematic Viscosity [m^2/s], ζ = Thermal Diffusivity [m^2/s]

The Prandtl Number (Pr) was dependent on the fluid state only, as opposed to Re which required the length scale (L) of the implementation. Pr described the Diffusion mechanisms of the mixing process. A large Pr (>> 1) implied that mixing was dominated by 'Momentum Diffusion'; where the Velocity of the fluids was conveyed by the viscous forces. A small Pr (<< 1) implied that mixing was dominated by 'Thermal Diffusion'; the Temperatures of the fluids rapidly distributed to achieve the Resultant. Both forms of Diffusion happened irrespective but, according to the Pr value, one mechanism occurred at a greater rate. A lower Pr (<< 1) was the objective for this Design.

11.1.2 Dimensionless Variable Implications

Flow Development (HFD and TFD)

Upon the entry of the SS stream into the Main stream, the Resultant flow underwent profile development until it achieved a uniform flow profile. According to Chakraborty [40], there were 2 measures of the flow development profile to consider in this implementation; the Hydraulic profile (HFD) and the Thermodynamic profile (TFD). At the point where the flow boundary layer grew to meet at the channel core, the Velocity profile was constant and regarded as Hydraulically Fully Developed (HFD). Munson [19] defined this length for Turbulent flow as:

$$\mathbf{L_{HFD}} = \mathbf{4.4} \cdot (\mathbf{Re}^{\frac{1}{6}}) \cdot \emptyset \qquad \text{… (35)}$$

Chakraborty [40] stated that Thermodynamically Fully Developed (TFD) flow was achieved when the relative Temperature profile did not change along the pipe length. Whilst TFD Flow was a primary concern in achieving the Resultant mixed flow, the respective incremental partial derivative analysis ($L_{TFD} = \frac{d}{dx} f_X\{T_{B\text{-}LAYER}, T_{MEAN}, T_{SURFACE}\}$) did not necessarily have to be performed. This was due to a 'convenient' relationship between HFD and TFD Flow; using Pr. The Pr was an indication of the ratio between the Velocity boundary layer thickness (Velocity BLT) and Thermal boundary layer thickness (Thermal BLT):

Pr < 1 → Thermal BLT grew faster than Velocity BLT, which by corollary → if HFD then also TFD

This relationship meant that if Pr < 1, the pipe length required for HFD Flow (L_{HFD}) inherently encompassed the pipe length required for TFD Flow (L_{TFD}).

Thermal Choking

For Parallel geometry concerning 2 compressible fluid streams, Otis [41] described the possible scenario of 'Thermal Choking' in the Resultant stream. The proposed model, as seen in Figure 24, showed the Resultant stream reaching 3 points of flow property equilibrium (in respective order): 1st = Pressure equilibrium, followed by 2nd = Velocity equilibrium, and finally 3rd = Temperature equilibrium. When mixing a Subsonic flow with a Supersonic flow, the Resultant stream could possibly Choke (M = 1) at the Temperature equilibrium point. This occurrence was determined by the dimensionless variable 'β'. This dimensionless 'β' variable, in relation to Point 3 in Figure 24, was defined in Otis [41] as:

$$\boldsymbol{\beta} = \left(\frac{\mathbf{2 \cdot M_{3*}}}{\mathbf{1+M_{3*}}^{\mathbf{2}}}\right)^{\mathbf{2}}, \text{ Where } \mathbf{M_{3*}} = \frac{\mathbf{V_3}}{\sqrt{\mathbf{R \cdot T_0 \cdot (\frac{2k}{k+1})}}} \qquad \text{… (36)}$$

The variable β categorized the mixing behaviour as:

β < 1 → Mixing was achieved without any form of Choking

β = 1 → Thermal Choking occurred during the mixing process

β > 1 → Flow became Choked before completely mixing

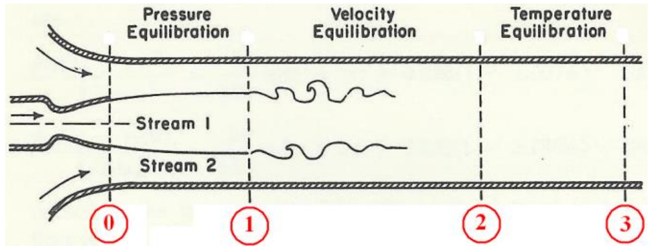

Figure 24. Ejector Mixing Model with proposed equilibrium points (0 = Mixing of flows, 1 = Pressure Equilibrium, 2 = Velocity Equilibrium, 3 = Temperature Equilibrium), edited from Otis [41]

This approach was usually limited to Ejector applications of flow entrainment, and not necessarily Temperature Mixing. That is to say, the Temperatures of the two hypothetical compressible streams in Figure 24 were comparably similar. The intention of the current Design was to mix two streams of significantly different Temperatures. The MC produced a Resultant stream with the Velocity of the Main Primary flow (i.e. $M_3 \approx M_{PRIMARY} = M_{MAIN} << 1$), and it was expected that $\beta < 1$.

11.2 Temperature Mixing Mechanisms

The geometrical MC concepts in this section focus exclusively on Parallel configurations; as the Final MC Design was based on this concept. The literature analysis of the Perpendicular configurations, used during the comprehensive concept generation, was included in Appx. G.6.3. The MC sizing was approximated using the minimum length (L) and diameter ($Ø_{MC}$) required in achieving the Resultant flow. These minimum dimensions were largely determined by the flow conditions of the SS stream. The theoretical Temperature Mixing concepts served only as the hypothetical start-points for the MC Design. This was due to certain compromising characteristics of the theoretical mechanisms, including:

- Mixing of 2 comparable flow streams (i.e. comparable Velocity, Viscosity, and composition).
- Focused exclusively on the mixed Resultant flow achieving a consistent flow profile, but not necessarily the preliminary development of the 2 contributing streams (Main or SS).
- Did not include the influence of significantly different Temperatures; objectives were not focused on any form of substantial cooling/heating.
- Did not include the influence of significantly different Velocities; particularly the 'mass velocity' and compressibility effects of the SS flow.

Prandtl Mixing Length (L_M)

L_M determined the energy transfer (through eddy viscosity) in Turbulent flows. Clarkson [42] described the Nikuradse 'Mixing Length for Pipe flow', seen in Figure 25 Part A, as:

$$\frac{\mathbf{L_M}}{\mathbf{r_0}} = \mathbf{0.14} - \mathbf{0.08}\left(\mathbf{1} - \frac{\mathbf{y}}{\mathbf{r_0}}\right)^{\mathbf{2}} - \mathbf{0.06}\left(\mathbf{1} - \frac{\mathbf{y}}{\mathbf{r_0}}\right)^{\mathbf{4}} \quad \text{... (37)}$$

Where r_0 = radius ($\frac{Ø_0}{2}$) [m], y = vertical distance of shear layer [m]

The maximum possible L_M occurred at the core of the flow ($y = r_0 = \frac{Ø_0}{2}$), resulting in: $L_M = 0.07 \cdot Ø_0$.

Jet Mixing Core Length (X_C)

Brodkey [43] described the secondary jet to maintain a core length over distance X_C before dissipation; as depicted in Figure 25 Part B. The jet diameter ($Ø_{JET}$) increased with distance (X) from the nozzle ($Ø_N$):

$$Ø_{JET} = Ø_N + 2 \cdot X \cdot \tan\left(\frac{\alpha_{EXP}}{2}\right) \quad \text{... (38a)}$$

Where $Ø_N$ = nozzle diameter [m], X = axial distance from nozzle [m], α_{EXP} = expansion angle (± 14°)

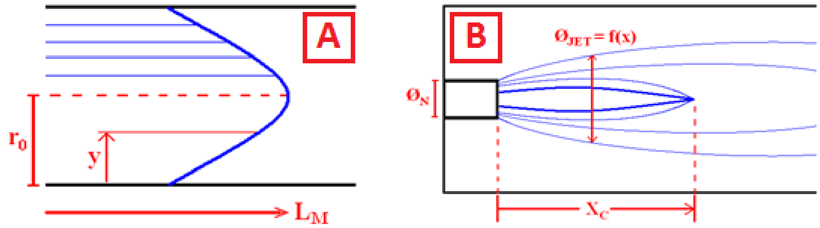

Figure 25. Parallel Mixing Mechanisms, Part A) Prandtl Mixing Length L_M proportional to Shear Layer (y), Part B) Jet Mixing Core Length X_C associated with $Ø_N$

The Jet core length (X_C) was the maximum axial distance of the jet flow; in which it retained its individual characteristics. X_C represented the minimum MC length required before the mixing process would occur. This definition was independent of jet expansion; i.e. $X_C \neq f_X\{Ø_{JET}\}$. It was instead dependent on the nozzle diameter ($Ø_N$) and flow characteristic (Re); defined for $10^4 < Re < 10^5$ as:

$$\mathbf{X_C = 2.13 \cdot Ø_N \cdot Re^{0.097}} \quad \text{... (38b)}$$

Potential Core Length Models ($L_{CO\text{-}FLOW}$)

Murakami [44] investigated examples of core length behaviour; where the SS flow (Primary) entered into a chamber with parallel flow of varying Velocity. There were 3 identifiable regimes:

1. Single Jet – Primary jet was expanded into a stagnant chamber; akin to the X_C model (eqn. 38b).
2. Co-Flowing Jet – Primary jet was expanded into a low speed Secondary flow. This was the typical layout of a wind tunnel designed to interpret jet flow expansion.
3. Co-Axial Jet – Primary jet was surrounded by a high Subsonic Secondary flow; which 'contained' (prevented the expansion of) the Primary flow.

The primary objective of the Murakami [44] experiment was to reduce SS Shock noise; through Mach Wave Elimination. This was accomplished by increasing the Velocity of the surrounding Secondary flow, but at the cost of elongating the Primary jet core length. Figure 26 showed the dimensionless elongation of the jet core length as the Secondary flow Velocity was increased (from stagnant to M0.9).

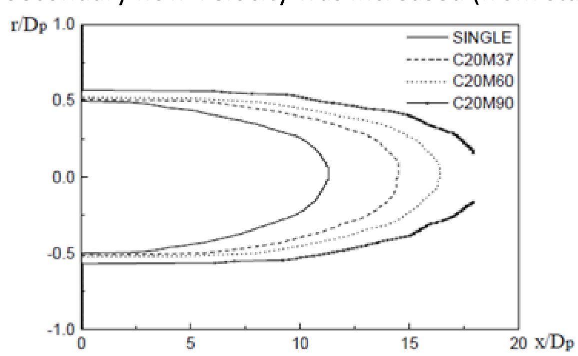

Figure 26. Dimensionless elongation of Potential Core Length (x) as the Secondary flow Velocity is increased (Single = Secondary Stagnant, C20M37 = Secondary M0.37, C20M60 = Secondary M0.6, C20M90 = Secondary M0.9), reproduced from Murakami [44]

The most prominent observation from Figure 26 was the distinct elongation in jet core length upon increasing the Secondary flow Velocity. Increasing the Secondary flow Velocity from stagnant to M0.6 resulted in a ±45% elongation of Primary flow core length. The approach to the Murakami [44] objective was the opposite of what was required for the MC. The objective of the current Design was to minimize SS flow core length and, by that distinction, the MC design process followed the Co-Flowing Jet model.

This model reduced the surrounding Secondary flow Velocity as much as possible. It increased the Primary SS shear layer, and reduced its potential core length. The model was implemented in the MC Design by increasing $\O_{MC}$; so as to reduce V_{MAIN}. The Potential Core Length Model for the Co-Flowing Jet ($L_{CO\text{-}FLOW}$) was described in Murakami [44] as:

$$\mathbf{L_{CO-FLOW}} = \frac{\O_{\mathbf{SS}}}{\mathbf{0.14}\cdot\frac{(\mathbf{1-r_V})(\mathbf{1+\sqrt{s_\rho}})}{\mathbf{1+r_V\cdot\sqrt{s_\rho}}}\cdot(\mathbf{0.23+0.77e^{-3.5\cdot M_C{}^2}})} \quad \dots (39)$$

Where $\O_{SS}$ = SS tunnel exit diameter [m], r_V = velocity ratio ($\frac{V_{secondary}}{V_{primary}}$), s_ρ = density ratio ($\frac{\rho_{secondary}}{\rho_{primary}}$),
M_C = average Mach number ($\frac{V_{primary}+V_{secondary}}{a_{primary}+a_{secondary}}$)

Summary of Mixing Mechanisms (Parallel Concepts Only)
These lengths (L_{HFD}, L_M, X_C, and $L_{CO\text{-}FLOW}$) formed the basis of the MC length (L) budget; for Parallel mixing concepts. The diameter of the MC ($\O_{MC}$) was sized to reduce V_{MAIN} as much as possible, without resulting in Main flow stagnation. It was also important to acknowledge the hierarchy of these lengths. The dimensionless variables of L_{HFD} and L_M formed the basis of the Fluid and Thermal Dynamics of the entering flows; i.e. the minimal length required before mixing would take place. The $L_{CO\text{-}FLOW}$, which was more relevant than the X_C length, determined the length required for the mixing of the various streams in achieving the Resultant flow. With these fundamental Mixing Mechanisms explained, the MC Analytical Model was developed in the next section (Section 12).

12 Mixing Chamber (MC) Analytical Modelling

The MC Analytical Model was used to interpret the conversion of Supply Device flow properties (Centrifugal and Rotary Compressors) to the Design Point WT Inlet requirements. The Analytical Model included the effects of both: the Fluid Mechanics in expanding the SS flow, and the Thermodynamics of mixing the 2 streams to achieve the Resultant flow. The Modelling procedure was performed in steps:

- Fluid Mechanics 'Base' Model – Incorporating the entry of the SS Flow into the MC. This analysis included the SS flow expanding and incurring the P_0 Sudden Expansion loss. This Base model formed the foundation for the Global MC In/Out variables.
- Temperature Mixing Mechanisms – Determining the MC dimensions (L and Ø) required to facilitate the mixing of the 2 streams, and achieve the eventual Temperature equilibrium.
- Identify Design Components – Investigating the geometric layouts, and the number/ positioning of Jets to be implemented. This produced the Final MC geometry.
- Analytical Model – Generating a complete MC Solution that produced the WT Inlet conditions from the specified Supply Devices. This Analytical Model concluded the mathematical estimate to serve as validation for the MC Numerical Model.

12.1 Base Model (MC In/Out)

At Design Point, the required MC Out/WT In conditions (Section 7.5) were: $\dot{m}$ = 22kg/s, P_0 = 98500 Pa, and T_0 = 240 K. The respective $\dot{m}$ contributions (SS flow = $\dot{m}_{SS}$ and Main flow = $\dot{m}_{MAIN}$) were determined by the balance in achieving the ResultantT_0. In Section 9.2, the Isentropic Cooling Mechanism calculation provided an estimate for the SS Supply Device. These conditions did not take into consideration the actual mechanics of introducing the SS flow into the MC. The Cooling Mechanism, by design, resulted in an immediate and significant P_0 loss; due to the sudden expansion of the SS Jet into the MC. This P_0 loss had to be factored into the Supply Mechanism itself; even prior to any isentropic MC model variations.

SS Jet Sudden Expansion Loss (K_{SE})

The Sudden Expansion loss, eqn. 20a, was a function of the respective areas for the SS Tunnel Exit ($Ø_{SS}$) and the MC ($Ø_{MC}$). The $Ø_{MC}$ could be varied to find the most effective space required for mixing. The $Ø_{SS}$ however, was a function of the required $\dot{m}_{SS}$ to decrease the Resultant flow $T_{0\ OUT}$. The $Ø_{SS}$ was limited in its variation due to the following:

- The $P_{0\ SS}$ was limited to 10.83 bar; Maximum output of the selected Device (Appx. O.2.5).
- The P_0 loss from the Sudden Expansion necessitated a higher $\dot{m}_{SS}$ contribution than previously estimated; since P_0 (after loss) << 10.83 bar.
- This $\dot{m}_{SS}$ contribution was limited by the $\dot{m}_{TOTAL}$ Design requirement (22 kg/s). This limit ensured the Design relevance of the Test Section flow (M0.7), and prevented choking at the OTS Inlet.

The net effect of these factors required that $\dot{m}_{SS}$ contributed as much of $\dot{m}_{TOTAL}$ as possible in order to achieve T_0 = 240 K. The $\dot{m}_{SS}$ however, could not exceed the fixed limit of 22kg/s.

Whilst the exact dimensions of the MC ($Ø_{MC}$) were specific to each geometric configuration, the Base Model utilized the Centrifugal Supply Exit as the starting point.

$\boldsymbol{Ø_{MC\ (BASE\ MODEL)}}$ **= 0.7 m** (≈ 0.755 m according to the selected Device in Appx. O.1.3)

The SS Tunnel Exit ($Ø_{SS}$) was sized to deliver the required $\dot{m}_{SS}$ in order to overcome the Sudden Expansion loss (K_{SE}). The K_{SE} loss was calculated using eqn. 20a.

$$\mathbf{K_{SE}} = \left(\mathbf{1} - \frac{\mathbb{A}_1}{\mathbb{A}_2}\right)^{\mathbf{2}} = \left(\mathbf{1} - \frac{\mathbb{A}_\mathbf{E}}{\mathbb{A}_\mathbf{MAIN}}\right)^{\mathbf{2}} = \left(\mathbf{1} - \frac{Ø_{\mathbf{SS}}{}^2}{0.7^2}\right)^{\mathbf{2}} \qquad \text{… (40)}$$

This equation (eqn. 40) presented a relationship between K_{SE} and $Ø_{SS}$. The $Ø_{SS}$ however, was exclusively dependent on the required $\dot{m}_{SS}$. The $\dot{m}_{SS}$ was controlled by the SS Tunnel Throat Choke (M_T = 1). Increasing $\mathbb{A}_T$ to increase $\dot{m}_{SS}$ would correspondingly increase $\mathbb{A}_E$ (and therefore $Ø_{SS}$); in order to maintain the designated Area Ratio (A.R.* = $\frac{\mathbb{A}_E}{\mathbb{A}_T}$). A.R.* was fixed by the Maximum Pressure Ratio available to achieve the SS Underexpansion (P.R.* = $\frac{P_{0\ SS}}{P_b} = \frac{10.83\ \text{bar}}{P_b}$). These relationships (between K_{SE}, $Ø_{SS}$, $Ø_T$, and $\dot{m}_{SS}$) were best demonstrated using a sample calculation; included in Appx. G.4. The important flow properties from the sample calculation were presented here. The calculation was performed with the SS flow contributing the total mass flow rate; i.e. $\dot{m}_{SS} = \dot{m}_{TOTAL}$ = 22kg/s, and $\dot{m}_{CENT}$ = 0. The SS flow was specified to enter the MC as Underexpanded. This was achieved by decoupling the P.R.* and A.R.* relationship from Section 9.1. The P.R.* affected the P_E, whereas the A.R.* directly and independently determined the M_E. This design choice of 'decoupled A.R.* - P.R.*' ensured that, even at the slightest contribution of SS flow (i.e. $\dot{m}_{SS}$→0, $\dot{m}_{CENT}$→22 kg/s), the flow was always Underexpanded.

The P.R.* was determined from $P_{0\ SS}$ and P_b (P.R.* = $\frac{P_{0\ SS}}{P_b} = \frac{1083000}{83000}$ = 13.048). The A.R.* was selected to correspond to a lower P.R.* value (P.R.* = $\frac{1083000}{97225}$ = 11.139) at A.R.* = 2.0508. The sample calculation produced the SS Tunnel Exit Area ($\mathbb{A}_E$) so as to evaluate eqn. 40 as: K_{SE} = 0.912. This K_{SE} value was applicable to the Maximum possible $\dot{m}_{SS}$ contribution (22kg/s). Decreasing the $\dot{m}_{SS}$ contribution from this point required decreasing $\mathbb{A}_E$, which consequently increased K_{SE}. It revealed an unavoidable and excessive P_0 loss during the expansion of the SS flow. For clarity on the relationship between the 'decoupled A.R.* - P.R.*' and the values of K_{SE} and $\dot{m}_{SS}$, a parameter optimization was included in Appx. C. This 'varying' procedure helped to optimize the loss coefficient, but the principle value of this Sudden Expansion loss (from $Ø_{SS}$ to $Ø_{MC}$) was still large; $K_{SE} \approx 0.9$ in the best case. To establish a starting point for the MC Base Model, the K_{SE} was optimistically assumed as:

$\mathbf{K_{SE}}$ **≈ 0.9** (at Maximum $\dot{m}_{SS}$ contribution)

Inlet Configuration (Pseudo-Isentropic) Model

The SS jet configuration was specified using multiple SS Outlets, as opposed to a single jet. This 'Multiple SS Outlet' version of the SS Supply had considerable advantages, such as:

- Allowing for a mechanical (and more pragmatic) means of varying $\dot{m}_{SS}$.

It allowed for the Altitude Temperature levels to be varied as desired. By shutting off one or more SS Supply streams, lower Altitude settings were achieved by cooling to a lesser extent. This version allowed for different levels of cooling without having to actively alter the dimensions of the SS Tunnels or the P_0 capacity of the Rotary Compressor.

- Economic utilization of Rotary Compressor Supply Mechanisms.

The Cooling Mechanism inevitably required multiple SS Supply Devices to adequately deliver the Design Point $\dot{m}_{SS}$. This was due to the significant K_{SE}, and the fixed Maximum P_0 output of the compressor. At lower Altitude simulations though, not all of this capacity was required. The 'Multiple SS Outlet' version allowed for non-essential Rotary Compressors to be shut-down.

- Staggered Temperature exchange reduced the incremental load on Turbulent Mixing.

By mixing the Centrifugal stream with incremental SS streams (as opposed to a single lumped stream), the length (and time to dissipation) of the SS Jet cores were reduced. The Resultant $T_{0\ OUT}$ was achieved through a continual supply of SS Jets; cooling in summation, rather than as a whole.

Using these Base Model features (Multiple SS Outlet and K_{SE}), an otherwise 'Isentropic' model was created. It identified the balance between the Inlets (SS and Centrifugal contributions) and Outlet (required T_0); to achieve the Fluid Mechanics analysis. The Inlet conditions were then used to outfit the different Temperature Mixing mechanisms, outlined in the next section (Section 12.2), to determine the most feasible MC Concepts. The process through which a typical geometry was evaluated was explained Section 12.3. For the purposes of this Pseudo-Isentropic model, the Design Point MC Inlet properties were extracted from the analysis in Section 12.3. The Inlet properties included: 3 SS Jets, P.R.* = 14.45, A.R.*= 1.982 (corresponding to a P.R.* = 10.5), and $Ø_{MC}$ = 0.7 m. Figure 27 depicted a hypothetical layout (not actual configuration) with the key locations (SS, T, E, L, MAIN, and END) from which the flow was analysed. SS (Supersonic), MAIN (Centrifugal), and END (Resultant) referred to the respective flow streams. T (Throat), E (Exit), and L (Sudden Expansion Loss) referred to the specific locations along the streamline of the Underexpanded SS Flow.

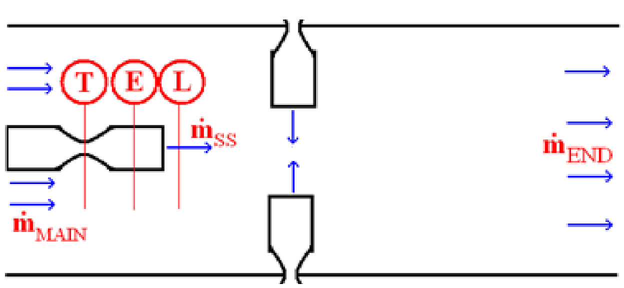

Figure 27. MC hypothetical layout with: 3 SS jet flows (including locations: T = Throat, E = Exit, and L = after Sudden Expansion Loss), MAIN (Centrifugal) Flow, and END (Resultant) flow

The relationship between the 3 major points in Figure 27 (SS, MAIN, and END) was established using the Continuity equation (eqn. 2) and the Modified Mixing Chamber Energy equation (eqn. 30). Equation 30, as explained in Section 9.1, reflected the energy contributions of each stream (Main, SS, and END). It also included the SS Sudden Expansion loss; via the exclusion of its respective Kinetic Energy (V_{SS}).

$\dot{m}_{END} = \dot{m}_{SS} + \dot{m}_{MAIN}$ = 22 kg/s

$\dot{m}_{MAIN}(T_{0\,MAIN}) + 3 \cdot \dot{m}_{SS}(T_L) = (\dot{m}_{END})(T_{0\,END})$ = (22 kg/s) x (240 K)

The sample calculation for the flow properties along the SS streamline (T, E, and L) was included in Appx. G.5, with the results presented here in Table 8. The flow conditions at Point L referred to the application of the K_{SE} loss, and not necessarily when the flow had fully expanded to $\varnothing_{MC}$. It implied that the Geometry and Static Pressure of the loss point (L) were retained from the SS Exit (E) conditions; i.e. $\mathbb{A}_L = \mathbb{A}_E$, and $P_L = P_B$. The 'SS Exit Actual (L)' column in Table 8 revealed the SS flow properties after incurring the K_{SE} loss. The significant P_0 loss resulted in M reduction (M2.19 to M1.01), and T increase (144.7 K to 235.0 K). This represented a significant loss in cooling potential. There were 2 properties from Table 8 that were important to the design of the Temperature Mixing Mechanisms: Mass Flow Rate ($\dot{m}$), and SS Exit Area ($\mathbb{A}_E$). $\mathbb{A}_E$ allowed for the iterative refinement of the K_{SE} value. $\dot{m}_{SS}$ = 6.8 kg/s reflected the contribution from 1 of 3 SS Tunnels; i.e. cumulative $\dot{m}_{SS}$ = 20.4 kg/s, and $\dot{m}_{MAIN}$ = 1.6 kg/s. Assessing the cumulative $\dot{m}_{SS}$ expected of the Rotary Compressor (20.4 kg/s), it was apparent that the K_{SE} loss had a considerable impact on the SSEC concept implementation. The Volumetric Flow Rate of the Supply Device was calculated, using Table 8 values, as: $\dot{\forall}_{SS\,(TOTAL)} = \frac{\dot{m}_{SS}}{\rho_{Throat}} = \frac{20.4}{7.41}$ = 2.75 m^3/s.

Table 8. Mixing Chamber Inlet results (calculated using EES)

Property	SS Stagnation (0)	SS Throat (T)	SS Exit Ideal (E)	SS Exit Actual (L)
P_0 [Pa]	950000	950000	950000	158354
P [Pa]	950000	501868	90672	$P_L = P_b$ = 83000
T [K]	283.2	236.0	144.7	235.0
ρ [kg/m^3]	11.69	7.41	2.18	3.72
M	-	1	2.19	1.01
V [m/s]	-	307.9	527.4	311.1
$\dot{m}$ [kg/s]	-	6.8	6.8	6.8
$\mathbb{A}$ [m^2]	-	2.98 x10^{-03}	5.91 x10^{-03}	$\mathbb{A}_L = \mathbb{A}_E$
Ø [mm]	-	61.58	86.70	$\varnothing_L = \varnothing_E$

This Supply capacity (2.75 m^3/s) could only be achieved with 6 of the specified Rotary Compressors (6 × 0.5 m^3/s > 2.75 m^3/s). The compressors were set in 3 pairs (connected in parallel) corresponding to the 3 SS Tunnels. The unavoidable reality of 6 SS Mechanisms (Compressors, Receivers and Accessories) effectively tripled the cost of the SSEC concept; this revision was addressed in the Design Specification (Section 14.3). With the results of the Pseudo-Isentropic Base Model ($\dot{m}_{SS}$, $\dot{m}_{MAIN}$, and T_{SS}), the various Temperature Mixing mechanisms were calculated in the next subsection (Section 12.2).

12.2 Temperature Mixing Mechanisms

The Temperature Mixing Mechanisms, as described in Section 11.2, fulfilled the fundamental MC purpose – efficient mixing of the Cold and Hot streams to produce the Resultant flow. This part of the Analytical Modelling concerned the immediate exposure of the Underexpanded SS stream into the Main

Centrifugal stream, and ended at the WT Inlet ($\dot{m}$ = 22kg/s at T_0 = 240 K). The calculations for the Mixing Mechanisms were included in Appx. G.6, along with the Perpendicular configuration results. The results for the Parallel configuration, which was the configuration used in the Final MC Design, were presented in this section. The compilation of results (L_M = 0.05 m, $L_{CO\text{-}FLOW}$ = 0.8766 m, X_C = 0.8464 m) were depicted in Figure 28 Part A. The MC Extension, depicted in Figure 28 Part B, was implemented immediately aft of the Parallel Mixing Mechanism (prior to the WT Inlet). It was designed using the Dimensionless Variables (Section 11.1) which produced: Pr = 0.015, $L_{HFD\ SS}$ = 5.218 m, and β_{SS} = 0.9731. These results produced: the length required for TFD Flow (where $L_{HFD} > L_{TFD}$; if Pr << 1), and the need for physical Convective Devices. The Convection Devices were designed specific to each application; to directly interact with the respective flow stream orientations. Using the Minimum dimensions (L_{MC} and $Ø_{MC}$), and the Fluid Mechanic–specific Inlet conditions (P_0, T_0, and $\dot{m}$), a range of MC concepts were generated in the next subsection (Section 12.3).

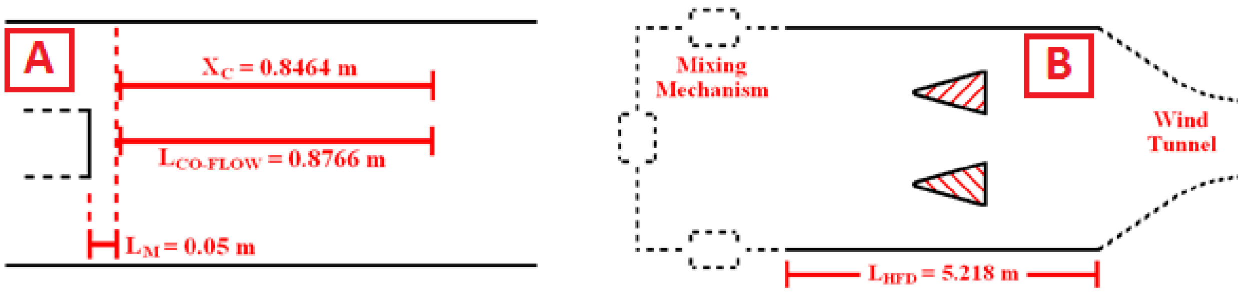

Figure 28. Temperature Mixing Mechanisms, Part A) Parallel Mechanism Compilation (L_M, X_C, and $L_{CO\text{-}FLOW}$), Part B) Mechanism Extension (L_{HFD}) with Convective Devices [NOT TO SCALE]

12.3 MC Concepts

The Base Model and Temperature Mixing Mechanisms provided the foundation (Inlet conditions and MC dimensions) from which to develop the MC concepts. However, at no point was this analytical approach capable of representing the actual 'mixing behaviours' within the MC. These behaviours included: Turbulent Diffusion, expansion of the SS Jet, obstruction of Main flow, and the benefit of Convective Devices in dispersing the flow cores. These behaviours were especially relevant in the MC Design, as the Velocities and $\dot{m}$ of the flows concerned were significantly different. Without a mathematical estimation method capable of determining these parameters, the Design relied on preliminary Numerical models (CFD) of a wide variety of MC concepts. The concepts were identified in 4 categories:

1. Angles of Entry for the SS and Main flows (with respect to the Resultant Flow).
2. Number of SS Jets utilized.
3. Positioning of the SS Jets within the MC.
4. Convective Mixing Devices placement and number.

The actual simulation sets comprised of variants across all 4 categories (compounding the techniques); in an attempt to determine the mixing effectiveness. This mixing effectiveness was largely quantified by:

- Resultant T_0 – in achieving the Design Point (T_0 = 240 K).
- Flow profile within the MC – producing a consistent Resultant flow profile prior to the WT Inlet.
- P_0 loss – minimizing SS P_0 losses in the Mixing Mechanisms, and achieving the required $P_{0\ WT\text{-}IN}$.

The development and evaluation of the various MC concepts proved to be a considerable portion of the Project; both in terms of computational time and analytical frameworks. The analysis consisted of simulating 3-D models of different possible configurations. With each configuration, the Inlet conditions and corresponding Mixing Lengths had to be calculated (specific to the concept). These analytical results were then incorporated into the respective preliminary CFD model. The CFD models were geared towards improving turnaround time, as opposed to resolving the finer Fluid Mechanics of each configuration (viz. near-wall behaviour, and eddy resolution). The Mesh cell sizes (coarse mesh) and Solution settings (1^{st} Order) were focused on reducing simulation times, and producing a solution that was indicative of the bulk flow behaviour. A limited range of these MC Concept variants, highlighting the distinct attributes of the respective categories, was included in Appx. P.1. The results of which were compiled using the same 4 categories as the variants, despite compounding techniques, and included in Appx. P.2. The concept parameters best suited to the current Design were listed in this section with a brief summary of intended benefits. It was important to note that these conclusions pertained to the final compound configuration, which was a combination of all these features, and not necessarily the properties of any single parameter taken in isolation.

Angle of Entry = Parallel (Appx. P.2.1)
- Reduced $P_{0\,SS}$ loss, since there were no collisions with MC walls (as with perpendicular flow).
- Predictable flow distribution of the SS Jet; effectively a 1-D Mixing Mechanism.
- Reduction of Main flow blockage, and avoidance of Main flow recirculation and reversal.

Number of SS Jets = 3 jets (Appx. P.2.2)
- Decreased flow per Jet prevented $\emptyset_{MC}$ obstruction and allowed space for Main flow occupancy.
- Reduced $\dot{m}_{SS}$ per SS Exit reduced each Jet core length (and therefore each Mixing Length).
- Multiple Jets allowed for variation of T_0 via 'shutting-off' of individual Jets. 3 Jets allowed for 4 immediate stages of Temperature variation (0 - 3 Jets active).

Positioning of SS Jets = In-line Sequence (Appx. P.2.3)
- Prevented each individual Jet from directly interfering with the $\frac{P_0}{P_B}$ relationship of other Jets.

Convective Devices = Intermediate Conical Pieces (Appx. P.2.4)
- Conical Pieces aft of each Jet allowed for the direct dispersion of each SS Jet core.
- The discontinuity associated with the abrupt backend of each Conical Piece was replaced with the subsequent Jet entry; resulting in a 'supplemented' continuity to the cumulative stream.

12.4 Component Sizing and Associated Losses

The MC Concept conclusions (Section 12.3), allowed for a fully realized geometric model to be constructed. The layout of the MC, depicted in Figure 29, consisted in respective order of:

7. Centrifugal Supply at the Main Inlet (MAIN IN).
8. Rotary Compressor Supply at each of the 3 SS Inlets (SS_X IN).
9. Convective Flow Divider prior to each SS Inlet.
10. Intermediate SS_X Mixing Length for each SS Flow introduction.
11. Minimal Length for Temperature Equilibrium ($T_0 \equiv$ Length) of the total flow; sized according to T_{HFD}.

The sizing, geometry details, and associated losses of the individual components were included in Appx. H.2. In keeping with the minimalistic geometric profiles of the WT, the MC also utilized basic geometries (limited curvature). The complete MC was presented in Figure 30.

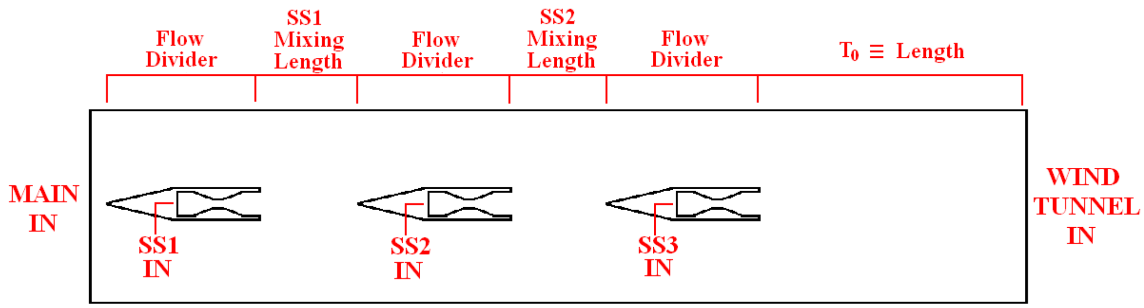

Figure 29. Mixing Chamber layout with components in respective order (NOT TO SCALE)

The numbering format depicted in Figure 30 corresponded to the 10 Key Points along the flow profile; used in developing the Analytical Model (Section 12.5). The Key Points (and associated losses) included:

1. Main Flow Inlet (**K_{NOZ} = 0.05**)
2. End of Nozzle
3ss. End of 1st Supersonic Inlet flow (including expansion loss **K_{SE} = 0.92**)
3. Mixing of 1st Supersonic and Main flows
4. Start of 1st Conical Splitter (**K_{SPLIT} = 0.11**)
5. End of 1st Conical Splitter
6ss. End of 2nd Supersonic Inlet flow (including expansion loss **K_{SE} = 0.92**)
6. Mixing of 2nd Supersonic and preceding flows
7. Start of 2nd Conical Splitter (**K_{SPLIT} = 0.11**)
8. End of 2nd Conical Splitter
9ss. End of 3rd Supersonic Inlet flow (including expansion loss **K_{SE} = 0.92**)
9. Mixing of 3rd Supersonic and preceding flows
10. End of Mixing Chamber

Certain components of the MC required additional design considerations:

- The Main Flow Inlet component consisted of the contraction from the Centrifugal Fan outlet diameter ($Ø_{CENT}$ = 755 mm) to the MC diameter ($Ø_{MC}$ = 700 mm).
- The SS Tunnels were modelled complete with a Contraction, Throat ($Ø_T$ = 62.5 mm), and Expansion ($Ø_{SS}$ = 88 mm). The losses for this component were based on the K_{SE} optimization (Section 12.1).
- The Conical Splitters served 2 functions: to aid in splitting the preceding SS Jet core, and to create the physical space required for the subsequent in-line SS Tunnel. The K_{SPLIT} loss associated with the Conical Splitter was estimated using the same CFD approach as $K_{ENG\ LOSS}$ (Section 6.2), and was included in Appx. I.2.

The assimilation of MC components was completed with intermediate lengths between the SS Inlets and Conical Splitters (2000 mm each), and an extended backend length beyond the 3rd SS Inlet (3500 mm). As detailed in Section 12.2, these MC lengths (intermediate and extended backend lengths) followed the Parallel mixing mechanisms: $L_{CO\text{-}FLOW}$ = 0.877 m (SS Jet core length) and L_{HFD} = 5.218 m (consistent Velocity profile). It was most economical (length wise) to dissipate each Jet core with $L_{CO\text{-}FLOW}$, and then develop the collective flow at the end using L_{HFD}. The actual MC lengths however, as depicted in Figure 30, used $L_{CO\text{-}FLOW}$ and L_{HFD} as the starting points. These lengths were subsequently refined / reallocated on the basis of the CFD results. The reallocation of the MC lengths was made for the following reasons:

- The $L_{CO\text{-}FLOW}$ was the minimum length required for the SS Jet core to dissipate. The continually increasing $\dot{m}_{MAIN}$ (with the addition of each preceding $\dot{m}_{SS}$) encapsulated the subsequent SS Jet cores even further (with the respective core length elongated).

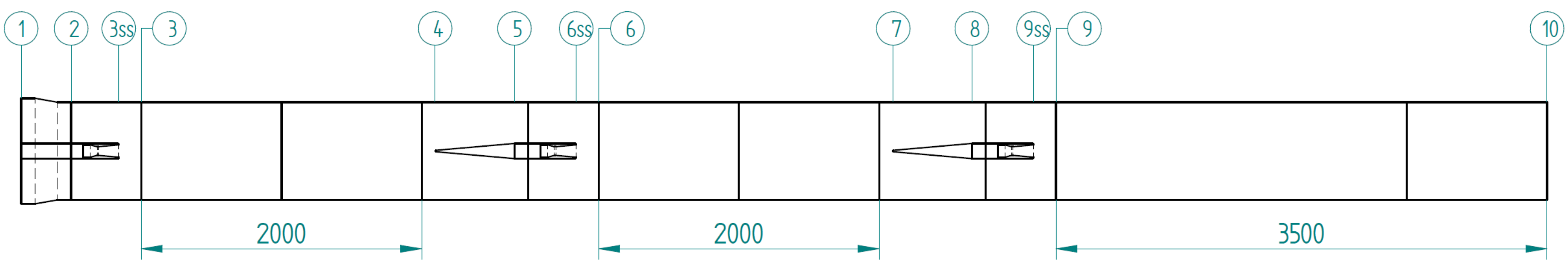

Figure 30. Complete Mixing Chamber (including intermediate lengths, $T_0 \equiv$ length, and Key Point numbering)

- The intermediate lengths (2000 mm) had to budget for the SS Jet core dissipation, and for the development of an intermediate mixed flow profile. As described in Chuech[45], flow mixing between the Main and SS flows only ensued in the subsonic region (aft of $L_{CO\text{-}FLOW}$). The intermediate length allowed for the subsequent Conical Splitter to alter the stream path of the intermediate mixed flow, as opposed to inferring the bulk of the Splitter P_0 loss on the SS stream.
- The main purpose of the extended backend length (3500 mm) was to achieve Temperature Mixing, and produce TFD flow. As established by Pr = 0.015 (Section 12.2), the flow was TFD well before it was HFD. It implied that the entire L_{HFD} was not necessary to achieve Temperature Mixing.

12.5 MC Analytical Model

The MC Analytical Model was created and verified using the same procedure as the WT (Section 6.3). The results of the MC Analytical Model provided the Supply Device Inlet conditions ($P_{0\ SS}$, $\dot{m}_{SS}$, $P_{0\ CENT}$, and $\dot{m}_{CENT}$) to satisfy the WT Inlet requirements (P_0, T_0, $\dot{m}$). The sample calculation, included in Appx. G.7, focused on the SS Expansion and Mixing. The important flow properties from the Analytical Model were presented in Table 9; in correspondence with the 10 MC Key Point locations. The properties for the SS Tunnels were common across all 3 entries (3_{SS}, 6_{SS}, and 9_{SS}), and were listed in Table 9 separate from the Key Point format. The flow properties included: Distance along MC length (X), Stagnation Pressure (P_0), Static Pressure (P), Stagnation Temperature (T_0), Static Temperature (T), Mach number (M), and Mass Flow Rate ($\dot{m}$). Table 9 displayed the MC objectives in boxed cells. The MC Outlet results compared to WT Inlet Requirements (Section 7.5) as: P_0 = 98425 Pa (required = 98500 Pa), T_0 = 240.1 K (required = 240 K), $\dot{m}$ = 22.03 kg/s (required = 22 kg/s).

The solution to the Analytical Model presented the Supply Device capacities (Rotary and Centrifugal) in achieving the MC Outlet requirements. T_0 and $\dot{m}$ were interpreted as the most relevant MC parameters in achieving the Test Section conditions; as these values could not be manipulated between the MC Outlet and OTS Inlet. These parameters were replicated by the MC Outlet with Max error ≈ 10^{-03}. The Main Inlet (Key Point 1) Supply requirements at Design Point represented the minimum Centrifugal Fan contribution across all Altitude levels. The $P_{0\ MAIN\ IN}$ requirement (83007 Pa) was only slightly discernible from JHB ISA Atmospheric Pressure (83000 Pa). However, when applied across the large diameter of the Main Flow supply 'interface' ($Ø_{MAIN\ IN}$ = 0.7 m), it resulted in a noticeable $\dot{m}$ contribution.

$P_{0\ MAIN\ IN}$ corresponded to the minimum $\dot{m}_{MAIN\ IN}$ contribution (1.64 kg/s). However, this $P_{0\ MAIN\ IN}$ did not necessarily imply the positive Pressure differential along the MC length; in order to dictate the Resultant flow path. The objective of the Analytical Model was to determine the corresponding $\dot{m}$ and T_0 contributions, from the various Supply Devices (Main and SS) in order to achieve WT Inlet conditions. On face value, $P_{0\ MAIN\ IN}$ presented a concern for the final compiled Design; i.e. MC and WT. This was because the WT Exit Static Pressure was very similar ($P_{WT\text{-}OUTLET}$ = 83000 Pa ≈ $P_{0\ MAIN\ IN}$ = 83007 Pa). It 'created the image' of the SS flows reversing upon entry into the MC, and exiting through the Main flow orifice; due to the path of lower Pressure resistance. It may be necessary that, in the development of the Numerical Model (Section 13.4), $P_{0\ MAIN\ IN}$ be increased to enforce the flow path direction within the MC. The increased $P_{0\ MAIN\ IN}$ however must maintain the $\dot{m}$ and T_0 contributions of the Analytical Model.

Table 9. Selected Results from Mixing Chamber Analytical Model (WT Inlet objectives boxed)

Point Number	X [mm]	P_0 [Pa]	P [Pa]	T_0 [K]	T [K]	Mach	$\dot{m}$[kg/s]
3_E, 6_E, 9_E	-	950000	90637	283.2	144.7	2.19	6.8
3_{SS}, 6_{SS}, 9_{SS}	-	158354	83000	283.2	235.4	1.01	6.8
1	0.0	83007	83000	298.2	298.1	0.01	1.64
2	356.0	83007	82997	298.2	298.1	0.01	1.64
3	856.0	97510	97335	247.6	247.5	0.05	8.44
4	2956.0	97505	97330	247.6	241.7	0.05	8.44
5	3516.0	97485	97301	247.6	247.4	0.05	8.44
6	4116.0	97895	97335	242.2	241.8	0.09	15.23
7	6216.0	97880	97320	242.2	241.8	0.09	15.23
8	6776.0	97815	97227	242.2	241.7	0.09	15.23
9	7376.0	98496	97335	240.1	239.3	0.13	22.03
10	10876.0	98425	97263	240.1	239.3	0.13	22.03

The SS Inlet (3_{SS}, 6_{SS}, 9_{SS}) Supply requirements at Design Point represented the maximum Rotary Compressor contribution across all Altitude levels. The $\dot{m}_{SS}$ requirement was collectively = 20.4kg/s. Grouping the Supply Devices, according to the 3 Jet entries, put a respective demand of 6.8 kg/s per Supply location. As described in Section 12.1, $\dot{m}$ = 6.8 kg/s corresponded to $\dot{\forall}$ = 0.92 m^3/s at each of the SS Supply locations. It was important to note that, even at Maximum SS Cooling (Design Point), the selected Supply Devices were still operating slightly below full utilization. The $P_{0\,SS}$ could be increased from 950000 Pa to 1083000 Pa, and the total $\dot{\forall}$ could be increased from 2.75 m^3/s to 3 m^3/s. This reservation allowed development room for unforeseen P_0 losses; without escalating equipment costs.

The T_0 values in Table 9, from Point 1 to Point 10, decreased with a diminishing effect upon each SS flow contribution (Point 3, 6, and 9). The 1st SS Jet contribution cooled the MC flow from 298.2 K to 247.6 K (i.e. $\Delta T_{0\,SS1}$ = 50.6 K). This cooling contribution 'appeared' significantly larger than the subsequent SS Jets; $\Delta T_{0\,SS2}$ = 5.4 K and $\Delta T_{0\,SS3}$ = 2.1 K. This was due to the existing MC T_0 at Key Point 3 (1st Jet). The Main flow had T_0 = 298.2 K, but only had $\dot{m}$ = 1.64 kg/s. The 1st Jet contribution, $\dot{m}$ = 6.8 kg/s at T_{SS} = 235.4 K, far outweighed that of the Main flow ($\dot{m}$ wise). Using the Modified Mixing Chamber Energy Equation (eqn. 30), the intermediate resultant T_0 (after the 1st Jet) reduced significantly. Equation 30 also explained why each subsequent SS Jet had a lower cooling capability. The accumulating $\dot{m}$ along the MC length, with each preceding SS Jet $\dot{m}_{SS}$ contribution, limited the influence of each subsequent SS Jet.

With the Analytical Model in place, demonstrating the cooling capacity of each SS Jet, the concept was represented using Numerical Methods in the next section (Section 13). The Numerical Model was based on the Supply Device Inlet flow properties and MC geometry from the Analytical Model. It determined the $P_{0\,MAIN\,IN}$ necessary to enforce the intended flow path within the MC, whilst maintaining the expected T_0 and $\dot{m}$ contributions. The model also interpreted the SS Jet core dissipation and Temperature Mixing in the subsonic regions; that were previously only predicted by dimensionless variables (Section 12.2).

13 Mixing Chamber (MC) Numerical Modelling

The Mixing Chamber (MC) Numerical Model was developed to identify the various Inlet settings (Centrifugal Fan and Rotary Compressor) required to achieve the Test Section conditions at Design Point (M_{TS} = 0.7 and T_0 = 240 K). The Numerical Model was compared to the respective Analytical Model to validate: MC Entrance/Exit conditions (Main IN, SS_X IN, Wind Tunnel IN), and the flow properties along the MC length. In order to interpret the effects of the MC model on the Test Section conditions, the Numerical Model had to comprise of both the MC (Figure 30) and WT (Figure 14). The Complete Geometry (MC+WT) was created in 3-D and halved along the vertical axis (axisymmetric). The MC had to be rendered in 3-D in order to capture the rotation and swirl of the Turbulent Mixing mechanisms.

The MC Numerical Modelling process followed from the conclusions of the WT Numerical Model (Section 7.5). In implementing these choices, two of the Roache [29] testing guidelines were relaxed:

- The Numerical Methods were of 1st Order Accuracy; detailed in Section 13.2.1.
  The Roache [29] guideline required ≥ 2nd Order Accuracy. In lieu of a more diffusive Turbulence Model, the Solution required the turbulence exaggeration inherent of 1st Order methods. It was also worth pointing out that 2nd Order Convergence would prove to be difficult due to the discontinuities (Shocks) within the flow. ANSYS [20] recommended defaulting to 1st Order accuracy for such cases.
- A Single Mesh was tested (no Mesh Independence performed); detailed in Section 13.1.1.
  The Roache [29] guideline required a range of solutions across multiple mesh grids. The Sensitivity Analysis was replaced with Dynamic Mesh Adaptation; as was previously concluded with the WT Mesh (Section 7.3.1). This was due to the method of extracting results (MWA); which did not converge to a singular asymptotic solution upon mesh refinement. The Complete Geometry (MC+WT) was meshed using the Archetype Cell Sizing; with Dynamic Mesh Adaptation.

The validation methods of the WT (using Solution Convergence, and comparison to Analytical Model) had to be refined for the MC application. The 1st Order methods reduced the accuracy of the converged Solution, and necessitated additional means of validation. This was accomplished using previously published externally sourced results; a form of validation described by Jauregui [30]. The exact application of the SSEC Concept prevented direct objective-based comparison to external results. The Concept concerned the far-field behaviour of an Underexpanded SS Jet in a moving flow, and focused on the Temperature Mixing in the resultant stream. Typical published results, however, focused on the core length of the supersonic jet expansion and the decay of the downstream subsonic core. None of these published result sets concerned Temperature Mixing. The comparisons were therefore made using the available parameters (potential core length and subsonic core decay). These comparisons were detailed in Section 13.3, and validated the implementation of the SS Jets in the MC. From this point of validated jet expansion behaviour, the MC Numerical Model then interpreted the Temperature Mixing within the resultant flow and compared the results to the MC Analytical Model.

13.1 Meshing (ICEM)

The meshing was performed using the same program and computer as the WT (Section 7.1). The Complete Geometry (MC+WT) mesh cell sizing was specified using the Archetype Mesh Settings from Section 7.3.1, barring a few SS Tunnel-specific modifications, as specified in the next subsection.

13.1.1 Mesh Cell Size Estimation

The Mesh Cell Sizing followed the same procedure as that of the WT Model (Section 7.1.1). The limitations that affected the cell count in the WT mesh (1 500 000 cells) were more restrictive here; as the MC geometry was modelled together with the existing WT geometry. The Complete Geometry (MC+WT) was rendered in order to demonstrate: how the various MC Inlet conditions affected the Test Section flow conditions, and how the intended flow path was maintained along the length of the Complete Geometry (MC+WT). Due to the size of the geometry, and limited cell count, the required 1st layer cell sizes for y+ compliance were not achievable. This analysis of MC 1st Layer Cell Size, with regards to y+ conformance, was included in Appx. J.2.The mesh instead focused on resolving the flow at the core of the MC; interpreting the performance measures of Turbulent Mixing and Thermal Diffusion. It was established in the WT Mesh Sensitivity Analysis (Section 7.3.1) that the particular method of extracting results in this Project (MWA - Mass Weighted Averages across vertical 'Ghost' planes) did not demonstrate any asymptotic behaviour between the multiple mesh variants tested. This method was significantly different from analysing a flow property along a single defined surface (such as Lift/Drag along an aerofoil). The WT results, across the ghost planes, were compromised by the unresolved wall conditions (y+ non-conformance) and the recirculation incurred during flow expansion (OTS and large Diffusers). Whilst this method made Mesh Independence unattainable, it did focus the analysis on the bulk flow behaviour at the WT core; allowing for the Global parameters to be monitored along the WT length. These issues were also faced in the MC Numerical Model. The SS Jet cores dissipated into the Main flow through dispersion and recirculation; partially due to the convective effects of the Conical Devices. These instances of recirculation occurred across the MWA 'Ghost' planes. It resulted in a net vector summation, due to different directional components, that did not conform to asymptotic behaviour upon mesh refinement. Therefore, extrapolation techniques could not be performed.

The MC Mesh was instead generated using the conclusions from the WT Mesh (Section 7.5), i.e. Standard Cell Size Archetype settings with Dynamic Gradient Mesh Adaptation, including:

- Archetype Mesh element size: Each surface spanned by ≥ 5 elements. The individual surfaces were meshed according to the Archetype $\frac{\text{size of surface}}{\text{number of cells}}$ ratio.
- Certain 'surfaces of interest' (such as Conical Splitter tips) received even greater cell refinement.
- Dynamic Mesh Refinement: The Solver was programmed with Gradient Adaptation.

These Archetype settings described the cell sizing for the various MC surfaces. The cell sizes for the SS Tunnels however, required a specific cell allocation ratio in order to capture the SS Jet expansion. The cell size was specified by Velikorodny [46] as being less than 1/16 of the SS Tunnel Exit diameter:

$$\textbf{i.e. SS Tunnel cell size} < \frac{\boldsymbol{\emptyset_E}}{\mathbf{16}} \qquad \ldots (41)$$

The Complete Geometry (MC+WT) Mesh was generated to capture the sudden expansion of the Underexpanded (UE) SS Jet into the MC. It captured the flow properties aft of the SS Tunnel Exit (ensuring UE flow), and the downstream Temperature Mixing of the subsonic jet core with the MC flow. The mesh however, was not fine enough to capture the repeated shock cell structure of the UE jet core; due to the limited cell count available. In order to compare the MC Numerical Model to published results, the scenario of the SS flow expansion had to be rendered in isolation. This method allocated the total cells available (1 500 000 cells) to rendering the UE shock cell structure. Whilst this method did not comprehensively resolve the discontinuity of each shock cell, it did render the macroscopic pattern of the repeated shock cell structure. This Isolated SS Model provided a means from which to compare the implementation of the SS Jet in this Design to the published sources; detailed in Section 13.3. It was important to state here that the UE repeated shock cell structure in the Isolated SS Model resulted in the extension of the supersonic region of the SS Jet core. Menon [53] encountered this scenario in comparing the shock cell length of UE Jets using experimental and numerical methods. In the thesis, the numerical result was produced using the Spallart-Almaras Turbulence Model which simulated a shock cell length longer than that observed in the experiment; due to the less diffusive nature of set Model. It was observed however, that the flow fields for both sets of results maintained qualitative agreement. The limited Turbulence Model only served to scale the respective shock cell lengths. This behaviour was also observed in this Project, when comparing the Isolated SS Model and the MC Numerical Model. The increased mesh resolution of the Isolated SS Model revealed a scaled extension to the shock cell structure, but the results maintained qualitative agreement with the MC Numerical Model. The behaviour delayed the mixing process, lengthwise, by offsetting the subsonic region of the Jet. This Jet core flow extension was pre-emptively factored into the MC Design, via extension of the intermediate lengths in Section 12.4 (2000 mm). These lengths allowed for the dissipation of the UE SS Jet shock cell structures before collision with the ensuing Conical Splitter (intended to act only on the subsonic jet core). With the exception of this extended supersonic Jet core, the MC Numerical Model represented the intended effects of the UE flow; including the large Shock Diamond immediately upon Jet entry.

13.1.2 MC Mesh

The mesh was generated for the Complete Geometry (MC+WT), depicted in Figure 31 Part A. The zoomed-in geometry of the MC was depicted in Figure 31 Part B; showing the specific MC surfaces. The surfaces of the model were defined (labelled in Figure 31 Part A and B), and meshed with the single Archetype Mesh cell size. The Isolated SS Model (not shown here) depicted a single SS Jet entering the MC flow, followed by an extended length (3500 mm) without any Convective Devices. This Isolated SS Model was meshed using the same Archetype mesh settings, but included a concentrated mesh density region that spanned the Jet core length. Both meshes were generated with Unstructured Tetra/ Mixed cells using the Robust (Octree) Method, and met the respective testing requirements. The Complete Geometry (MC+WT) mesh captured the Temperature Mixing of the various flows (within the Subsonic region), and the Isolated SS mesh captured the UE SS Jet expansion (including the Supersonic shock diamonds). The detailed mesh procedures, including the mesh cell sizes, were included in Appx. K.2.

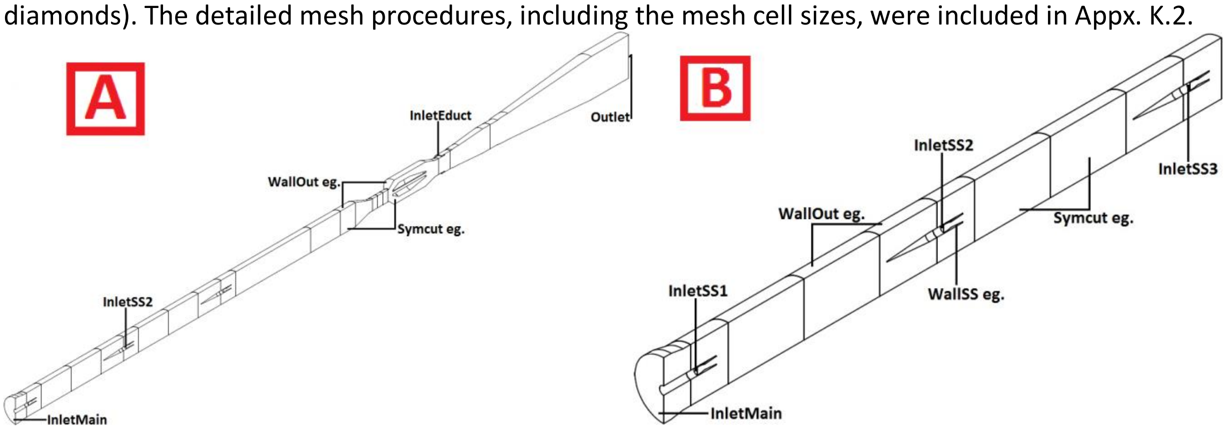

Figure 31. Isometric View of model geometries with symmetrical cut along the vertical axis. Part A) Complete Geometry (MC+WT), Part B) Isolated MC

13.2 Solution (Fluent)

The solution was obtained using the same program and computer as the WT (Section 7.2). The following procedure detailed the settings for both the Complete Geometry (MC+WT) and Isolated SS Model.

13.2.1 Solver Settings

The Fluent Solver was run with the mesh of the Complete Geometry (MC+WT). The Design Point conditions at the Test Section (M0.7, T = 219 K, and runtime = 5 min) were still the performance measures, but the locations for Inlet specifications were changed (viz. Main Centrifugal Inlet, and 3 SS Inlets). The Solver retained certain settings from the WT Numerical Model (Section 7.2.1), and amended others that pertained specifically to the MC implementation. The amendments concerned the Turbulence Modelling, 1st Order Solution methods, and the respective contingencies. The definitions of, and reasoning behind, the setting selections were included in Appx. L.3.

- **Retained Solver Settings (from Section 7.2.1)**

Density based (capable across transonic regime), Coupled (with rudimentary Under-Relaxation factors and Artificial Time Step), Steady State (Pseudo Steady Defined by Cr), Implicit Solver (Cr = 1). Compressible Boundary Types (Pressure Inlets and Pressure Outlet) with Operating Pressure = 0 Pa.

- **Turbulence Modelling (Realizable k_{TKE} - ε_{TDR}, T.I. and $Ø_H$)**

The decision was then to retain the Realizable k_{TKE} – ε_{TDR} model (from Section 7.2.1), despite the k_{TKE} – ω_{SDR} model being best suited to interpreting Turbulent Diffusion. This was in response to the y+ non-conformance of the mesh cell size; in an attempt to prevent solution divergence. The lack of diffusivity and Jet core deterioration of the k_{TKE} - ε_{TDR} model, discussed in Appx. L.3.1, adversely affected the interpretation of the Mixing Mechanism within the MC. The over-simplification of the mixing had to be compensated for by other means. This was done using 1st Order Solution methods, as described in the next subsection, to exaggerate the Turbulent Diffusion.

- **Solution Methods (1st Order Upwind)**

The MC Numerical methods were performed with 1st Order Accuracy only. In the WT Numerical Model (Section 7.2.2), the solution was performed to 1st Order convergence (Qualitative), and then refined to 2nd Order methods (Quantitative - Global $\dot{m}$ balance). The reason the WT 1st Order solution had incorrectly tracked the Global $\dot{m}$ balance was due to turbulence exaggeration (identified in Section 7.5). This behaviour, described by Bakker [47] as 'False Diffusion', was discussed in Appx. L.3.2. It was utilized here in the MC Numerical Model as an asset; in lieu of a more diffusive Turbulence Model. The 1st Order Solution emphasized the Mixing Mechanism, and implied greater Turbulent Diffusion along the inter-stream boundaries. By implementing this approach, the accuracy of the Global $\dot{m}$ balance had to be resolved through other means; since there was no 2nd Order refinement. The Convergence Criteria (both Qualitative and Quantitative) had to be changed, from that of the WT (Section 7.2.1), in order to reflect the intentions and contingencies of this pursuit.

- **Convergence Criteria (Continuity and Energy RMS < 0.00025)**

The Quantitative Convergence across the Complete Geometry (MC+WT) was tracked using a similar monitor to that implemented for the WT, including: the Main Inlet, 3 SS Inlets, Eductor Inlet, and Outlet flow. Due to the 1st Order exaggeration of recirculation in the MC, it was necessary to implement further means of Continuity tracking. This was achieved using stricter RMS requirements for the cell-to-cell tracking. The Qualitative Convergence criteria for Continuity and Energy were refined even further than the Archetype residual (0.0005 from Section 7.3.2) to 0.00025, with all other Archetype residuals retained. The simulation was performed to 1st Order convergence according to these refined RMS residuals. This converged solution was then continually iterated at these RMS specifications, Energy and Continuity < 0.00025, until Quantitative Convergence was achieved as close as possible ($\sum \dot{m}_{IN} = \dot{m}_{OUT}$).

13.2.2 Solving Outline

The Complete Geometry (MC+WT) mesh was read into the Fluent Solver; using the previously defined surfaces. The Solution was performed to 1st Order residual convergence, and iterated beyond until Quantitative Convergence. The Global mass flow rate balance ($\dot{m}_{IN} = \dot{m}_{OUT}$) at convergence was:

$\dot{m}_{MAIN}$	$+ \dot{m}_{SS1}$	$+ \dot{m}_{SS2}$	$+ \dot{m}_{SS3}$	$+ \dot{m}_{EDUCT}$	$= \dot{m}_{OUT}$	
1.05	+ 3.41	+ 3.42	+ 3.42	+ 2.64	= 13.94	→($\Delta\dot{m}$) = 0 kg/s

The values of the various RMS residuals at 1st Order convergence were:

Continuity = 2.498 $\times 10^{-04}$	Energy = 2.049 $\times 10^{-04}$	
X- Velocity = 4.286 $\times 10^{-04}$	Y- Velocity = 1.534 $\times 10^{-04}$	Z- Velocity = 1.134 $\times 10^{-04}$
k (TKE) = 2.780 $\times 10^{-04}$	ε (TDR) = 3.087 $\times 10^{-04}$	

There were 2 important residual values that stood out: the X- velocity and Continuity. All residuals converged to the specified requirements (Energy and Continuity < 0.00025, all others < 0.0005), but the Continuity and X-Velocity residuals both approached the respective limits. This behaviour was attributed to the recirculation within the MC. The expansion of each of the SS Jets created intermittent blockages of the preceding Main flow; resulting in a rubber-banding effect in the cell-to-cell tracking of both the X-Velocity and Continuity. The detailed Solving procedure, including the convergence analysis, was included in Appx. L.4. The results of the MC Numerical Model were presented and analysed in Section 13.4. Before this analysis however, the current SS implementation (via the Isolated SS Model) was compared to the published sources in the next subsection.

13.3 Solution Validation (Appx. D)

Previously, in the WT Numerical Model (Section 7), the validation methods included the Numerical Solution Convergence and comparison to the Analytical Model. The MC Numerical Model, which formed the research component of the Project, utilized Turbulent Diffusion mixing mechanisms that were not readily identifiable using conventional analytical modelling. The Model validation required additional methods of comparison; in the form of previously published experimental data. The analyses of these published sources included: SS Tunnel Exit flow properties, Potential Core Lengths, and the subsonic Velocity Decay. The MC Numerical Model analysis however, concerned the far-field Temperature Mixing of the SS Jets. As such, the MC Model domain was much larger; focusing on the downstream locations rather than the near-field SS Jet entries. The cell sizes for the MC were larger and more evenly spaced; and were unable to adequately resolve these near-field flow properties for comparison purposes. As stated in Section 13.1.1, this was addressed by rendering the SS Jet flow expansion in isolation. It allocated the total cell count (1 500 000 cells) to the resolution of the UE SS shock diamond structure. This Isolated SS Model was presented in Figure 32. The model replicated the geometry of the MC entry and 1st SS Jet (SS1). SS1 was selected (as opposed to the other 2 Jets) for model replication due to the limited influence of the surrounding Main flow; providing a Solution more comparable to published data. The Isolated SS Model, however, excluded the 1st Conical Splitter. It replaced the Convective Device with a constant diameter length equivalent to the extended MC backend length (3500 mm); so as to assess the subsonic Jet core Velocity Decay without obstruction. The mesh was enhanced via a cell concentration (max cell size = 10) at the SS Jet Exit; dimensions included $Ø = 1.5 \times Ø_{SS}$ and L = 1500 mm. This limited concentrated volume was sufficient to capture the shock diamond formation; detailed in Section 13.3.1. The Isolated SS Model was simulated using the same settings as the MC Numerical Model (Section 13.2.1). The Isolated SS Model Outlet conditions (P_{EXIT}) however, were varied to achieve the respective $\dot{m}$ contributions from the Main and SS1 Inlets as close as possible. The detailed Solving procedure, and convergence analysis, for the Isolated SS Model was included in Appx. L.5.

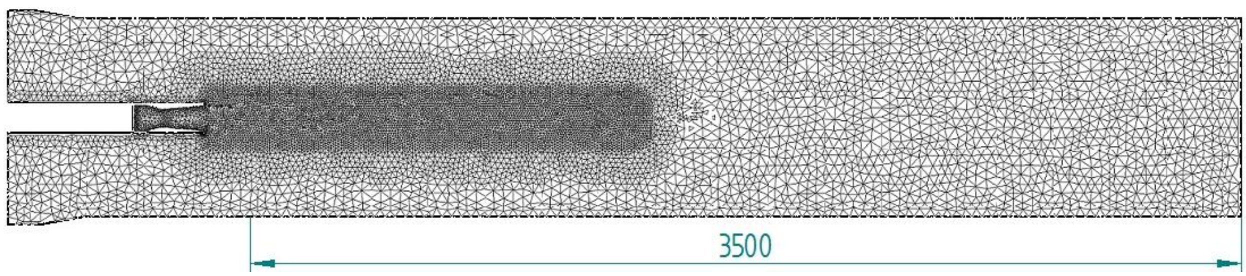

Figure 32. Isolated SS Model Mesh, showing cell concentration in UE SS Jet core

The results for the Isolated SS Model were presented in the form of Visual Contours (Static Pressure and Mach number), and assessed in Appx. D.1. The analysis compared the near field expansion of the UE SS Jets (SS1 in the MC Model, and the Isolated SS Model). The comparisons showed that the MC mesh had in fact replicated the SS Exit flow conditions necessary for the SSEC mechanism. It captured the SS Jet entry conditions, interpreted the UE SS flow regime, and produced a result set suitable for the purposes of the MC Numerical Model analysis (Section 13.4). The limited MC Model cell count however, depicted the flow to expand to MC conditions ($P_{SS} \approx P_{MAIN}$) over a much shorter axial length. This was due to the oversimplification of the repeated shock diamond pattern. Whilst this was tolerable for interpreting the SSEC mechanism, which involved the Turbulent Mixing within the downstream subsonic region, it was not adequate for comparison to the published sources. The remainder of the validations were then performed using the Isolated SS Model; which fully resolved the repeated shock diamond pattern and provided a more accurate depiction of the UE SS Jet core length. The Isolated SS Model revealed an extension to the supersonic region of the SS Jet core; due to the repeated shock diamond structures. It effectively delayed the mixing process, lengthwise, by offsetting the subsonic region of the Jet. This Jet core flow behaviour was pre-emptively factored into the MC Design, via the extension of intermediate lengths in Section 12.4 (2000 mm > $L_{CO\text{-}FLOW}$ = 877 mm). As detailed in Section 13.3.1, this length was sufficient for the Jet core flow to become subsonic. With the exception of this Jet core supersonic region extension, the MC Numerical Model fully represented the intended effects of the UE SS flow.

13.3.1 Potential Core Length (Appx. D.2)

The Potential Core Length was defined by Karthikeyan [51] as the non-dimensional Axial Length required for the SS Jet Exit flow to become subsonic. The analysis for this application was performed in 2 phases: the repeated shock diamond stage (flow property oscillation), and the predictable SS expansion stage.

- The 1st Phase (flow property oscillation) was identified by Lovaraju [48] as the core length specific to UE SS flow. The non-dimensional 'flow property oscillation' length for the Isolated SS Model was identified as $L_{CFD\ OSC}/Ø_E$ = 12.47; detailed in Appx. D.2.
- This oscillation length ($L_{CFD\ OSC}/Ø_E$ = 12.47) corresponded well with the Velikorodny [46] UE SS core length expectation ($X_P/Ø_E$ = 12.72); resulting in an error of 2%.
- The 2nd Phase (predictable SS expansion) was identified as the Potential Core Length in typical SS Jet expansions; the length for the Jet flow to become subsonic. The non-dimensional Potential Core Length for the Isolated SS Model was identified as $L_{CFD\ POT}/Ø_E$ = 10.82; detailed in Appx. D.2.
- This Potential Core Length was validated against the results of 2 published sources; $L_{POT}/Ø_E$ = 10.29 from Zaman [49] and $L_{SINGLE}/Ø_E$ = 10.74 from Murakami [44]. The largest error from these 2 comparisons amounted to 5%.
- The near-field expansion of the SS Jets, used in the Isolated SS Numerical Model, produced an accurate depiction of the expected behaviour.

13.3.2 Subsonic Velocity Decay (Appx. D.3)

The Potential Core Length analysis, in the previous subsection, concerned the near-field supersonic flow behaviour of the Isolated SS Jet. The Velocity Decay analysis, in this subsection, concerned the far-field subsonic flow behaviour (downstream of the Potential Core Length). After the Jet core had become subsonic, it experienced centreline Velocity Decay that conformed to a 'normalized' rate described by Yüceil [50]. The non-dimensional Velocity (V_E/V) and Axial Length ($x/Ø_E$) were normalized to account for complete flow expansion and fluid compressibility; resulting in the 'corrected values' (V_2/V and $x/Ø_2$). The relationship between these normalized parameters produced a universal gradient that defined the Velocity Decay rate (K_{DEF}). The analysis was included in Appx. D.3, with the results presented here.

- The SS Jet application in this Design expanded the flow within the SS Tunnel structure using A.R.* ($Ø_T$ and $Ø_E$). The flow exited the SS Tunnel and expanded to the MC requirements. It did not have to be normalized to account for compressibility. This was demonstrated by comparing the respective values at the SS Tunnel Exit and the hypothetical complete expansion location (Point 2); in Appx. D3. The analysis continued with the normalized values; to maintain conventions during the comparison.
- The plot of normalized non-dimensional Velocity Decay (V_2/V vs. $x/Ø_2$) produced a linear trend-line gradient of K_{DEF} = 0.1524. This K_{DEF} value correlated well with the universal 'corrected' Yuceil [50] expectation of $K_{DEF\ CORR}$ = 0.16; error = 4.75%.
- The far-field behaviour of subsonic Jet Decay, used in the Isolated SS Numerical Model, replicated the expected experimental behaviour.

The Isolated SS Model was successfully validated against the published data (both near-field and far-field). The near-field behaviour (Supersonic Expansion) corresponded with published sources for both the UE repeated shock diamond formation (flow property oscillation) and the potential core length of the Supersonic Jet core ($M > 1$). The far-field behaviour (Subsonic core) corresponded with the predicted rate for normalized Velocity Decay. The MC Model was constructed with the same geometry and layout as the Isolated Model, but did not have the same mesh resolution (so as to capture the minute expansion details). The bulk flow behaviour though, was common between the Models. These included the UE SS Regime, SS Exit flow properties, and downstream subsonic flow conditions. The MC Numerical Model was deemed adequate for the analyses of the Temperature Mixing objectives (SSEC Concept).

13.4 Solution Analysis

The series of decisions taken in the development of the MC Numerical Model (including: the limited cell count available for y+ conformance, the oversimplified $k_{TKE} – \varepsilon_{TDR}$ turbulence model, 1^{st} Order Solution Methods, and revised RMS residuals) produced a result that exaggerated the Turbulent Diffusion within the MC. The adverse effects of this implementation included the exaggerated turbulence within the WT components prone to recirculation (OTS and Diffusers). The detailed discussion of the y+ impact on the Numerical Model quality was included in Appx. J.3, but a major finding was to 'partition' the MC Numerical Model results to exclude the WT components prone to recirculation. The Solution analysis was then limited to all components prior to the OTS Inlet; thus avoiding the known recirculation offenders of the OTS and Diffusers. This approach provided a 'limited control volume' (Main Inlet to OTS inlet) with a 'Partitioned $\dot{m}$ balance', within the Complete Geometry control volume (Main Inlet to WT Outlet) with the Global $\dot{m}$ balance. With these measures in place, the current mesh provided a solution that focused on the exclusive effects of the MC on the Test Section objectives.

13.4.1 Numerical Results

The 1^{st} Order Solution was presented using the Mass-Weighted Averages (MWA) at the Key Point locations along the Complete Geometry (10 Key Points along the MC length, and at certain Key Points along the WT). This allowed for the flow behaviour to be tracked along the MC length, and compared to the Analytical Model. The comparison would achieve a triangulated solution for the Supply Device Inlet flow properties. The flow properties at the Key Points along the WT length were assessed to determine the effectiveness of the current MC configuration. The Solution analysis did not concern the flow profile attributes downstream of the OTS Inlet (i.e. Diffuser and OTS). It focused only on the segments upstream; with the objective of obtaining the OTS Inlet specifications.

The fluid properties were listed in Table 10 for the 10 MC Key Point locations (identified in Figure 30), with the following parameters including: Distance along the Tunnel length (X), Stagnation Pressure (P_0), Static Pressure (P), Mach number (M), Stagnation Temperature (T_0), Static Temperature (T), and Mass Flow Rate ($\dot{m}$). The $\dot{m}$ values in Table 10 were doubled to account for the Symcut surface; this allowed for direct comparison to the Analytical Model values (Table 9). Table 10 also included the flow conditions of the Inlets (Main Inlet, 3 SS Inlets, and Eductor Inlet) and the WT Outlet; so as to readily identify the Global $\dot{m}$ balance. The OTS Inlet conditions were included to assess the capability of the MC in achieving Design Point conditions.

It was important to point out here that, unlike the MC Analytical Model, the flow conditions at the Exit of each SS Tunnel could not be readily attained using the 'MWA across Ghost planes' approach. The MC Numerical Model analysis of the SS flow was limited to either:

- The point of entry into the Control Volume; at the respective SS Inlet conditions. Such as the Key Point 'SS2 Inlet' in Table 10.
- The point of expansion into the Main flow; taking the combined influence of both flows across the MC diameter. Such as the Key Point '6' in Table 10.

It was also important to state that, due to geometrical considerations put into effect for the benefit of the Numerical Model, the Eductor P_0 was inflated to $P_{0\ EDUCT}$ = 92000 Pa (to overcome the nominal intermediate length not included in the Analytical Model). Table 10 displayed the Design objectives in boxed cells. The various Inlet conditions were specified to achieve these PRS objectives: M_{TS} = 0.75 (Objective = 0.7), T_{TS} = 222.2 K (Objective = 219 K), and P_{EXIT} = 83000 Pa (Objective = 83000 Pa).

Table 10. Selected Results from Complete Geometry (MC+WT) Numerical Model (Objectives Boxed)

Point Number	X [mm]	P_0 [Pa]	P [Pa]	T_0 [K]	T [K]	Mach	ṁ(x2)[kg/s]
Main Inlet	0.0	83010	82984	297.9	297.9	0.02	2.09
SS1 Inlet	392.7	950000	887523	283.2	277.7	0.31	6.82
SS2 Inlet	3652.7	950000	890958	283.2	278.0	0.30	6.84
SS3 Inlet	6912.7	950000	887708	283.2	277.7	0.31	6.84
2	356.0	83011	82973	284.4	284.4	0.03	1.65
3	856.0	293992	85608	276.7	223.1	0.95	8.59
4	2956.0	97050	84740	262.9	253.7	0.35	9.15
5	3516.0	90006	89673	251.5	251.2	0.07	10.40
6	4116.0	262586	92087	262.5	221.3	0.76	17.80
7	6216.0	112432	90396	259.2	245.1	0.46	18.13
8	6776.0	99502	94396	258.3	254.5	0.25	18.51
9	7376.0	209219	97290	258.7	230.7	0.57	25.55
(MC-Out/WT-In) 10	10876.0	107634	102056	253.0	249.2	0.24	23.04
OTS In	12476.0	100519	69541	246.8	222.2	0.75	23.27
Eductor Inlet	14259.5	92000	75106	290.0	273.7	0.55	5.27
WT Outlet	20531.5	83444	83000	244.4	244.1	0.08	27.87

Inspecting the boxed Design objectives in Table 10, it was identified that despite T_{TS} being slightly higher than the objective (222.2 K > 219 K), M_{TS} was still higher than required (M0.75 > M0.7). It implied that there was a higher energy profile in the WT flow than anticipated. This excess WT energy had to be addressed before assessing the MC Design performance (T_0 and ṁ) and the OTS Inlet conditions (M_{TS}, T_{TS}). The excess energy investigation was performed by focusing on the MC-Out/WT-In Key Point location (i.e. Key Point 10 in Table 10). This Key Point isolated the resultant output of the MC and the expected input for the WT. Ideally this would be performed by comparing the MC-Out from Table 10 to the WT-In from Table 6. However, due to the Solver Setting differences (1st Order MC Solution vs. 2nd Order WT Solution, and MC RMS > 0.00025 vs. WT RMS > 0.0005), this comparison was not impartial. Instead, the comparison was made between Table 10 and the WT 'Strict-RMS' variant from the Sensitivity Analysis (Section 7.3.2). The MC Numerical Model and the 'Strict-RMS' WT variant (included in Appx. M.1) were both performed using 1st Order Solution Methods only, and utilized stricter RMS requirements for the Continuity and Energy residuals (<0.00025). The corresponding MC Out/WT In conditions (Key Point 10 in the Complete Geometry, and Key Point 1 in the 0.00025-WT-SA) were compared in Table 11. The most glaring difference between the 2 sets of results was P_0. The $P_{0\ WT\text{-}IN}$ value for the Complete Geometry (MC+WT) was 6661 Pa higher than when simulating the WT in isolation.

Table 11. Comparison of Complete Geometry (MC+WT) and 0.00025-WT-SA at MC Out/WT In

	Complete Geometry (Point 10)	0.00025-WT-SA (Point 1)
P_0 [Pa]	107634	100973
T_0 [K]	253.0	240.0
$\dot{m}$ [kg/s]	11.52	11.08

This higher P_0 was attributed to the influence of the SS Jets; as the Main Inlet (Centrifugal Fan) P_0 was too low to play a significant role in boosting the conditions at this location (Key Point 10). It was evident that the SS flows had not expanded fully; to achieve the desired 'lower' Pressure (P_B). This 'unfulfilled' SS expansion was also noted to affect the resultant T_0 in Table 11 (253.0 K > 240 K). If the Complete Geometry (MC+WT) $P_{0\ MC\text{-}OUT}$ was hypothetically equal to the isolated WT $P_{0\ WT\text{-}IN}$, with the Temperature comparison maintained at $T_{0\ MC\text{-}OUT} > T_{0\ WT\text{-}IN}$, it could be concluded that the Turbulent Mixing mechanism was not effective. However in this case, where $P_{0\ MC\text{-}OUT} > P_{0\ WT\text{-}IN}$, it implied that the SS flow had not accomplished the complete expansion within the MC (irrespective of any Mixing Mechanism). This incomplete expansion within the MC length resulted in a higher P_0 profile ($P_{0\ WT\text{-}IN}$ > 98500 Pa), and an 'under-cooled' Main flow ($T_{0\ WT\text{-}IN}$ > 240 K). The higher Pressure profile ensured that, despite the higher T_0, the OTS Inlet Mach number objective was still achieved. The higher T_0 however, affected the Altitude objective; effectively simulating M0.75 at a lower corresponding Altitude.

The higher P_0 profile within the MC was investigated in Appx. E; by comparing the MC Numerical Model (Table 10) and MC Analytical Model (Table 9) P_0 values at the 10 Key Points along the MC length. This analysis identified the P_0 contribution of each SS Jet to the Main flow Pressure profile. With each SS Jet flow addition, the cumulative Main flow prevented the complete expansion of the subsequent SS Jet. Instead of extracting the complete Cooling potential of the subsequent SS Jets, the Main flow had inherited a higher P_0. This was particularly noticeable for the 2nd SS Jet. The incomplete expansion of the Jets wasted the cooling potential of the SS flow. Instead, it retained a higher P_0 in the MC. This was detrimental to the MC objective of Altitude Temperature; thereby reducing the Design Quality. This set of MC Resultant flow conditions (higher P_0 and T_0) were reflected by the OTS Inlet conditions; affecting the Design Point objective. This revised Design Point objective was evaluated in the next subsection.

13.4.2 MC Numerical and Analytical Model Comparison

The analysis in this subsection concerned the MC Design comparison (T_0 and $\dot{m}$) and Design Point objective comparison (OTS Inlet conditions); to triangulate the MC Inlet specifications. The complete Contour Plot analysis of T_0 and Mach number along the MC length was included in Appx. N.4. The Contour Plot analysis focused on the visual interpretation of the SS Jet expansions and Turbulent Mixing mechanisms. The implications of these visual results were readily identifiable using the Numerical Result data in Table 10 (with the discussions in this subsection), and therefore the Contour Plots were excluded for brevity. These plots did however confirm and demonstrate the concept of the flow becoming TFD before HFD for Pr < 1 (from Section 11.1.2). The Main flow developed a consistent Temperature profile before it developed a consistent Velocity profile. This was true for each of the 3 SS Jet intermediate mixing stages, and the final Resultant Flow mixing.

Objectives Comparison (T_0 and $\dot{m}$)

The parameters pertinent to the MC Numerical Model evaluation were limited to T_0 and $\dot{m}$. The objective of this segment was to achieve the required Test Section T_0 (at the OTS Inlet) by varying the contributions of Supply Devices ($\dot{m}_{MAIN}$ and $\dot{m}_{SS}$). Figure 33 depicted the T_0 and $\dot{m}$ variation (from Table 10); along the geometry length from the Main Inlet (Key Point 1) to the Test Section Inlet (Key Point OTS In). This limited the scope of the analysis up to the point of the Design Objective (OTS Inlet). The plot depicted the staggered $\dot{m}$ contributions of the 3 SS Jets (X_{SS1} = 856.0 mm, X_{SS2} = 4116.0 mm, and X_{SS3} = 7376.0 mm), and the associated effects on the MC Main flow Stagnation Temperature ($T_{0\ MAIN}$).

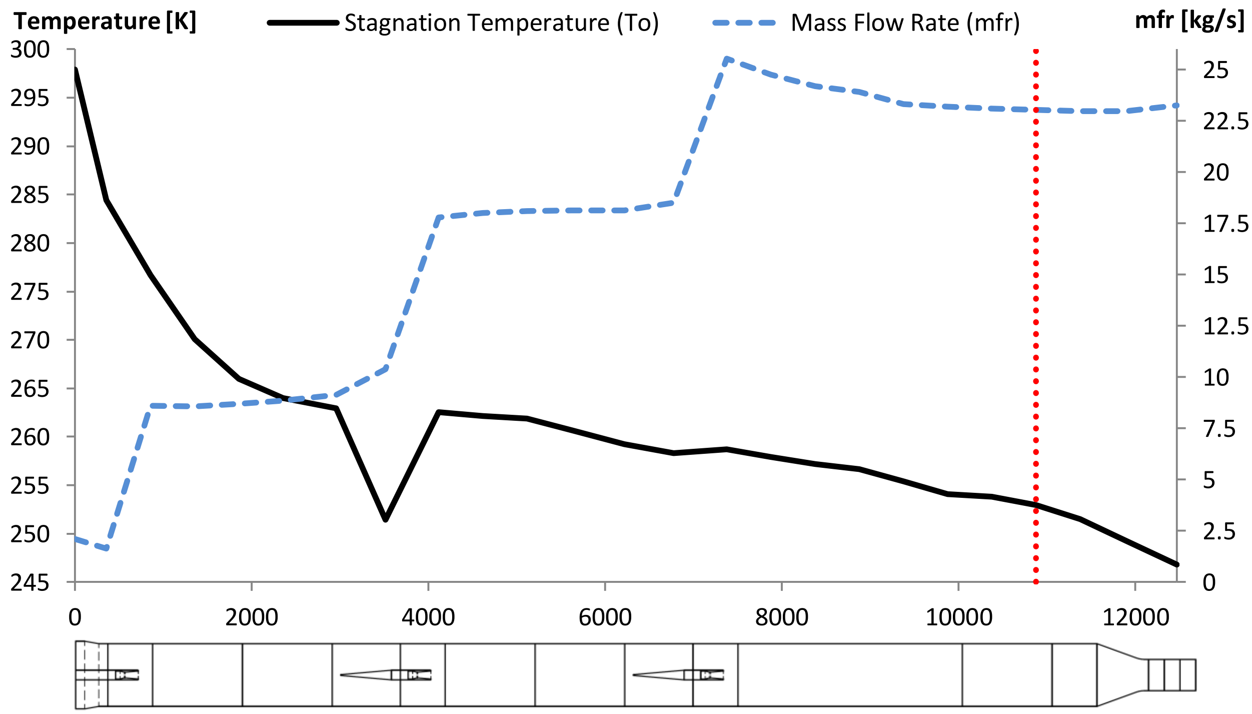

Figure 33. Stagnation Temperature (T_0) and Mass Flow Rate ($\dot{m}$) variation of Numerical Model over Mixing Chamber length and a segment of the Wind Tunnel (up to the OTS Inlet), RED vertical marker distinguished the Mixing Chamber Outlet from Wind Tunnel Inlet

Focusing on the $\dot{m}$ curve, the 3 staggered SS Supply mechanisms followed the intention of the Analytical Model. Each Jet supplied the desired $\dot{m}$ = 6.8 kg/s; the specified $P_{0\ SS}$ resulted in the required $\dot{m}_{SS}$. The curve should have remained as a straight horizontal with each flow addition (as was expected from the Analytical Model $\dot{m}$ column in Table 9). Instead, the curve demonstrated a gradient prior to each SS Jet entry. This $\dot{m}$ inconsistency was due to the turbulence exaggeration of the 1st Order Solution Methods. The scale and positioning of these $\dot{m}$ tracking inconsistencies were due to respective $\dot{m}$ contributions at each point. At the 1st SS Jet entry, $\dot{m}_{SS}$ (6.82 kg/s) was greater than $\dot{m}_{MAIN}$ ($\dot{m}_{MAIN\ IN}$ = 2.09 kg/s). The SS Jet expansion resulted in the obstruction and recirculation of the miniscule Main flow. This behaviour explained the negative gradient of the curve prior to the SS1 Jet entry (dropping by 0.44 kg/s); in which the Main flow was displaced and reversed. It was important to state here that, despite the displacement and obstruction, there was no reversed flow at the Main Inlet face (Centrifugal Fan Inlet).

At the 2nd SS Jet entry, the Main flow weighting was larger than SS2 ($\dot{m}_{MAIN\ IN}$ +$\dot{m}_{SS1}$ > $\dot{m}_{SS2}$). The cumulative mass of the Main flow decreased the displacement dominance of the SS2 Jet expansion; and prevented the Main flow reversal. The $\dot{m}$ curve displayed a positive gradient along the 1st Conical Splitter (prior to the SS2 Jet entry). This was due to the obstructive nature of the Jet expansion, which resulted in a build-up of the Main flow prior to the Jet entry (increasing by 1.25 kg/s). The $\dot{m}$ curve displayed a lesser gradient along the 2nd Conical Splitter (prior to the 3rd SS Jet entry). Instead, the $\dot{m}_{MAIN}$ build-up was registered at the Jet expansion point. This was due to the eventual cumulative increase in Main flow $\dot{m}$ that resulted in a much larger and more dominant flow; occupying $Ø_{MC}$. This 3rd SS Jet $\dot{m}$ contribution registered the largest $\dot{m}_{MAIN}$ value at 25.55 kg/s; larger than the Resultant Mixed flow exiting the MC at 23.04 kg/s. This inconsistent $\dot{m}$ reading was due to the turbulence exaggeration of the 3rd Jet expansion. The $\dot{m}$ curve returned to the expected MC Out value at halfway along the extended backend length. With the exception of this peak value (at the 3rd SS Jet expansion), the maximum $\dot{m}$ tracking inconsistency along the MC length (using the MWA method) registered at 11%. Given the amount of recirculation and obstruction caused by the multiple SS Jet expansions within the MC, this result was tolerable using 1st Order methods. The MC Out $\dot{m}$ (23.04 kg/s) was only 4.6% larger than the Analytical Model value (22.03 kg/s). This increased value (±1 kg/s) was partially due to the inconsistent $\dot{m}$ tracking within the MC, but also due to the slight excess contributions of the various inlets. The SS Inlets all contributed the required $\dot{m}$ (±6.8 kg/s); with a combined erroneous addition of 0.1 kg/s. The Main Inlet, despite being specified close to the Analytical Model P_0 value (83010 Pa ≈ 83007 Pa), delivered 2.09 kg/s (instead of the Analytical Model $\dot{m}_{MAIN\ IN}$ = 1.64 kg/s). This additional 0.45 kg/s was the result of the low Static Pressure profile at the MC entry created by the aspiration effect of the 1st SS Jet.

The T_0 curve in Figure 33 showed the drop in cumulative Main flow T_0 over the MC length. There were 2 important flow attributes that were interpreted from this curve: Absolute Minimum T_0 (246.8 K at the OTS inlet), and the Temperature Mixing Length required. Looking at the Cooling effect of the 1st Jet, the T_0 in the MC continually decreased until the 2nd Jet (reaching a minimum of T_0 = 251.5 K). The T_0 upon the 2nd Jet entry spiked up to 262.5 K, before cooling again. This 'spike-decline' pattern was repeated at the 3rd Jet; but to a lesser extent. These spikes were due to the method in which these flow properties were taken; Mass-Weighted Averages (MWA) across Ghost planes. The MWA of T_0, taken aft of each SS Tunnel Exit, averaged the flow property across $Ø_{MC}$. The flow property (T_0) was interpreted across the Ghost plane according the respective $\dot{m}$ contribution of each stream (Main and SS). If one flow outweighed the other, it would have a greater representation in the result. This explained why the T_0 curve in Figure 33 spiked at each SS Jet entry, but the value of each subsequent spike diminished (due to the cumulative $\dot{m}$ of the Main Flow with each previous SS flow addition). Looking at this 'spike-decline' behaviour from the Main Inlet to 1st Jet, the T_0 was seen to drop from $T_{0\ MAIN\ IN}$ = 297.9 K to $T_{0\ SS\ IN}$ = 283.2 K. This was due to the respective $\dot{m}$ contributions of each flow on the MWA; $\dot{m}_{MAIN\ IN}$ = 2.09 kg/s, and $\dot{m}_{SS1}$= 6.82 kg/s. The SS flow outweighed the Main flow by more than ×3, and had a greater representation in the MWA T_0 at the Ghost plane. Proceeding to the 2nd Jet spike, $\dot{m}_{MAIN}$ = $\dot{m}_{MAIN\ IN}$ + $\dot{m}_{SS1}$ = 8.91 kg/s. This value outweighed the 2nd Jet contribution ($\dot{m}_{SS2}$ = 6.84 kg/s). The Ghost Plane T_0 at the 2nd Jet Exit was impacted more so by the Main flow (T_0 = 251.5 K) than the 2nd Jet (T_0 = 283.2 K); which resulted in the MWA of 262.5 K. This behaviour was also exhibited with the 3rd Jet, but of course to a greater extent due to $\dot{m}_{MAIN}$ = $\dot{m}_{MAIN\ IN}$ + $\dot{m}_{SS1}$ + $\dot{m}_{SS2}$ > $\dot{m}_{SS3}$.

The T_0 curve also demonstrated the rate at which Temperature Mixing occurred. In the Analytical Model (Table 9), this mixing was assumed to occur immediately upon contact with each $\dot{m}_{SS}$ contribution. The Model did not include any measure to interpret the Turbulent Diffusion. It only estimated the minimum axial length, downstream of each SS Jet, required for mixing (from Section 12.2). These axial lengths however, did fulfil the respective purposes in the Numerical Model T_0 curve (Figure 33). The spikes in the T_0 curve reflected the T_0 of each SS Jet core. The Jets retained the SS flow attributes ($T_{0\ SS}$ and M_{SS}) in the core until dissipation. The curve interpreted the Main flow T_0 to cool gradually over the budgeted axial length within the subsonic region (aft of each SS Jet core). The curve also showed that the axial mixing length required (per Cooling Jet) increased as $\dot{m}_{MAIN}$ increased. This was in keeping with the $L_{CO\text{-}CLOW}$ concept (eqn. 39): potential core length extension due to increased co-flowing $\dot{m}_{MAIN}$.

That is to say, at the 1st SS Jet (where $\dot{m}_{MAIN} = \dot{m}_{MAIN\ IN}$) the Main flow achieved the optimum Cooling potential (T_0 = 251.5 K) within the budgeted intermediate length (2000 mm). Whereas after the 3rd Jet (where $\dot{m}_{MAIN} = \dot{m}_{MAIN\ IN}+\dot{m}_{SS1}+\dot{m}_{SS2}$), the Main flow did not even achieve the optimum Cooling potential within the extended backend length (3500 mm). It resulted in further Cooling within the WT Geometry. The flow continually decreased from the MC Out/WT In (T_0 = 253.0 K) to the OTS Inlet (T_0 = 246.8 K). The 2nd Jet in particular did not achieve the complete mixing; as the T_0 prior to the 3rd Jet entry (258.3 K) was still higher than the T_0 prior to the 2nd Jet entry (251.5 K). The mixing process for the 2nd SS Jet appeared to be postponed until after the 3rd Jet entry, to be completed in the extended backend length. This occurrence, whilst not ideal, was tolerated within the Design; since the lowest possible T_0 from the Mixing Mechanism was achieved prior to the OTS Inlet. This was accomplished using the 'convective mixing effects' implied by the WT Nozzle contraction (prior to the OTS Inlet). Despite this WT Nozzle flow agitation, the Numerical Model Resultant flow T_0 (at the OTS Inlet) was still higher than the Analytical Model prediction; i.e. 251.5 K > 240.1 K.

In saying this, the Turbulent Mixing objective (complete mixing of different Temperature streams) was successful, but the Resultant flow T_0 objective was not. The higher Resultant flow T_0 (251.5 K) was the result of incomplete expansion of the SS Jets. The latter Jets in particular (SS2 and SS3). This was described in the previous subsection (and Appx. E); in which the Main flow inherited the P_0 of the incompletely expanded SS Jet flows instead of completely extracting the respective Cooling potential. This behaviour was distinct from the Analytical Model interpretation; which assumed near-complete assimilation of SS flow into the Main flow P_0. It was recommended, based upon the T_0 Contour analysis in Appx. N.4, that additional convective devices be placed within the extended backend MC length to agitate the Main flow. This approach would facilitate further mixing within the allotted MC length at the expense of the excess P_0. This was evidenced by the additional Cooling extracted downstream of the MC; by the convective effects of the WT Nozzle contraction. The T_0 Contour (Appx. N.4) displayed a consistent Temperature profile (across $Ø_{WT}$) after the WT Nozzle contraction. This consistent T_0 profile was maintained along the intermediate length preceding $Ø_{OTS\text{-}IN}$. It indicated that the flow had reached Temperature Equilibrium, even though the Mach Contour (Appx. N.4) displayed a flow Velocity core that was still developing prior to $Ø_{OTS\text{-}IN}$. This occurrence was in keeping with the Pr < 1 prediction; that the flow would become TFD before it became HFD.

OTS Inlet – Design Point Comparison

The current incomplete SS Jet expansions resulted in a different, but not irrelevant, set of Test Section Conditions. The OTS Inlet flow conditions for both the MC Numerical Model (from Table 13) and WT Analytical Model (from Table 5) were presented and compared in Table 12. The percentage deviations of the Numerical Model flow properties from the Analytical Model were calculated as $\frac{K_{CFD} - K_{MATH}}{K_{MATH}} \times 100$; and were also included in Table 12. The 2 Design Point objectives pertinent to the Design Quality were the Mach number (M_{TS} = 0.7) and Static Temperature (T_{TS} = 218.2 K, Altitude replication for 35000 ft).

Table 12. Comparison of WT Analytical Model and MC Numerical Model at the OTS Inlet

OTS Inlet	WT Analytical Model (Table 4)	MC Numerical Model (Table 10)	% Deviation
M	0.70	0.75	+7.14
$\dot{m}$ [kg/s]	22.16	23.27	+5.01
P_0 [Pa]	96140	100519	+4.56
T_0 [K]	240.0	246.8	+2.83
T [K]	218.2	222.2	+1.83
P_{JUMP} [Pa]	13140	17519	+33.33
T_{DROP} [K]	58.2	51.4	-11.68

The Mach number was over-achieved by the MC Numerical Model by 7.14 %; resulting in M_{TS} = 0.75. The WT geometry was, however, pre-emptively designed to avoid possible choking at this narrowest segment ($Ø_{TS\ IN}$ = 0.35 m) in the event of a Main flow with a higher energy profile or flow rate. The Mass Flow Rate ($\dot{m}$) only overshot the objective by 5.01 %, and fulfilled the M_{TS} objective without choking at $Ø_{TS\ IN}$. The MC Numerical Model had succeeded in this Design Point objective. The other Design Point objective was the Static Temperature (T_{TS} = 218.2 K); to simulate the Design Point Altitude (35000 ft). According to Table 12, the MC Numerical Model T_{TS} was 4 K higher than the WT Analytical Model T_{TS}; resulting in a 1.83 % deviation. This was explained in the previous subsection as the result of incomplete expansion of the SS flows within the MC. In fact, the $P_{0\ OTS\text{-}IN}$ of the MC Numerical Model was 4379 Pa higher than the $P_{0\ OTS\text{-}IN}$ of the WT Analytical Model. The Model deviations for P_0 (4.56 %) and T_{TS} (1.83 %) did not seem like large differences; at least not large enough to change the OTS Inlet conditions. Taking these values compared to Ambient conditions however, revealed the extent of the deviations. These comparative values were included in Table 12 as P_{JUMP} and T_{DROP}.

The P_{JUMP} was the increase in P_0 over Ambient (83000 Pa). The T_{DROP} was the drop in T_0 from Ambient (298.2 K). These values isolated the effectiveness of the delivery Devices. The MC Numerical Model T_{DROP} under-achieved the target set by the WT Analytical Model by 11.68 %. The Cooling Mechanism underperformed by 6.8 K; directly correlating with an Altitude reduction and thus reducing Design Quality. The MC Numerical Model P_{JUMP} on the other hand significantly overshot the WT Analytical Model target by 33.33 %. It produced an OTS Inlet flow that was 4379 Pa higher than required. Whilst this did not choke the OTS inlet, it did over-specify the Pressure energy. It was not an accurate depiction of the required Velocity, in testing the Ram effects at the Test Piece Engine, and therefore affected the Design Quality. These 2 parameters (T_{DROP} and P_{JUMP}) however, served to offset each other in achieving the required M_{TS}. The higher Pressure Energy, when converted to Kinetic Energy, allowed the MC

Numerical Model to achieve M0.75 despite the higher T_{TS}; using eqn. 6: $M = \frac{(\uparrow V)}{\sqrt{k \cdot R \cdot (\uparrow T)}}$. According to the MC Numerical Model, the flow was capable of accomplishing the Design Point Engine Performance requirement (M_{TS} = 0.75 > 0.7), but not the Design Point Altitude requirement (T_0 = 246.8 K < 240 K). The T_0 of the MC Numerical Model corresponded to an Altitude = 32000 ft (< Design Point Altitude = 35000 ft). The quality of this Design was then compromised until additional means of SS Jet expansion were investigated; to fully extract the Cooling potential.

13.5 MC Numerical Model Conclusions

The conclusions of the MC Design were based on the Numerical Model. The Analytical Model served as the validation for the various MC Inlet specifications (Main Inlet and SS Inlets). The Numerical Model interpreted the Mixing Mechanisms involved, to achieve the Design Point OTS Inlet conditions of M0.75 at T_{TS} = 222.2 K (equivalent Altitude = 32000 ft). These results served as the Revised Design Point. The SSEC Concept was successful (achieving 88.32% of the required Cooling), and the modelling was an adequate representation of the Concept. The MC+WT achieved a Design Point that was representative of the PRS. The Design Point Supply Device requirements were triangulated with high confidence as:

$P_{0\ MAIN\ IN}$= 83010 Pa,	**$T_{0\ MAIN\ IN}$= 297.9 K,**	**$\dot{m}_{MAIN\ IN}$ = 2.09 kg/s,**	**$Ø_{MAIN\ IN}$ = 755 mm.**
$P_{0\ SS}$ = 950000 Pa,	**$T_{0\ SS}$ = 283.2 K,**	**$\dot{m}_{SS}$ = 3 × 6.8 = 20.4 kg/s,**	**$Ø_{SS}$ = 88 mm.**

The major findings from the MC Modelling approach were listed here, together with the complications of the Meshing and Solver programs, as:

- The limited cell count available (< 1 500 000 cells), not only prevented the full resolution of the repeated Shock Diamond cell structure of the UE SS Jet cores but also, limited the applicable Turbulence Model to the Realizable k_{TKE} - ε_{TDR}. The over-simplifications of the k_{TKE} - ε_{TDR} model required the turbulence exaggeration of 1^{st} Order Solution methods; in order to simulate the Turbulent Diffusion of the SSEC Concept.
- The required mixing length for each subsequent SS Jet increased as $\dot{m}_{MAIN}$ increased. The cumulative $\dot{m}_{MAIN}$ suppressed the latter SS Jets, and prevented the complete expansion of the respective SS flows. The Main flow ultimately inherited part of the $P_{0\ SS}$ energy (boosting the $P_{0\ MAIN}$ energy profile), instead of fully extracting the Cooling potential.
- The T_0 Contour (Appx. N.4) revealed that the flow had achieved a consistent T_0 profile (across $Ø_{WT}$) prior to the OTS Inlet. The Mach Contour (Appx. N.4), however, displayed a flow Velocity core that was still in development. The flow was TFD, but not completely HFD, prior to the OTS Inlet.

14 Design Specification

The Design Specification was divided into the 2 parts that comprised the Complete Geometry; the WT and the MC. The WT specifications identified the MC Outlet/ WT Inlet flow conditions required to achieve the Design Point (M0.7, T = 219 K) at the Test Section. The MC specifications identified the Supply Devices required to achieve the conditioned flow at the MC Outlet/WT Inlet. The relevant Supply Devices were listed with the associated costs; identifying the best possible Delivery mechanism options. This distinction (WT from MC) allowed for future modularity of the MC Design.

14.1 WT Summary

The WT Geometry (Section 6.2) was designed in keeping with the PRS (Section 3): the Primary objective of testing a Turbine Engine (Ø = 0.35 m) at Altitude (35000 ft), and the Secondary pursuit of testing a Propeller Engine ($Ø_{BLADE}$ = 2 m). The Design geometry comprised of the following: Open Circuit WT, Blowdown configuration, and Open Test Section (with free-jet Test Section flow). The Tunnel components included (in sequential order): Plenum Chamber (with flow straightener), Nozzle Contraction, OTS, Eductor Device, 2x Diffuser Expansions, and Mesh Screen (at WT Exit). The Open Test Section (OTS) chamber length was sized to accommodate the length of the Gas Turbine Test Piece Engine. The OTS chamber diameter however, had an arbitrary value for the purposes of Numerical Model continuity. The actual diameter of this chamber was not limited to any size, and allowed for the substitution of the Gas Turbine Engine with the Propeller Engine.

In testing the Propeller Engine, certain components upstream of the OTS (viz. Plenum Chamber and Nozzle Contraction) had to be substituted with a gradual Diffuser expansion into a larger OTS; as described in Appx. Q.1.2. The Plenum Chamber served as an intermediate length; prior to the implementation of the MC. The Eductor device was included to create a region of lower Pressure (partial vacuum effect) downstream of the OTS. It served to draw out the Engine exhaust flow; in the event of hazard. The placement of the component imparted the additional benefit of reduced OTS pulsation. The current implementation of the Eductor served merely as a placeholder. Its role was limited to entering the WT with a higher P_0 and M than the Main flow, and creating an aspiration effect in the immediate space. The actual optimization of this component was addressed in Appx. Q.3.2. The Numerical Model (Section 7.4) was performed to determine the WT Inlet requirements in achieving the Test Section objectives. The Numerical Model was validated by the Analytical Model, and confirmed the intended flow path and various component losses.

Design Objectives
M_{TS} = 0.70, T_{TS} = 218.5 K, P_{EXIT} = 83000 Pa.
WT Inlet Requirements
$P_{0\ WT\text{-}IN}$ = 98500 Pa, $T_{0\ WT\text{-}IN}$ = 240 K, $\dot{m}$ = 22.02 kg/s.

The WT Design (as summarized in Section 7.5) was capable of achieving the Design Point objectives (Velocity ≥ M0.7, and Static Temperature ≤ 219 K corresponding to 35000 ft) from the stated Inlet conditions. The $P_{0\ WT\text{-}IN}$ discrepancy between the Analytical Model and Numerical Model stemmed from the inaccurate resolution of the friction losses within the Intermediate length preceding the OTS. These simulation deficiencies were addressed in Appx. Q.2.1.

14.2 MC Summary

The MC Geometry (Section 12.4) was designed to deliver the WT Inlet requirements ($P_{0\ WT\text{-}IN}$, $T_{0\ WT\text{-}IN}$, and $\dot{m}$); from the appropriate readily available Supply Devices. The primary role of the MC was to cool the Main Supply airflow to the corresponding Altitude Temperature. In order to simulate the Design Point (35000 ft), the Cooling mechanism had to achieve the minimum T_0 = 240 K without changing the air composition. This application of Cooling rendered conventional applications (Vapor Cycle and Dry Ice Sublimation) inadequate. The final Cooling Mechanism was designed around the investigative concept of Supersonic Expansion Cooling (SSEC).

The SSEC concept utilized 3 Secondary Underexpanded SS Jets (P_{0SS} **>>** $P_{0\ WT\text{-}IN}$) to cool the Primary Main flow (≈ $P_{0\ WT\text{-}IN}$) through Turbulent Diffusion. The outer MC geometry was a constant diameter duct from Main Supply Inlet to WT Inlet ($Ø_{MC} = Ø_{WT\text{-}IN}$). The MC contained 3 SS Jets (with respective SS Supply Inlets and 'Shock Tube' Tunnels) with a parallel alignment (arranged in-line as a staggered sequence). The geometry also consisted of Intermediate lengths between each SS Jet (with an extended length at the MC back-end), and Conical Splitter Convective Devices at the end of each Intermediate length (except at the extended back-end length). Having 3 SS Jets, instead of a Single Jet, allowed for modular Cooling levels without changing the SS Tunnel geometry. The Altitude test range demonstrated in Appx. Q.1.1 showed how, through the different combinations of active Jets, the complete Altitude Temperature range (from JHB I.S.A to Design Point) was achieved. The Parallel in-line staggered arrangement ensured minimal SS stream P_0 loss; by avoiding direct-collision contact with the MC walls. This alignment also benefited the Main Inlet Supply, preventing recirculation and reversed flow at the Inlet face.

The high $P_{0\ SS}$ Jet was positioned so as to draw the Main flow into contact with the SS stream; using an aspiration effect. The staggered arrangement allowed for incremental cooling; reducing the responsibility of each cooling interaction. The intermediate lengths were budgeted using the theoretical mixing lengths, and then refined using the Numerical Model. The Conical Splitters divided each respective preceding Jet core; forcing the SS flow into the path of the surrounding Main flow. These Convective Devices were found to be a necessary inclusion in the MC Design; as Turbulent Diffusion alone did not achieve the desired mixing rate. In fact, additional Convective Devices were required within the MC back-end length to fully realize the Cooling potential; as described in Appx. Q.3.4. The Numerical Model (Section 13.4) was performed to determine the Supply Device requirements in achieving the Test Section objectives. The Numerical Model was validated by the Analytical Model, and confirmed the budgeted mixing lengths and Temperature Mixing expectations.

Design Objectives
$P_{0\ TS}$ = 100519 Pa, $T_{0\ TS}$ = 246.8 K, $\dot{m}$ = 23.27 kg/s, M_{TS} = 0.75, T_{TS} = 222.2 K.
MC Supply Device Requirements
$P_{0\ MAIN}$ = 83010 Pa, $P_{0\ SS}$ = 950000 Pa, $T_{0\ MAIN}$ = 297.9 K, $T_{0\ SS}$ = 283.2 K, $\dot{m}_{MAIN}$ = 2.09 kg/s, $\dot{m}_{SS}$ = 20.4 kg/s.

The Temperature Mixing continued beyond the length of the MC. It was for this reason that the MC performance measures were shifted from the WT Inlet ($_{WT\text{-}IN}$ subscript) to the Test Section Inlet ($_{TS}$ subscript). The Velocity objective had been over-achieved (M_{TS} = 0.75 > 0.7), but the Altitude Temperature objective was not met (T_{TS} = 222.2 K > 219 K). The reason for this set of conditions was the incomplete expansion of the latter SS Jets. The $P_{0\ TS}$ for the MC Numerical Model was higher than that required in the WT Analytical Model ($P_{0\ WT\text{-}IN}$ = 100519 Pa > 96140 Pa). This was due to the Main flow inheriting part of the Pressure Energy of the latter SS Jets, instead of fully extracting the respective Cooling potentials. The Turbulent Diffusion mechanisms were not sufficient, and further convective measures (within the extended back-end length) were warranted. These convective measures would be in the form of intrusive physical devices; so as to directly impact the Jet cores. Variation of the outer MC walls ($Ø_{MC}$) would not directly affect these cores, as described in Section 12.3, and would also negatively impact the aspiration effect of the Jets on the Main flow (especially at the Main Inlet). The convective devices would disturb the flow profile and create turbulence; thus dissipating the excess P_0. The Test Section results of the Numerical Model confirmed the capability to achieve the Design Point Velocity objective (M_{TS} >0.7), but at a lower Altitude Temperature ($T_{0\ TS}$ = 246.8 K) corresponding to 32000 ft.

14.3 Supply Device Cost Estimate

The Cost breakdown followed from the analyses in Sections 8.1 and 10. The cost breakdown did not include the materials and manufacturing costs of the Complete Geometry (MC+WT). Instead, it was based on the MC Supply Device evaluations; Airflow and Cooling using readily available machinery. Focusing on the cost breakdown of the Selected MC Supply Devices, the components were allotted into 2 groups: the Main Inlet Supply Device, and the 3 SS Inlet Supply Devices.

Main Inlet Supply Device

Primary Selection:	Centrifugal Fan Howden Donkin Series HBC-M Size 1250(E) 1.0
	Cost per Test (1 hr) = R 141.46
Back-Up Solution:	Air Cylinder Nuvair NUVT 4500 Spec DOT-E10869-4500/TC-SU4369-310
	Cost per Test (13.6 min) = R 288.46

SS Inlet Supply Device (x 3)

Primary Selection:	Rotary Screw Compressor CompAir Series L200 RS
	Air Receiver BOGE Vertical Air Receiver Galvanized 5000L 11bar
	Cost per Test (1 hr) = R 407.24 x 3 = R 1221.72
Back-Up Solution:	Air Cylinder Nuvair NUVT 4500 Spec DOT-E10869-4500/TC-SU4369-310
	Cost per Test (13.6 min) = R 1145.04 x 3 = R 3435.12

Total Cost Summary

The complete Cost per Test (1 hr) at Design Point was the combination of the 2 Primary Selections:
Cost per Test (1 hr) = 141.46 + 1221.72 = R 1363.18

This cost only pertained to the MC Delivery Mechanism. It did not include the cost evaluation of the SS Air Dryer component. The Cost Summary also excluded the Supply requirements for the Eductor flow. The cost exclusion of these specific Devices was based on the respective immediate relevance to the flow profile analysis in the Design.

14.4 Critical Analyses

The Critical Analyses were divided into 3 sections:

1) The analysis of the Design in meeting the PRS objectives.
2) The analysis of the Methods used in this Project to achieve the Design. This section assessed the decisions made in the design process, and evaluated the outcomes. It also critiqued the implementation of the SSEC Concept (the research aspect of the Project).
3) The analysis of the PRS rationality. This section evaluated the pragmatism of the Design Quality measures, and determined whether the current Design addressed the original Project Brief.

14.4.1 Critical Analysis of Design

The Project focused on achieving the Design Point conditions with the inherent capability of all stages encompassed by these conditions; i.e. achieving M0.7 at 35000 ft would imply achieving lower Velocities at lower Altitudes as well. With this reasoning in place, certain PRS requirements were addressed using the Isentropic 'Base Model' proposals; to demonstrate the intended behaviour. These requirements were addressed here and directed to the relevant sections in Appx. Q. Certain PRS objectives that formed the Measures of Compliance were addressed in that specific section; to avoid repetition.

Primary Requirements

- *Air supply that was capable of performing engine tests including Hot Soak, Cold Soak, Windmilling, Spooldown, and Starting Limits (Take-off altitude).*

The WT was capable of delivering the conditioned air to an inactive Test Piece Engine; the Tunnel did not require the Engine contribution in creating the intended flow path. This allowed for the Tunnel to be in operation, and producing the Altitude air conditions, before the engine needed to be activated. This fulfilled the requirements of testing an idle Engine in an existing flow stream. The Starting Limit Take-Off Altitude requirement (14764 ft) was also encompassed by the WT Altitude capability (up to 32000 ft).

- *Primary equipment (Air Supply and Air Conditioning) that was capable of simulating the test conditions for at least (≥) 5 minutes.*

The Supply Devices selected for the Air Supply and Cooling Mechanism were both capable of running continuously over the required duration (5 minutes). The devices supplied the air dynamically; with the Rotary Compressor requiring an Air Receiver to buffer the 'rotary' air pulsations. The Numerical Models confirmed the intended Steady State flow path that was present for the 5 minute duration.

Constraints

- *WT feature that allowed engine exhaust products to be drawn out in event of hazard.*

The WT was designed with an Eductor; immediately downstream of the OTS. The component supplied the WT with a supplementary flow that had a higher M and P_0 than the Main flow; at the immediate location. The Eductor specification was meant to create an aspiration effect in the immediate space downstream of the OTS. It drew out the exhaust products of the Engine, and served to suffocate the Engine in the event of hazard. This device was implemented merely as a placeholder; with a contribution that reflected that intended purpose. The actual design and optimization of this component was left as Further Work in Appx. Q.3.2.

Measures of Compliance

- *The ability to achieve the Design Point altitude condition (35000 ft); through the effectiveness of the Cooling mechanism.*

The Cooling mechanism implemented in this Design (SSEC concept) achieved a level of Cooling far superior to the alternative listed for selection (Vapor Cycle). However, it did not achieve the Design Point Altitude requirement of 35000 ft (T_0 = 240 K). The maximum Altitude simulated in this Design was 32000 ft (T_0 = 246.8 K). This was due to the incomplete expansion of the SS flows within the MC. The current Design Cooling capacity was considered a success; achieving 88.32 % of the required Cooling. This was especially true when compared to capability of the Back-Up selection (Vapor Cycle); which could only achieve 45.69 % of the required Cooling.

- *The ability to achieve the Design Point airflow velocity (M0.7); through the effectiveness of the Air Supply mechanism.*

Despite the Cooling mechanism falling short of the Altitude requirement, the Design over-achieved the Velocity requirement corresponding to the revised Altitude; M0.75 at 32000 ft. The incomplete expansion of the SS flows resulted in a higher Main flow P_0; which produced a higher V_{TS}. This higher V_{TS} compensated for the increased T_{TS}, and achieved the Design Point Mach number objective ($M_{TS} > 0.7$).

- *The efficiency of the Open Circuit WT flow path in achieving Design Point conditions; reducing excessive Pressure Energy wastage.*

The WT geometry was designed to optimize the utilization of the Inlet flow. It achieved the Test Section flow Velocity conditions with the minimal $\dot{m}$ contribution ($\dot{m}_{WT-IN}$ = 22 kg/s); by optimizing the Inlet-OTS-Outlet Pressure relationship. The flow achieved the OTS requirements from the WT Inlet specifications and exited to Atmosphere with minimal energy wastage ($P_{0\ WT-OUT}$ = 83303 Pa, compared to $P_{WT-OUT} = P_{ATM}$ = 83000 Pa). The excess P_0 (303 Pa) energy served to prevent backflow at the WT Outlet; when the Test Piece Engine was inactive. The MC however, in implementing the SSEC concept, resulted in a significant P_0 loss due to the expansion of the SS Jets. This loss was necessary for the SS flow expansion, but resulted in a Sudden Expansion loss of K_{SE} = 0.92. The loss, estimated using the MC Analytical Model (Section 12.5), reduced $P_{0\ SS}$ from 950000 Pa to 158354 Pa (± 83% loss). There was no way to avoid this, as the Sudden Expansion facilitated the contact between the Hot Main flow and Cold SS flow; and was thus accepted as part of the Design. The WT Design, in isolation, presented a highly efficient utilization of WT Inlet conditions. The MC Design however, represented a significantly inefficient, but necessary, way of expanding flow. The Complete Design (WT+MC) was therefore a success in the utilization of Supply specifications; to achieve the Test Section Design Point conditions.

- *The cost effectiveness of the Supply Device utilization in achieving the Design Point conditions; in keeping with the designated academic purposes.*

The Supply Devices (and associated support equipment) were selected from readily available market options. At no point did the Tunnel Inlets require custom made Devices (or support equipment). The costs were based on the specific academic application of the Devices (5 minute testing time buffered by safety intervals), and were presented on the basis of utilization. This utilization cost (R 1363.18) however, presented a significant hurdle when considering the initial investment. The Supply Devices included a Centrifugal Fan (Capital Cost = R 315 693.00) and 6 Rotary Compressors (Capital Cost = 6 × {R 695 100.00 + R 91 762.40} = R 4 721 174.40). Considering that the application was strictly for academic purposes, with little to no commercial reimbursement, this cost presented a significant barrier to the feasibility of the Design and was left to stakeholder decision processes.

- *The modularity of the Supply Device capability; to achieve the incremental altitude replication.*

The Cooling Mechanism (Altitude replication) of this Project was designed with the intention of modular Supply levels. The SS Supply Devices were positioned in pairs at 3 Key Point locations. The 3 SS flow streams entered as Jets along the MC length, and each Jet contributed an equal amount to the Cooling contribution. This allowed for intermediate Cooling levels; between JHB ISA and Design Point. It was achieved by deactivating 1 or more of the Jets, and supplementing the flow with the Centrifugal Fan Supply. This process was left as Further Work in Appx. Q.1.1.

- *The modularity of the WT Test Section in achieving the Secondary Objectives (Propeller Testing and Inlet Distortion Pattern Testing).*

The Test Section was designed as an Open Test Section (OTS) with an arbitrary chamber diameter. This chamber diameter could theoretically be scaled to accommodate the Propeller diameter ($Ø_{BLADE}$ = 2 m), but was sized in this Project to maintain continuity in the Numerical Model. The components upstream of the OTS (Plenum Chamber, Nozzle, and intermediate length) could be substituted with a gradual Diffuser to facilitate the required flow expansion; so as to accommodate the Propeller Blades. The current Supply Device capability however, would result in a significantly lower M_{TS}. It would warrant the re-evaluation of these Devices to meet the Propeller Testing requirements. These design concerns were left as Further Work in Appx. Q.1.2. The Analytical and Numerical Models were both designed with an intermediate length prior to OTS. This length could easily be retrofitted with a designated Distortion Pattern. The WT Inlet conditions could then be scaled back, to avoid Choke at the OTS Inlet, and swirl testing could be performed. This analysis was not attempted due to the comparative purposes of Distortion Pattern testing and the Design objectives of this Project; detailed as Further Work in Appx. Q.1.3. The modularity of these components formed the Secondary Requirements of the PRS. Whilst it was possible to include these components in the current Design, the respective implementations did not influence the Design Quality.

14.4.2 Critical Analysis of Method

This section encompassed the major decisions taken during the development of the WT and MC models; and the respective impacts on the validity of the Design. These decisions were categorized as:

1) Unique components of the WT geometry
2) Decisions taken in the WT Numerical Model
3) Mixing Mechanism of the MC (SSEC Concept)
4) Decisions taken in the MC Numerical Model

WT Components

The Eductor component was implemented as a placeholder; with the optimization left for Further Work in Appx. Q.3.2. This device was placed downstream of the OTS; to create an immediate 'partial vacuum'. The energy contribution of this flow was minimal, when compared to the Main flow, and did not impact the WT Design Point objective. The positioning of this component, downstream of the OTS, ensured that it did not affect the flow conditions upstream. The Test Piece Engine, within the OTS, was simulated as a geometrical feature only; i.e. 'bluff body'. The Design ignored the contribution of the Engine (ingestion and exhaust); this active Engine state was left as Further Work in Appx. Q.3.1. In reality, the Engine would produce a significant EGT that would boost the energy profile of the flow exiting the Tunnel. The Design proactively accounted for this additional energy by the over-sizing of the Collector lip at the OTS Exit (the narrowest WT segment downstream of the Engine). This ensured that the potential energy contribution of the Test Piece Engine would not Choke the flow downstream. The current Open Circuit WT Design was capable of testing the Engine within an OTS, under Altitude-specific conditions. It allowed for the analysis of RAM effects, and emitted the combined exhaust flow (WT + Engine) without the need for air reconditioning or risking the integrity of sensitive WT equipment (Supply Devices).

WT Modelling

The purpose of the WT Model was to obtain the MC Out/WT In requirements (T_0 and $\dot{m}$), and not necessarily to assess the effectiveness of each WT component. The performance validation for each of the WT components was limited to the comparison between the Numerical Results and the Analytical estimates (flow-specific theoretical expectations). The WT Numerical Model was meshed with a 1^{st} Layer cell size that prevented y+ conformance; due to the limited cell count available. This non-conformance ruled out the implementation of the 'ideally suited' $k_{TKE} – \omega_{SDR}$ Turbulence Model. This particular model would have adequately simulated: Boundary Layer Separation of the OTS free-jet, and Adverse Pressure Gradient of the Eductor aspiration effect. The decision was to implement the $k_{TKE} – \varepsilon_{TDR}$ Turbulence Model; and treat the OTS effectively as a 'black-box'. The approach involved monitoring the OTS Inlet and OTS Exit using Mass Weighted Averages (MWA); to attain the bulk flow parameters. This approach suited the Design application, as the performance measures were in the bulk flow behaviours. These bulk flow measures included maintaining Global $\dot{m}$ balance, and attaining the core flow behaviour at the OTS Inlet. The only exception to this exclusive approach (focusing on core, and ignoring near-wall) was the intermediate length prior to the OTS. This length was designed to develop a potential core flow profile prior to the OTS, and utilized the friction within this length to increase Mach number. This length did perform as intended, but was artificially exaggerated (slightly) by the inflated Viscous Sublayer. The exaggeration however, did not affect the bulk flow objectives in a meaningful way. The decision to implement the larger mesh, and focus on the core flow bulk behaviour, provided a solution that accurately defined the WT flow.

MC Mixing Mechanism

The Temperature Mixing mechanism investigation was based on 'Classical Thermodynamics', using macroscopic flow properties (P, V, T), instead of the molecular-scale approach of the 'Gas Kinetic Model'. The SSEC concept involved the Sudden Expansion of High Pressure Ambient Temperature airflow, to achieve an Underexpanded (UE) SS flow. During the expansion of the SS flow Jet into the MC, it was assumed to lose its entire Velocity component (V_{SS}). The Jet had to use its Thermal energy ($T_{0\ SS}$) to maintain the mechanical energy stream path with the MC flow. The extent of this SS Jet expansion loss was further refined upon the K_{SE} loss coefficient optimization. The principle value (K_{SE} = 0.92) however, was still high enough to justify this assumption of complete SS flow Velocity head loss in the MC Energy balance. The Jet flow entered with low Static Temperature (T_{SS}), and performed the expected Temperature reduction of the Main flow. Even with the accumulating Main flow $\dot{m}$ within the MC, all Jets entered as UE SS Jets. The Temperature Mixing of the Cold SS flow Static Temperature (T_{SS}) and Hot Main flow Stagnation Temperature ($T_{0\ MAIN}$), to achieve the Resultant Stagnation Temperature ($T_{0\ WT\text{-}IN}$), was a valid concept demonstrated by the Numerical Results. The insufficient Cooling, i.e. not achieving the Design Point Altitude, was the result of the incomplete expansion of the SS flow in the MC. The latter SS Jets were encapsulated by the accumulating Main flow $\dot{m}$ (due to contributions of the preceding SS flows), and were prevented from completely expanding to $Ø_{MC}$. This occurrence increased the disparity between the respective 'reduced K_{SE} loss' and the assumed 'complete V_{SS} loss'. The Main flow inherited part of the high Pressure energy of the SS flows, instead of extracting the respective Temperature reduction potential. This resulted in a higher $P_{0\ MAIN}$ and $T_{0\ MAIN}$ than the Analytical prediction. This was the main deficiency in the Final Design. It prevented the Design from achieving the

Primary PRS Altitude requirement (35000 ft). The SSEC Concept however, was still valid and considered a success. It achieved 88.32 % of the required Cooling. The SSEC Concept was inefficient with regards to Pressure energy wastage (due to the Sudden Expansion), but it was effective in achieving the Absolute Minimum Temperature (T_0 = 246.8 K). The Concept was capable of rapidly cooling large amounts of airflow without changing the flow chemical composition. Typically, this phenomenon of Supersonic Cooling was analysed as a detrimental side-effect to supersonic flight (i.e. surface icing). However, in this Project, the Cooling Concept was shown to be more effective than both Vapor Cycles (superior $\dot{Q}$ and $T_{0\ MIN}$) and Dry-Ice sublimation (superior $\dot{Q}$ and retained k_{AIR}) in achieving the required Cooling. It was capable of providing the Altitude-conditioned airflow suitable for Test Piece Engine ingestion. Altitude could be replicated without having to house the Test Piece Engine in a vacuum chamber, or having to create a Pressure differential using High and Low Pressure sources at the Engine Inlet and Outlet respectively. Not only did this alleviate the concerns of the WT equipment risk and Engine Exhaust Gas reconditioning, it also allowed for the analysis of the RAM effects available with the current OTS Design. The SSEC Concept was a successful application for the current Project, and proposed a valid option for other possible applications where:

- The Minimum Temperature required is beyond the capabilities of typical Chillers ($T_{0\ MIN}$ < -7 °C).
- Large amounts of continuous (uninterrupted) airflow needs to be Cooled.
- Airflow integrity is of importance to the Cooling application; air composition needs to be retained.

MC Modelling

The 1st Layer cell size restrictions, and consequences, of the WT were also faced with the MC Numerical Model. Unlike the WT though, the $k_{TKE} - \omega_{SDR}$ feature set could not necessarily be ignored by treating the free-jet occurrences as 'black boxes'; via MWA on either side. Even though the Design objectives lay within the bulk flow behaviour (as opposed to near-wall), the $k_{TKE} - \omega_{SDR}$ Turbulence Model was needed to interpret the 'inter-flow' boundary layer dissipation of the SS Jets into the Main flow. This Turbulent Diffusion was a defining characteristic of the SSEC Mechanism. The decision to implement the valid alternative $k_{TKE} - \varepsilon_{TDR}$ Turbulent Model had to be compensated for; using other indirect methods of exaggerating turbulence. This was accomplished by limiting the Model to the numerically diffusive 1st Order Solution Methods. These decisions to enhance Turbulence Diffusion, given the inadequate $k_{TKE} - \varepsilon_{TDR}$ Model, produced a solution that confirmed the SSEC Concept and reflected the Temperature Mixing within the MC. The Solution however was of 1st Order, and involved manipulating the Solver capability to reflect the desired intention of exaggerating turbulence. It did not conform to the Roache [29] guidelines for publishing; thereby reducing the relevance of the Model. The Solution therefore served as a proof of the Cooling Concept, rather than a quantifiably accurate benchmark. The limited cell count, that affected the 1st Layer cell size, also affected the resolution of the repeated shock cell structure within the UE SS Jet flow core. This limitation necessitated the simulation of an Isolated SS Model. It dedicated the entirety of the limited cell count to resolving the SS Jet core; for comparison to published sources. The Isolated SS Model revealed an elongation of the SS Jet flow core, compared to the MC Model interpretation, before becoming subsonic. The MC Design however, was pre-emptively designed to accommodate the elongated Jet flow cores, and was still relevant. The repeated shock cell structure merely offset the Turbulent Mixing process (within the subsonic region), and did not negate the fundamental SSEC implementation. The current modelling of the MC successfully captured the

Temperature Mixing, and the Cooling objectives, inherent of the SSEC Concept. It provided a Solution that demonstrated the bulk flow workings of the mechanism, and proved the SSEC Concept a success.

14.4.3 Critical Analysis of PRS

The Primary Performance Requirements (Section 3.1) were all realisable propositions. These Primary Requirements comprehensively described the Tunnel capabilities needed in order to perform Gas Turbine testing to military standards. The Complete Geometry (MC+WT) met all the Primary requirements (Altitude modularity, testing time, and an independent continuous Air Supply), but at a revised Design Point. The Design achieved the specified Design Point Velocity requirement (M0.75 > 0.7), but fell just short of the Design Point Altitude requirement (32000 ft < 35000 ft). With the proposed alterations, described as Further Work in Appx. Q.3.4, the Design could increase its capability from the Revised Design Point Altitude limit to the Primary Performance Requirement. The flow path of the Open Circuit WT was designed to be energy efficient; minimizing component losses. However, this Measure of Compliance would have to be revised to the respective applications of the MC and WT. The Tunnel geometry was designed to provide the Test Section conditions with minimal WT Inlet specifications. The MC Cooling Mechanism however, required the expansion of SS Jets which resulted in a substantial Pressure energy loss for each respective Jet. These expansion losses dwarfed all other energy losses and, when taken in consolidation with the WT, rendered all Tunnel efficiency measures moot. This Measure of Compliance would then have to be isolated to the WT flow path alone, and not the Cooling Mechanism within the MC. The Secondary Performance Requirements (Section 3.2), involving the modularity of the OTS, would have to be revised with consideration of the Project scope. The Inlet Distortion Pattern Testing, described as Further Work in Appx. Q.1.3, distinguished the respective purposes of the Numerical Modelling in this Project and the hypothetical Distortion Testing of an Engine Inlet. Given that the Design was based on the performance of the WT (and preceding MC), the Inlet Distortion Pattern Testing was not a pertinent Measure of Compliance. The Propeller Testing Secondary Requirement, described as Further Work in Appx. Q.1.2, necessitated the complete overhaul of the OTS and the re-evaluation of the Supply Devices; in order to supply the Design Point conditions across $Ø_{BLADE}$ = 2 m. This Measure of Compliance would have to either be relaxed, to a decreased capacity, or be removed entirely from the Design requirements. The current Supply Device capacities were not conducive to Propeller Testing. The Compliance Measure of Cost Effectiveness, with regards to the designated academic purposes, presented a significant hurdle to the Design feasibility. The Design made every attempt to be economical in utilization costs, but the pursuit of the Primary Performance Requirement of Design Point Altitude necessitated the inclusion of multiple Rotary Compressors. The high, and arguably unfeasible, Capital and Utilization costs were necessary. This Measure of Compliance would have to be relaxed significantly; in order to fully realize the Design capabilities. With the exception of these revisions to the Measures of Compliance, and certain Secondary Performance Requirements, the Design had successfully satisfied the Performance Requirement Specifications (Section 3). The Design was theoretically capable of performing military-standard testing for the specified UAV Gas Turbine Engine. With the proposed Numerical Modelling and Design Geometry refinements (described as Further Work in Appx. Q.2 and Q.3 respectively), and the Scaled Physical Model to provide a direct experimental result contribution (described as Further Work in Appx. Q.1.4), the Design would provide an effective and comprehensive solution to the Project Brief.

References

1 Wits MIA, ER 000 Masters (R) Degree Brief, University of Witwatersrand (EBE), 2011

2 Ledger University Research Program, *BALLAST: Gas Turbine Technology Skills Development*, https://ledger.wikispaces.com/BALLAST, 2018

3 Rolls Royce Ltd, *The Jet Engine*, Rolls Royce, 1969

4 NASA, *Technology Opportunity – Wind Tunnels at Glenn*, NASA Glenn Research Centre, https://facilities.grc.nasa.gov

5 AEDC, *Propulsion Wind Tunnel*, AEDC Public Affairs, Release # 2005 -392

6 ONERA, *Modane S3 Technical Specification*, Grands Moysens Techniques, www.onera.fr

7 DERA Brochure, *Pyestock Cell 3 Technical Specification*, DERA 1995-2001

8 G.S. Markovich, *Wind Tunnels and Their Instrumentation*, Jerusalem: IPST, 1996

9 NASA, *Beginner's Guide to Wind Tunnels*, NASA Glenn Research Centre, www.grc.nasa.gov/WWW/k-12/airplane/tunoret.html(Open WT),www.grc.nasa.gov/WWW/k-12/airplane/tuncret.html (Closed WT)

10 M. Davis, W. Baker, G. Power and D. Beale, *A Proposal for Integration of Wind Tunnel and Engine Test Programs for the Evaluation of Airframe-Propulsion Compatibility Using Numerical Simulations*, Volume 124, Severdrup Technology Inc. AEDC, July 2002

11 DERA Brochure, *Pyestock Cell 1 Technical Specification*, DERA 1995-2001

12 The RAND Corporation, *Technical Report: Wind Tunnel and Propulsion Test Facilities*, National Defense Research Institute, 2004

13 Arthur M. Halpern, *Chemistry Encyclopaedia – Gases*, Chemistry Explained: Foundations and Applications,www.chemistryexplained.com, 2013

14 FAA, *Federal Aviation Regulation (FAR), Section 33*, U.S. Department of Transportation
FAA, *Advisory Circulars (AC), AC 20 and AC 43*,U.S. Department of Transportation

15 MIL-E-5007D, *General Specification for Engine, Aircraft, Turbojet and Turbofan*, US DoD, 1995
JSSG-2007A, *Engines, Aircraft Turbine*, US DoD, 1998

16 Hsiao-Wei D. Chiang et al., *Miniature Liquid-Fuelled Turbojet Engine*, United States Patent No: 5782079, 7/21/1998

17 AMT Brochure, *AMT Nike EVP Specification*, www.amtjet.com/Nike.php, 2014

18 Patrick H. Oosthuizen and William E. Carscallen, *Compressible Fluid Flow*, McGraw Hill, 1997

19 Munson, Young and Okishi, *Fundamentals of Fluid Mechanics*, 5th Edition, John Wiley Inc., 2006

20 ANSYS Help 14.5, *FLUENT User's Guide, Theory Guide, and Tutorial Guide*, SAS IP Inc., 2012

21 I.E. Idelchik, *Handbook of Hydraulic Resistance*, 4th Edition, Begell House, 2008

22 Donald S. Miller, *Compressible Internal Flow*, BHRA Fluid Engineering, 1984

23 A. J. Reynolds, *Thermofluid Dynamics*, John Wiley and Sons Inc., 1971

24 Grant Nordwall, Jigger Jumonville and Terryl Matthews, *Desktop Use of Computational Fluid Dynamics to Design and Troubleshoot Compressors and Turboexpanders*, Proceedings of the 32nd Turbomachinery Symposium (Page 71-84), 2003

25 R.C. Pankhurst, *Wind-tunnel technique: an account of experimental methods in low- and high-speed wind tunnels*, London: I. Pitman, 1952

26 Mark Rennie, *Effect of jet length on pressure fluctuations in ¾ open-jet wind tunnel*, www.researchgate.net, 2000

27 Andrew J. Green, *Jet pumps and ejectors*, www.thermopedia.com, 2011

28 Robert G. Sargent, *Verification and Validation of Simulation Models*, Proceedings of the Winter Simulation Conference, 2011

29 Patrick J. Roache, Kirti N. Ghia, Frank M. White, *Editorial Policy Statement on the Control of Numerical Accuracy*, JFE (Journal of Fluids Engineering), ASME, 1986

30 R. Jauregui, F.Silva, *Numerical Validation Methods, Numerical Analysis - Theory and Application*, Universitat Politècnica de Catalunya (UPC), http://www.intechopen.com/books/numerical-analysis-theory-and-application/numerical-validation-methods, 2011

31 John Kaiser Calautit, Hassam Nasarullah Chaudhry, Ben Richard Hughes, Lik Fang Sim, *A validated design methodology for a closed-loop subsonic wind tunnel*, Volume 25, Journal of Wind Engineering and Industrial Aerodynamics, 2014

32 Peter Moonen, Bert Blocken, Staf Roels, Jan Carmeliet, *Numerical modeling of the flow conditions in a closed-circuit low-speed wind tunnel*, Volume 94, Journal of Wind Engineering and Industrial Aerodynamics, 2006

33 LEAP Australia Computational Fluid Dynamics blog (CFD), *Tips and Tricks: Turbulence Part 2: Wall Functions and y+ Requirements*, www.computationalfluiddynamics.com.au, 2012

34 NASA, *Examining Spatial (Grid) Convergence*, www.grc.nasa.gov/WWW/wind/valid/tutorial/spatconv.html, 2008

35 Fluent Software Training, *TRN-99-003 Solver Settings*, Fluent Incorporated, 23/02/2001

36 Harmadipedia blog, *Rotating Machinery Design Basis – Compressor*, www.harmadipedia.blogspot.com/2013/06/rotating-machinery-design-basis.html, 2013

37 Beric W. Skews, *MECN Compressible Flow Course Notes*, University of Witwatersrand, 2001

38 E.T. Sweeney, *An Introduction and Literature Guide to Mixing*, BHRA Fluid Engineering, 1978

39 G.L. Shires, *Process Heat Transfer – Prandtl Number*, CRC Press, www.thermopedia.com, 1994

40 S. Chakraborty, *Fully Developed Pipe and Channel Flows*, IIT Kharagpur, 2006

41 D. R. Otis, *Choking and Mixing of Two Compressible Flow Streams*, ASME JFE, June 1976

42 Clarkson.edu, *Prandtl's Mixing Length Hypothesis*, Research Projects - Clarkson University New York, web2.clarkson.edu/projects/fluidflow/courses/me639/downloads/32_Prandtl.pdf, 2013

43 Robert S. Brodkey, *Turbulence in Mixing Operations: Theory and Application to Mixing and Reaction*, Academic Press Inc. New York, 1975

44 Erina Murakami, Dimitri Papamoschou, *Mixing Layer Characteristics of Coaxial Supersonic Jets*, AIAA (American Institute of Aeronautics and Astronautics)-2000-2060, 2000

45 S. G. Chuech, M.C. Lai, and G. M. Faeth, *Structure of Turbulent Sonic Underexpanded Free Jets*, AIAA (American Institute of Aeronautics and Astronautics) - VOL. 27 NO. 5, 1989

46 Alexey Velikorodny, Sergey Kudriakov, *Numerical Study of the Near-Field of Highly Underexpanded Turbulent Gas Jets*, Volume 37, International Journal of Hydrogen Energy, 2012

47 André Bakker, *Lecture 5 - Solution Methods - Applied Computational Fluid Dynamics*, http://www.bakker.org, © André Bakker (2002-2006),© Fluent Inc. (2002)

48 P. Lovaraju, E. Rathakrishnan, *Experimental Studies on Co-flowing Subsonic and Sonic Jets*, Volume 87, Flow Turbulence Combust, 2011

49 K. B. M. Q. Zaman, *Asymptotic spreading rate of initially compressible jets—experiment and analysis*, Volume 10, American Institute of Physics - Physics of Fluids, 1998

50 K. Bülent Yüceil, M. Volkan Ötügen, *Scaling parameters for underexpanded supersonic jets*, Volume 14, American Institute of Physics - Physics of Fluids, 2002

51 N. Karthikeyan, B.T.N. Sridhar, *Experimental and CFD analysis on coaxial turbulent jets with different velocity ratios*, Volume 38, Elsevier - Procedia Engineering, 2012

52 Mark H. Carpenter, Nail K. Yamaleev, *On Accuracy of Adaptive Grid Methods for Captured Shocks*, NASA/TM-2002-211415, NASA Langley Research Center, August 2002

53 Nandkishore Menon, *Analysis of non-axisymmetric underexpanded jet flow fields*, PhD Thesis, University of Witwatersrand (EBE), July 2009

References pertaining to electronic Appendices (prefix 'SD') were included on the Supplementary Disc.

Appendix A – Isentropic Sizing (WT)

A.1 Test Section Diameter ($Ø_{TS}$) Sizing

The Test Section diameter ($Ø_{TS}$) directly affected the required mass flow rate ($\dot{m}$) within the Wind Tunnel. In this section, the $Ø_{TS}$ was calculated using an Isentropic Model. The sample calculation set (with relevant isentropic equations) was presented in Appx. G.1. The set of equations were solved simultaneously using EES software. By varying the $Ø_{TS}$ with all other values held constant, the relationship between $\dot{m}$ and $Ø_{TS}$ was developed. The relationship, depicted in Figure A1, showed an exponential increase in $\dot{m}$ required with an increase in $Ø_{TS}$. The $Ø_{TS}$ in this Design was set to 0.35 m, which was smaller than the Test Piece Engine at 0.4 m total diameter (incl. dress). It actually required the $Ø_{TS}$ jet flow to expand within the OTS, prior to reaching the engine frontal area. The retained potential core of the Tunnel flow entered the OTS, and the boundary layer of the jet had to grow. If the $Ø_{TS}$ were hypothetically increased to 0.5 m, so that the unperturbed flow profile completely immersed the Test Piece Engine, the required $\dot{m}$ would increase from 19.05 kg/s to 39.03 kg/s. Not only did this relationship promote the initiative of $Ø_{TS}$ minimization, but the actual value of $\dot{m}$ was limited by the maximum capacity of the Supply Devices. Doubling the required $\dot{m}$, by increasing the $Ø_{TS}$ such that it immersed the engine ($Ø_{TS} \approx 0.5$ m), would have effectively required 2 Supply Mechanisms. It was for this reason that the Design $Ø_{TS}$ was retained at 0.35 m. It focused the core of the airflow on the engine frontal area, rather than producing a uniform unperturbed flow profile that immersed the total engine diameter = 0.4 m (incl. dress). The Tunnel flow achieved the Design Point conditions at the Engine Inlet face, with the minimum Supply Device requirements.

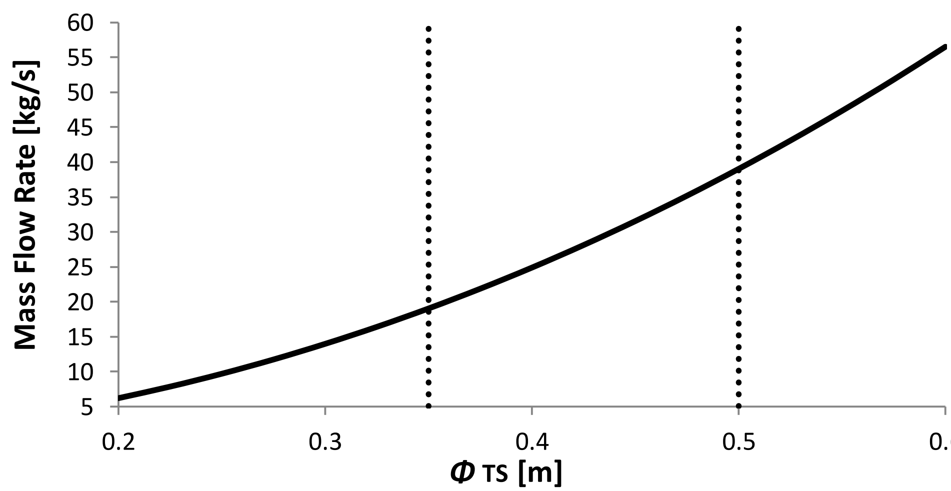

Figure A1. Relationship between Test Section Diameter ($Ø_{TS}$) and Required Mass Flow Rate ($\dot{m}$) with comparison markings at $Ø_{TS}$ = 0.35m and $Ø_{TS}$ = 0.5m

A.2 Outlet Diameter ($Ø_E$) Sizing

The sizing of the Outlet (as pertaining to Figure 12) was optimized to reflect a balance between the lowest achievable Static Pressure at the Test Section (P_{TS}), and the smallest Outlet Diameter ($Ø_E$).

- Reducing the P_{TS} allowed for a lower Inlet Stagnation Pressure (P_0) in achieving the required Test Section Mach number. This required less work to be done by the Supply Device.
- Reducing the $Ø_E$ allowed for less geometric expansion of the flow from $Ø_{OTS}$. This resulted in reduced expansion component losses, and a reduction in overall Wind Tunnel length.

The isentropic relationship between the flow properties at the Test Section and the Outlet was described using the previously listed ideal gas equations (Section 5.1). The equations were detailed with: flow properties from Figure 12, $Ø_{TS}$ = 0.35 m, and $Ø_E$ to be varied manually [0.35 – 5 m]. Using the Isentropic equation set from the previous subsection (Appx. G.1), and varying the $Ø_E$ with all other values held constant, the relationship between the Outlet size ($Ø_E$) and Test Section Static Pressure (P_{TS}) was depicted in Figure A2. The figure showed that P_{TS} decreased exponentially with increasing $Ø_E$, and reached the maximum trade-off at $Ø_E \approx 1$ m. By increasing $Ø_E$ from 0.35 m (equivalent to $Ø_{TS}$) to 1 m, the isentropic evaluation of P_{TS} dropped from 83000 Pa to 60000 Pa. This presented a significant saving in Supply Device requirements (P_0 capability), especially considering the Pressure Ratios concerned. For the sake of component robustness (in anticipation of non-isentropic flow), $Ø_E$ was selected as 1.25 m.

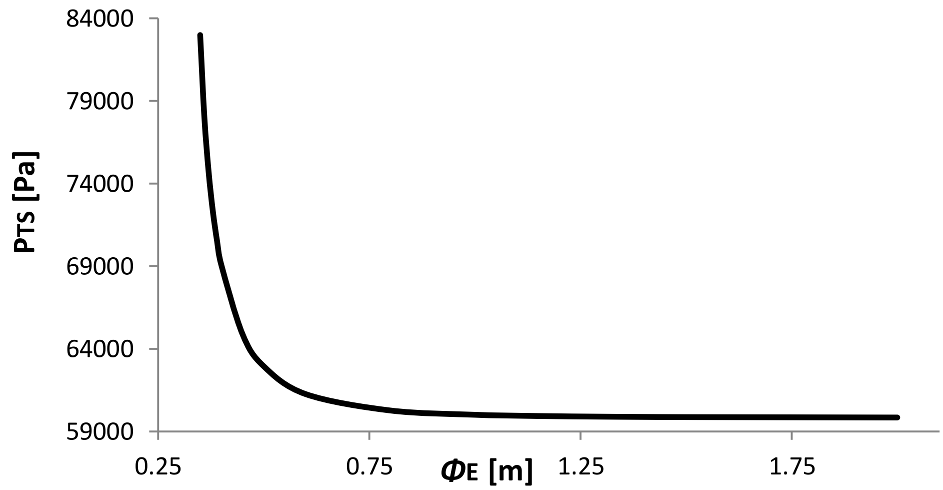

Figure A2. Relationship between Outlet Diameter ($Ø_E$) and Test Section Static Pressure (P_{TS})

Appendix B – Mechanism Design Study

B.1 Air Supply Design Point Optimization

The hypothesis was tested using the Analytical Model equation set from the WT design; Appx. G.2. $P_{0\ MAIN}$ was varied, and the resulting $\dot{m}$ and M_{TS} were recorded. All other WT flow specifications were retained, with exception of $T_{0\ MAIN}$. The $T_{0\ MAIN}$ had to varied, with each $P_{0\ MAIN}$ tested, in order to achieve the Design Point altitude requirement (T_{TS} = 219 K). This $T_{0\ MAIN}$ 'matching' was done because the parameter analysis in this optimization concerned only the variation of M with respect to P_0 and $\dot{m}$ (i.e. Air Supply), not altitude temperature (i.e. Cooling). The parameter of Mach number was chosen as the measure of cost compromise; due to the Primary Product Requirements (Section 3.1). The PRS stated that the test needed to be performed at several altitudes (10 in fact) within the ceiling limit (35 000ft) at the Design specific Mach number (M0.7). The Static Temperature (T) identified the altitudes, whereas the Mach number identified the Design capability at each respective altitude. So it was necessary for the entire spectrum of T [219-278.15 K] to be tested, whereas M was defined by the capability of the Engine being tested. In saying this, the capacity of the WT could be scaled back (if machinery cost necessitated) by testing the Engine at a lower M. The Design would still meet the PRS requirements for an altitude wind tunnel; albeit never truly testing the Test Piece Engine to full potential (M0.7).

Figure B1 showed M_{TS} and $\dot{m}$ responses to the respective $P_{0\ MAIN}$. The $P_{0\ MAIN}$ was varied from 85500 Pa to 108000 Pa; with the resultant M and $\dot{m}$ increasing accordingly. The rate at which these results (M and $\dot{m}$) increased with increasing $P_{0\ MAIN}$ (respective gradients) allowed the most efficient range to be identified. Figure B1 revealed that reducing the Test Section Mach objective from M0.7 (P_0 = 98500 Pa, $\dot{m}$ = 22 kg/s) to M0.5 (P_0 = 91250 Pa, $\dot{m}$ = 17.25 kg/s) resulted in a saving of P_0 = 7250 Pa and $\dot{m}$ = 4.75 kg/s. The saving in $\dot{m}$ was readily identifiable as a ± 22% reduction. The saving in P_0 however, was best interpreted as the respective Pressure increase from ambient by the Supply Mechanism (i.e. $P_{JUMP} = P_0 -$ 83000 Pa). This interpretation, as $P_{JUMP\ (M0.7)}$ = 15500 Pa and $P_{JUMP\ (M0.5)}$ = 8250 Pa, identified the saving as a ±47% reduction in Supply Mechanism P_{JUMP} requirement. This represented a significant reduction in overall Supply Mechanism requirements; more so with respect to P_{JUMP} than with $\dot{m}$.

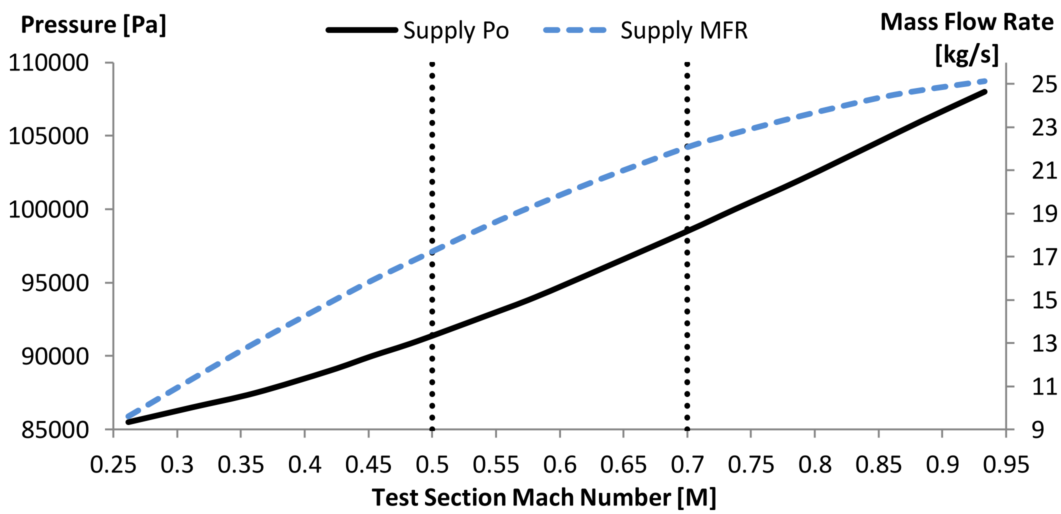

Figure B1. Supply Mechanism requirements (P_0 and $\dot{m}$) as a function of Test Section Mach Number (at the Design Point altitude) with comparison markings at M0.5 and M0.7

These relationships were substantiated by the respective behaviour of the parameter plots seen in Figure B1. The required P_0 increased with increasing M, whereas the required $\dot{m}$ displayed a logarithmic increase with increasing M (until the eventual Choke at M = 1). These curve behaviours implied that making an economic compromise on the Supply Mechanism P_0 capability, within reason, had a lesser impact on the M capability. i.e. decreasing M requirement from M0.7 to M0.5 could reduce P_{JUMP} requirement by nearly half.

The $\dot{m}$ supply capability could always be addressed by connecting multiple Supply Mechanisms in parallel (to deliver a combined effort). The P_0 supply capability, on the other hand, presented a considerable hurdle in the choice of applicable machinery. The Harmadipedia [36] compressor map showed the various Supply Mechanisms (Compressors and Fans) with capability limits; as a function of P_{JUMP} and Volumetric Flow Rate ($\dot{\forall} = \frac{\dot{m}}{\rho}$). It was possible that, by reducing the P_{JUMP} by half (for economic compromise), an entirely different type of Supply Mechanism could be implemented; not just a lower specification model of the same type. It was reiterated here though, that in retaining the altitude condition (T_{TS} = 219 K) at each of the M values in Figure B1, $T_{0\ IN}$ had to be adjusted to reflect the change in P_0. The corresponding $T_{0\ IN}$ for the Test Section M plot was depicted in Figure B2.

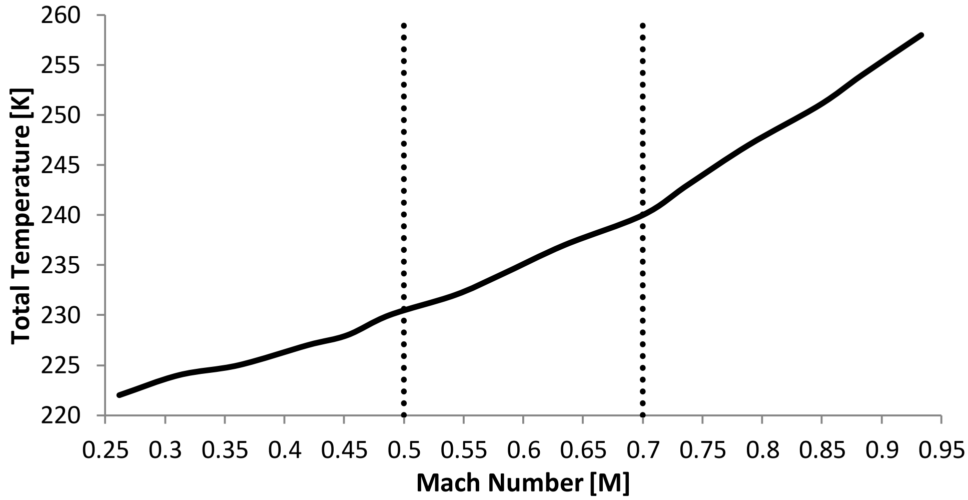

Figure B2. Resultant Main Inlet Stagnation Temperature ($T_{0\ IN}$) in attempting Design Point altitude (T_{TS} = 219 K) at the varying Mach number (corresponding to Figure B1)

From Figure B2, it was seen that decreasing M, from M0.7 to M0.5 (as was done in the hypothetical scenario in Figure B1), actually decreased the required Supply T_0 by 9.5 K (from 240 K to 230.5 K). The plot behaviour in Figure B2 demonstrated an exponential increase in $T_{0\ IN}$ requirement with increasing M; as was the case with the P_0 curve in Figure B1. It was important to note here that a higher T_0 was preferable. The flow would require less cooling from ambient temperature ($T_{0\ AMBIENT}$ = 278.15 K); i.e. less capacity required from the Cooling Mechanism. This decreased capacity was identified by comparing the cooling requirement (ΔT_0 = 278.15 – T_0) of each of the hypothetical Mach numbers (M0.5 and M0.7). This interpretation, $\Delta T_{0\ (M0.7)}$ = 38.15 K and $\Delta T_{0\ (M0.5)}$ = 47.65 K, revealed an increase in cooling capacity required by 20%, when M was decreased by 29%. Whilst this was not an immediate concern in the Air Supply Mechanism Evaluation, it did present a considerable consequence on the Cooling Mechanism Evaluation. It was shown in Section 10 that the costs and 'capability/limitation balances' of the Cooling Mechanism far outweighed that of the Air Supply Mechanism. In pursuit of an economically viable design, it was in the best interest to increase the required T_0 as much as possible. According to Figure B2, increasing T_0 implied a higher M. The Design Point was then retained at M_{TS} = 0.7 at $T_{0\ IN}$ = 240 K; requiring the Air Supply Mechanism to deliver $\dot{m}$ = 22kg/s at P_0 = 98500 Pa.

B.2 $P_{0\ SS}$ vs. $\dot{m}_{SS}$ (variable $T_{0\ OUT}$) Parameter Optimization

When developing the Isentropic Model for Ideal Expansion Condition, the parameter of Mach number defined the Critical Point ratios: P.R.*, T.R.*, and A.R.*. To that extent, each Testing Option could be represented by either the Mach number or one of these 3 Critical Point ratios interchangeably. For the sake of parameter clarity, each Testing Option was represented by the corresponding P.R.*. Using the P.R.* to identify each Ideal Expansion Condition scenario allowed for direct calculation (and plotting) of the required SS Supply Device P_0. It was reiterated explicitly here that P.R.* referred to the Critical Point ratio ($\frac{P_{O\ SS}}{P_b} = \frac{P_{O\ SS}}{97225}$), and not the P.R. used in typical Compressor specifications ($\frac{P_{O\ SS}}{P_{ATM\ (ISA)}} = \frac{P_{O\ SS}}{83000}$). The ratio pertained to the P_B specific to the application in Figure 21, as opposed to the hypothetical scenario of exiting to Atmosphere.

Figure B3 showed the required SS Mass Flow Rate contribution ($\dot{m}_{SS}$) for each P.R.* level, in order to achieve the resultant WT Inlet Stagnation Temperature ($T_{0\ OUT}$). The $T_{0\ OUT}$ effectively indicated the corresponding altitude. The $T_{0\ OUT}$ vertical axis in Figure B3 ranged 240 – 298 K. This range corresponded to the altitude requirements of 35000 ft (Design Point) – 8500 ft (Minimum altitude requiring cooling) respectively. Figure B3 revealed:

- **P.R.* < 5 was irrelevant**. The required $\dot{m}_{SS}$ increased beyond 11 kg/s at the Design Point altitude ($T_{0\ OUT}$ = 240 K). This was especially true with P.R.* = 2.5; where it required $\dot{m}_{SS}$ = 15.22 kg/s at Design Point. This was no easy task when the corresponding P_{JUMP} = 160337 Pa. This P_{JUMP} was well out of range of the flow rate capable options (Axial/Centrifugal Fans). These P.R.* levels required multiple high Pressure compressors in parallel to achieve the $\dot{m}_{SS}$.
- **P.R.* = 5 was identified as best $\dot{m}$ reduction**. This step in P.R.* level represented the most valuable $\dot{m}$ saving at Design Point altitude ($T_{0\ OUT}$ = 240 K); with regard to $\frac{\Delta \dot{m}_{SS}}{\Delta P.R.^*}$. This option (P.R.* = 5) reduced $\dot{m}_{SS}$ by 31% when doubling from P.R.* = 2.5. At no further increase in P.R.* level was the $\dot{m}_{SS}$ gain this profitable.
- **P.R.* > 10 revealed massively diminishing returns**. This was especially true at the lower altitude of 21000 ft ($T_{0\ OUT}$ = 270 K). Comparing P.R.* = 10 and P.R.* = 15 at this altitude revealed a saving of $\dot{m}_{SS}$ = 0.37 kg/s (10% decrease) at the expense of additional P_{JUMP} = 486670 Pa (50% increase). This rendered P.R.* > 10 highly inefficient.
- **P.R.* = 10 represented the limit of validity in increasing P.R.*.** This was not just the limit at the Design Point altitude; where increasing the P.R.* by 25% beyond this point (P.R.* = 12.5) resulted in a 5% saving in $\dot{m}_{SS}$. It was also the limit (more so) at lower altitude $T_{0\ OUT}$; where $\dot{m}_{SS}$ reduction was almost inconsequential.
- **The applicable P.R.* range = [5 – 10].** This range was applicable for Ideal Expansion Condition across the entire altitude spectrum. The optimum selection was defined by what Supply Device capabilities were available, but ultimately:

  P_{JUMP} range = 403675 – 890351 Pa   with corresponding $\dot{m}_{SS}$ range = 10.44 – 8.30 kg/s

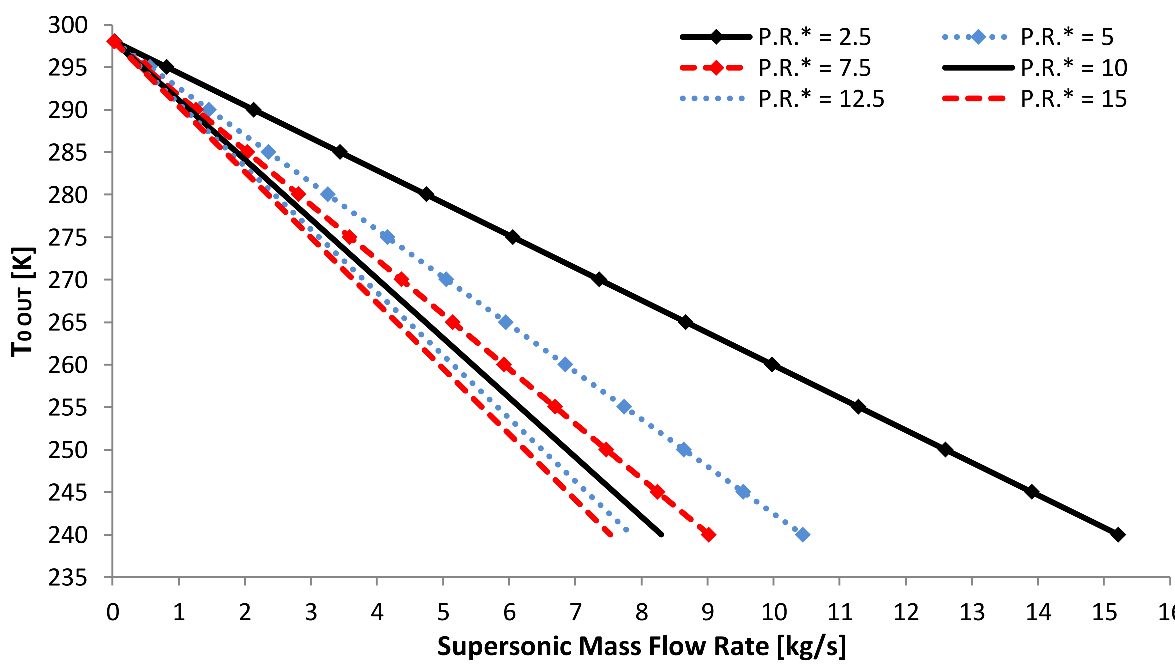

Figure B3. Range of P.R.* options (at Ideal Expansion Condition) to determine the required $\dot{m}_{SS}$; to achieve the respective altitude ($T_{0\ OUT}$)

Appendix C – K_{SE} vs. $\dot{m}_{SS}$ Parameter Optimization

Figure C1 depicted the relationship between K_{SE} and $\dot{m}_{SS}$ for 3 scenarios of 'decoupled A.R.* - P.R.*':

1. The Sample Calculation Model (Appx. G.4) – where the P.R.* = 13.05 and the A.R.* = 2.05 (corresponding to an Ideal Expansion at P.R.* = 11.139)
2. The Lower P.R. Model – where the P.R.* was reduced to 11.45 and the A.R.* retained at 2.05 (corresponding, as before, to a P.R.* = 11.139). This brought the P.R.* closer to what the A.R.* represented, but still ensured Underexpanded Flow.
3. The Lower A.R. Model – where the P.R.* was retained at the Sample Calculation value (13.05), and the A.R.* was reduced to 1.935 (corresponding to an Ideal Expansion at P.R.* = 10.04). This rendered the flow further Underexpanded, and at risk of Shock Diamond formation.

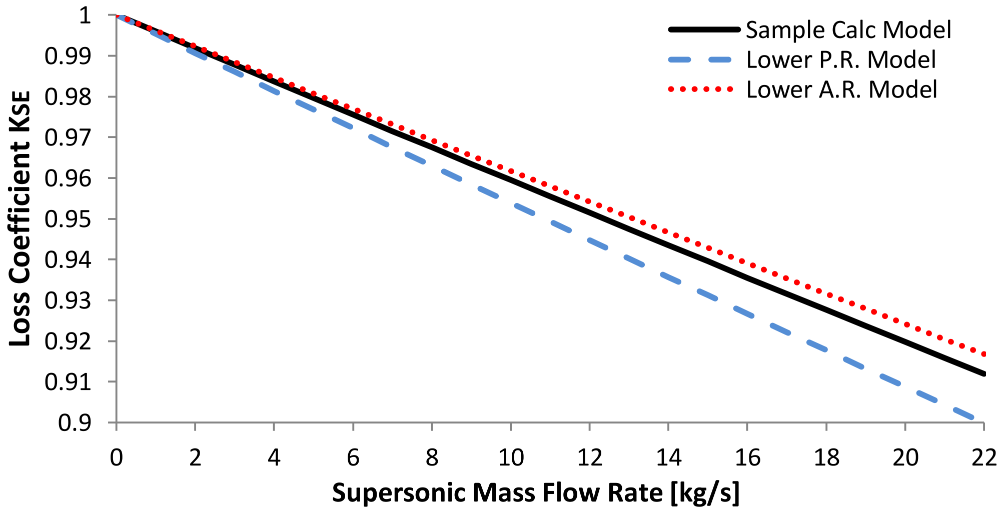

Figure C1. K_{SE} vs. $\dot{m}_{SS}$ relationship for 3 'decoupled P.R.* - A.R.*' scenarios: Sample Calculation Model (P.R.* = 13.05, A.R.* = 2.05), Lower P.R. Model (P.R.* = 11.45, A.R.* = 2.05), and Lower A.R. Model (P.R.* = 13.05, A.R.* = 1.935)

The difference in gradient between the 3 lines (Models) in Figure C1 showed that the closer the P.R.* was to the respective Ideal Expansion P.R.* (represented by the associated A.R.*), the lower the loss co-efficient (K_{SE}). The Lower P.R.* model best reflected this behaviour; when compared to the other 2 models. This K_{SE} vs. 'decoupled A.R.* - P.R.*' behaviour was important in that:

- The A.R.* was limited at Maximum by the $\dot{m}_{TOTAL}$ limit: $\dot{m}_{SS} < 22$ kg/s
- The P.R.* was limited at Maximum by the Compressor: $P_0 < 1083000$ Pa

Previously, the goal was to maximize the P.R.* ratio at P_0 = 1083000 Pa; so as to decrease T_{SS} as much as possible. The $\dot{m}_{SS}$ could then be delivered as per requirement; by varying the A.R.*. Now, it appeared beneficial to vary both P_0 and A.R.*; to meet the required $\dot{m}_{SS}$. This method reduced the difference between the Supply Device P.R.* and the geometry locked P.R.* (described by the A.R.*), and thus effectively reduced the K_{SE}. This 'varying' procedure helped to optimize the loss coefficient, but the principle value was still large; $K_{SE} \approx 0.9$ in the best case. This value was refined, after the SS Tunnel Exit Area ($\mathbb{A}_E$) was calculated per iteration, to reflect a more appropriate estimate. The iterative process was depicted in Figure C2; starting at K_{SE}. According to Figure C2, the K_{SE} was initially set to 0.9. This K_{LOSS} value implied the respective loss to $P_{0\,SS}$, and subsequently the P_E. The reduced P_E resulted in a higher T_E; higher than if the SS flow had entered the MC in an isentropic manner. The decreased cooling potential of the T_E required a larger $\dot{m}_{SS}$ contribution to $\dot{m}_{TOTAL}$. This increased $\dot{m}_{SS}$ compensated the Energy

Balance; in hope of achieving the required $T_{0\ OUT}$. In order to achieve this higher $\dot{m}_{SS}$, the SS Tunnel Throat ($\mathbb{A}_T$) had to be increased; as the flow was Choked at this narrowest location. In maintaining the corresponding A.R.*, the $\mathbb{A}_E$ then also had to be increased accordingly. The larger $\mathbb{A}_E$ ($Ø_E$) resulted in a smaller K_{SE}; which restarted the iterative process.

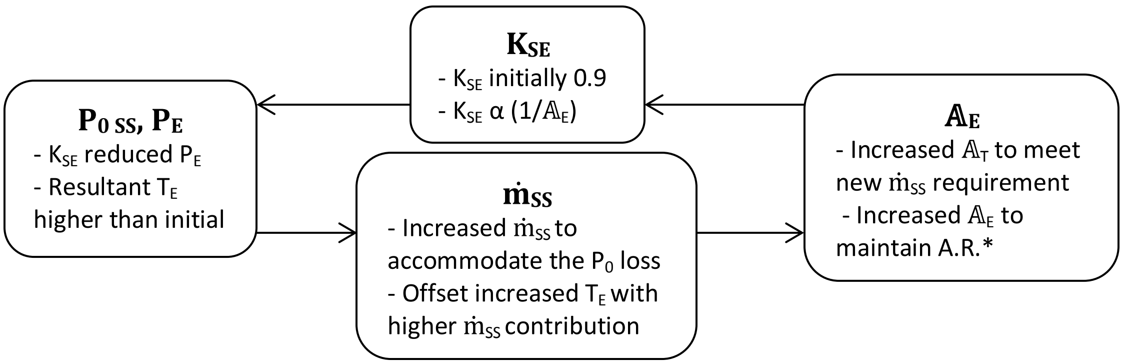

Figure C2. Flowchart of K_{SE} iteration process (Starting at K_{SE} = 0.9)

Appendix D – MC Numerical Solution Validation

D.1 MC and Isolated SS Model Comparison

The near-field supersonic flow behaviours for both the MC Model (SS1) and the Isolated SS Model were investigated in this section. The comparisons were made on the basis of the Contour Plots for Static Pressure and Mach number. The investigation highlighted the distinct purpose of the isolated SS Model in providing a relevant Numerical Model for comparison with published data. It was important to reiterate here that the 'jagged' near-wall contour appearance of the Symcut did not necessarily represent the full resolution of the mesh; adjacent wall surface meshes were excluded.

Static Pressure (P) Contour

Figure D1 Part A displayed the contour for the 1^{st} SS Jet in the MC (SS1). The Static Pressure (P) range was limited to the applicable spectrum concerning the SS1 Jet. The Max P value was displayed near the SS Tunnel Exit (Point 1 = 114–115 kPa). The flow exited the SS Tunnel with P greater than that of the MC (Point 2 = 81–84 kPa); confirming the UE SS flow requirement of $P_B > P_E$. The UE SS Jet flow then underwent the repeated shock diamond formation; expansion (Prandtl Meyer Fans) followed by compression (Oblique Shocks) of the flow. This was identified by the P oscillation: Low P at Point 3 (60–63 kPa), High P at Point 4 (93–96 kPa), Low P at Point 5 (75–78 kPa), and High P at Point 6 (84–87 kPa). The limited cell count within the MC mesh depicted P_{SS} to equalize P_{MAIN} within 2 shock diamond formations. This, however, was a gross simplification of the UE SS expansion process. The large MC cell size could not provide the resolution necessary to replicate the macroscopic repeated shock cell structure. Figure D1 Part B displayed the contour for the Isolated SS Jet. The contour depicted the Max P value near the SS Tunnel Exit (Point 7 = 113–117 kPa). The SS flow entered the MC with $P_E > P_B$ (Point 8 = 80–83 kPa). It underwent the expected flow expansion (Point 9 = 50–53 kPa), and compression (Point 10 = 107–110 kPa).The flow then repeated the shock diamond formation. The P oscillation however, continued beyond the length predicted by the MC Model (> 2 shock diamonds). The increased cell count of the Isolated SS Jet Model, and refined cell concentration within the Jet core, allowed for the

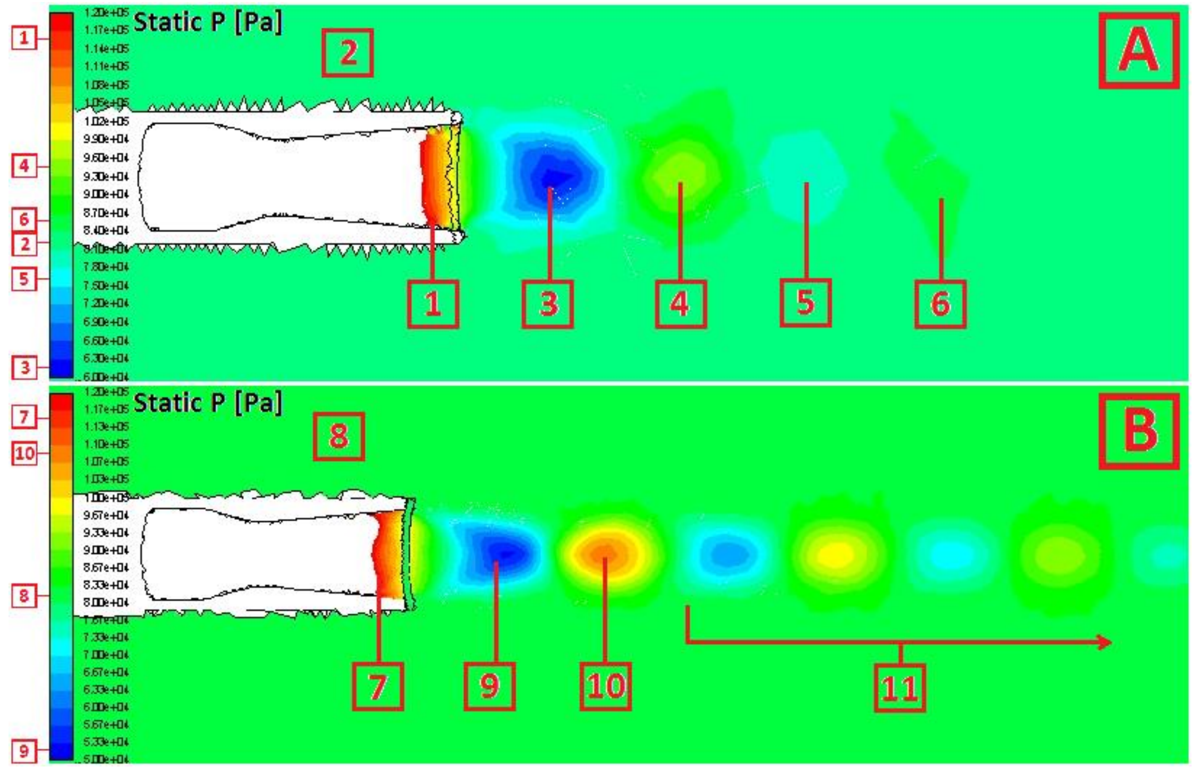

Figure D1. Static Pressure Contours for Part A) SS1 in MC Model, and Part B) Isolated SS Model; showing the decrease from P_E to P_B

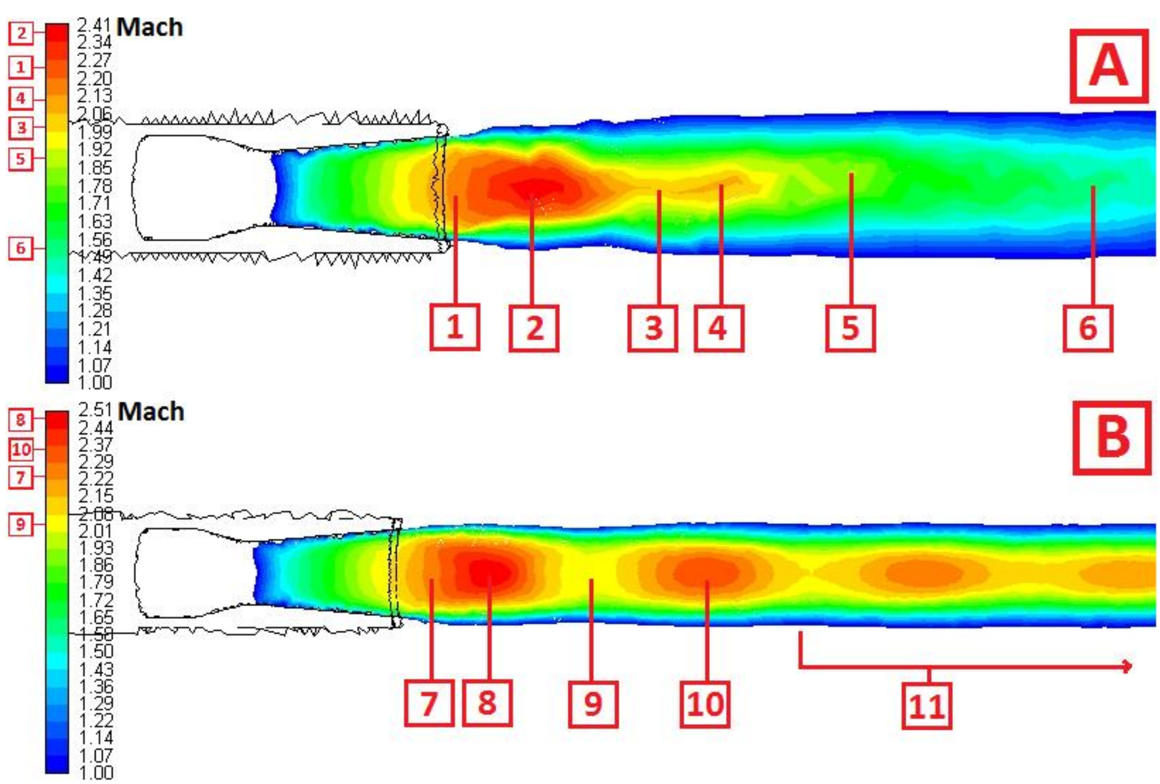

Figure D2. Mach number Contours for Part A) SS1 in MC Model, and Part B) Isolated SS Model; showing M_E > UE SS flow requirement

macroscopic structure of the repeated shock diamonds to be resolved. The smaller cell size adequately captured the discontinuities, and presented the subtle P oscillations that resulted in an extended UE SS core length before $P_{SS} = P_{MAIN}$.

Mach (M) Contour

To achieve UE SS flow within the MC, the SS Jet Exit flow had to exceed the Mach number prescribed by the SS Tunnel specific A.R.* = 1.982. The M_E upon entry into the MC had to exceed M > 2.19; as listed in the Analytical Model (Table 9). Figure D2 Part A displayed the Mach contour for the MC (SS1). The contour depicted the flow to enter the MC at Point 1 (M2.2–2.27); ensuring UE SS flow. The flow Mach number then increased to Max value (Point 2 = M2.34–2.41); in correspondence with the 1st expansion in the P contour (Point 3 in Figure D1 Part A). The Mach contour then oscillated; increased with each expansion (Point 4 = M2.06–2.13) and decreased with each compression (Point 3 = M1.99–2.06 and Point 5 = M1.85–1.92). However, due to the limited resolution of the MC mesh, the Jet core Mach number diminished (to Point 6 = 1.49–1.56) over a very short length. The contour clearly depicted only 2 shock diamonds (Points 2 and 4). This was not the case for the Isolated SS Jet in Figure D2 Part B. The contour depicted the flow to enter the MC, exceeding the A.R.* requirement (Point 7 = M2.22–2.29), and continued to expand to Max value within the 1st shock diamond (Point 8 = M2.44–2.51). The refined cell concentration was able to clearly render the shock structures; showing the distinct Mach oscillation pattern (4 visible shock diamonds). The subtle oscillations (Point 9 = M2.01–2.08 and Point 10 = M2.29 – 2.37) showed the preservation of SS Jet Mach number and the extension of SS Jet core length (Point 11).

Comparison Conclusion

The comparisons showed that the MC Mesh had in fact replicated the SS Exit flow conditions necessary for the SSEC mechanism. It was able to capture the Jet entry conditions and interpret the UE SS flow regime (replicating 2 shock diamonds). The limited cell count of the MC Model however, depicted the flow to expand to MC conditions over a shorter length by oversimplifying the repeated shock diamond pattern. This interpretation assumed P_{SS} to equalize P_{MAIN}, and M_{SS} to become subsonic over a shorter MC length. Whilst this was tolerable for interpreting the SSEC Concept, which involved Turbulent Mixing within the downstream subsonic region, it was not adequate for comparison to published sources. The remainder of the validations were then performed using the Isolated SS Model; which fully resolved the repeated shock diamond pattern and provided a more accurate depiction of the SS Jet core length.

D.2 Potential Core Length

The centreline Mach number plot of the Isolated SS Jet, as a function of non-dimension axial distance ($x/Ø_E$), was presented in Figure D3. The plot was accessorized with a vertical marker at $x/Ø_E = 12.47$; which indicated the endpoint of Mach number oscillation. Lovaraju [48] identified this length as the core length of the UE SS flow. The flow was still supersonic at this location, but the flow property oscillation had stopped. From this point, the flow then expanded predictably according to empirical SS Potential Core Length Models. This flow property oscillation length ($L_{CFD\ OSC}/Ø_E = 12.47$) was validated using the empirical relationship developed by Velikorodny [46]. The relationship estimated the UE SS core length on the basis of the SS Tunnel Throat (subscript '$_T$') conditions, and the Mach Disk location (X_M).

This relationship was interpreted, with respect to the current Isolated SS Jet application, as:

$$\frac{X_P}{\emptyset_E} = \frac{\emptyset_T}{\emptyset_E} \times 8 \times X_M = \frac{\emptyset_T}{\emptyset_E} \times 8 \times \frac{1}{2} \times \sqrt{k} \times \sqrt{\frac{P_T}{P_\infty}} \times \left(\frac{k+1}{k-1}\right)^{\frac{1}{4}} \quad \text{... (D1)}$$

$$\frac{X_P}{\emptyset_E} = \frac{0.0625}{0.088} \times 8 \times \frac{1}{2} \times \sqrt{1.4} \times \sqrt{\frac{485261}{83000}} \times \left(\frac{2.4}{1.4}\right)^{\frac{1}{4}} = 12.72$$

The Velikorodny [46] UE core length estimate ($X_P/\emptyset_E$ = 12.72) corresponded well with the Numerical Model oscillation length ($L_{CFD\ OSC}/\emptyset_E$ = 12.47); resulting in an error of 2%.

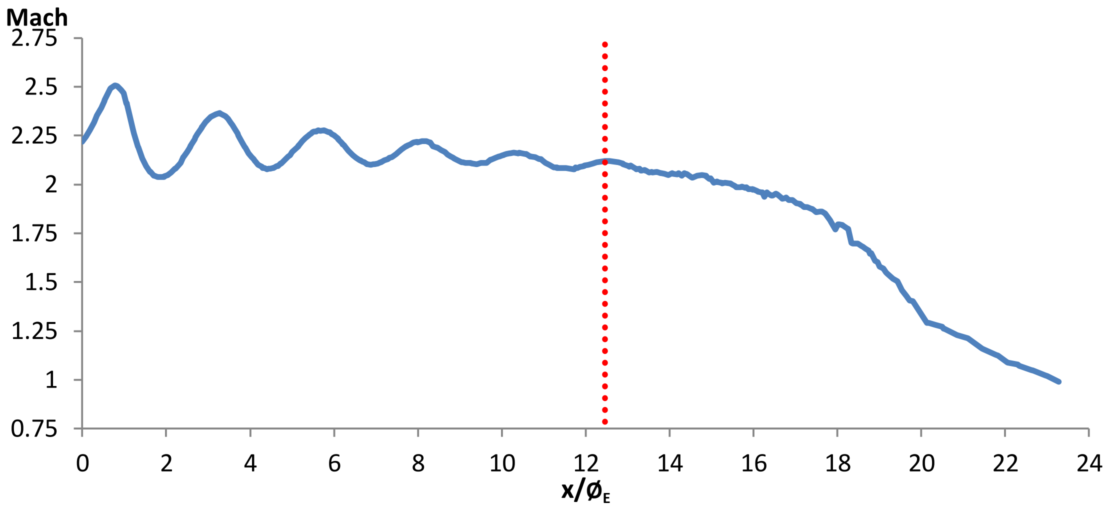

Figure D3. Jet centreline Mach number (M) over the non-dimensional Axial Length from SS Exit ($x/\emptyset_E$), including vertical marker at $x/\emptyset_E$ = 12.47

Proceeding beyond this oscillation length, into the predictable SS expansion length, the centreline Mach number in Figure D3 continued until subsonic (M < 1) at $x/\emptyset_E$ = 23.28. The length from the end of oscillation ($L_{CFD\ OSC}/\emptyset_E$ = 12.47) to the point of subsonic flow ($x/\emptyset_E$ = 23.28), represented the Potential Core Length for the SS Jet flow ($L_{CFD\ POT}/\emptyset_E$ = 10.82). This length was validated using 2 empirical relationships. Zaman [49] proposed a model applicable to all SS regimes (PE, UE, and OE), and focused on the flow core downstream of the initial expansion (so as to avoid screech). The relationship estimated the Potential Core Length using the post-oscillation SS Exit flow conditions (M_E and T_E) and the ambient Static Temperature (T_A) as:

$$\frac{L_{POT}}{\emptyset_E} = 4.3 + 1.2 \cdot {M_E}^2 + 1.2 \cdot \left(1 - \frac{T_E}{T_A}\right) \quad \text{... (D2)}$$

$$= 4.3 + 1.2 \cdot (2.12)^2 + 1.2 \cdot \left(1 - \frac{149.6}{297.2}\right) = 10.29$$

The other empirical relationship was the Murakami [44] model for the isolated SS Jet ($L_{SINGLE}/\emptyset_E$):

$$\frac{L_{SINGLE}}{\emptyset_E} = \frac{1}{0.14 \cdot (1+\sqrt{s}) \cdot (0.23 + 0.77 e^{-3.5 \cdot {M_C}^2})} \quad \text{... (D3)}$$

Where $s = \frac{\rho_E}{\rho_\infty} = \frac{1.88}{1.01} = 1.86$, and $M_C = \frac{V_E}{\sqrt{k \cdot R \cdot T_\infty} + \sqrt{k \cdot R \cdot T_E}} = \frac{519.44}{\sqrt{1.4*287*297.2} + \sqrt{1.4*287*149.6}} = 0.88$

$$\frac{L_{SINGLE}}{\emptyset_E} = \frac{1}{0.14 \cdot (1+\sqrt{1.86}) \cdot (0.23 + 0.77 e^{-3.5 \cdot (0.88)^2})} = 10.74$$

The Zaman [49] Potential Core Length estimate ($L_{POT}/\emptyset_E$ = 10.29) erred only by 5% from the Numerical Model Potential Core Length ($L_{CFD\ POT}/\emptyset_E$ = 10.82). The Murakami [44] estimate erred only by 0.7%. These different empirical relationships ($L_{CFD\ OSC}/\emptyset_E$ and $L_{CFD\ POT}/\emptyset_E$) produced results consistent with expectations; largest error = 5%. The near field expansion of the SS Jets used in the Numerical Model produced an accurate depiction of the expected empirical behaviour.

D.3 Subsonic Velocity Decay

The centreline Velocity Decay measured the non-dimensional Velocity (V_E/V) of the Isolated SS Jet from the point the flow became subsonic ($x/Ø_E$ = 23.28 in Figure D3). Yuceil [50] investigated the subsonic decay for a range of SS flow regimes (PE, UE, and OE), to determine a universal 'compressibility-corrected' Decay rate K_{REF}. The investigation normalized the non-dimensional values (V_E/V and $x/Ø_E$) with respect to Jet initial conditions and compressibility effects. This normalization resulted in the 'corrected' values (V_2/V and $x/Ø_2$); from which K_{REF} was obtained. The normalized values where obtained using the following equation set:

$$u = \frac{P_E}{P_\infty}, \qquad \frac{V_2}{V_E} = 1 + \frac{u-1}{k \cdot M_E{}^2 \cdot u},$$

$$\frac{\rho_2}{\rho_E} = \frac{2k^2 \cdot M_E{}^2 \cdot u}{2k \cdot M_E{}^2 \cdot u(k+u-1) - (k-1)(u-1)^2}, \qquad \frac{Ø_2}{Ø_E} = \sqrt{\frac{2k \cdot M_E{}^2 \cdot u(k+u-1) - (k-1)(u-1)^2}{2k^2 \cdot M_E{}^2 \cdot u + 2k(u-1)}} \quad \text{... (D4)}$$

The Yuceil [50] experiment was performed with the SS flow exiting at the Tunnel contraction ($\mathbb{A}_E = \mathbb{A}_T$), before fully expanding to Atmospheric Pressure at Point 2 (V_2, ρ_2, and $Ø_2$). In the MC Model however, the SS Tunnel was designed to expand the flow using the specific A.R.* values for $Ø_T$ and $Ø_E$ (prior to entering the MC). The flow conditions at the Isolated SS Jet Exit (V_E = 531.23 m/s, ρ_E = 2.203 kg/m^3, and $Ø_E$ = 0.088 m) represented the equivalent expansion of Point 2; demonstrated as:

$$u = \frac{83227}{83000} = 1.003, \qquad \frac{V_2}{531.23} = 1 + \frac{1.003-1}{1.4 \cdot 2.217^2 \cdot 1.003} \quad \rightarrow V_2 = 531.44 \text{ m/s}$$

$$\frac{\rho_2}{2.2029} = \frac{2(1.4)^2 \cdot 2.217^2 \cdot 1.003}{2(1.4) \cdot 2.217^2 \cdot 1.003(1.4+1.003-1) - (1.4-1)(1.003-1)^2} \quad \rightarrow \rho_2 = 2.025 \text{ kg/m}^3$$

$$\frac{Ø_2}{0.088} = \sqrt{\frac{2(1.4) \cdot 2.217^2 \cdot 1.003(1.4+1.003-1) - (1.4-1)(1.003-1)^2}{2(1.4)^2 \cdot 2.217^2 \cdot 1.003 + 2(1.4)(1.003-1)}} \quad \rightarrow Ø_2 = 0.0881 \text{ m}$$

The greatest deviation was the Ø (≈ 0.1%). This close correlation was due to the UE ratio (u = 1.003) when the Isolated SS Jet entered into the MC (x = 0.716 m). However, in maintaining parameters for direct comparison with the Yuceil [50] data, the analysis was presented in the form of the 'corrected' data (V_2 and $Ø_2$). The plot of the normalized non-dimensional subsonic Velocity Decay (V_2/V vs. $x/Ø_2$) was presented in Figure D4. The gradient of the linear trend-line for the data, also included in Figure D4, represented the Decay rate objective (K_{DEF}). This value K_{DEF} = 0.1524 correlated well with the universal 'corrected' Yuceil [50] expectation of $K_{DEF\ CORR}$ = 0.16; error = 4.75%. The subsonic decay of the SS Jets used in the Numerical Model replicated the expected experimental behaviour.

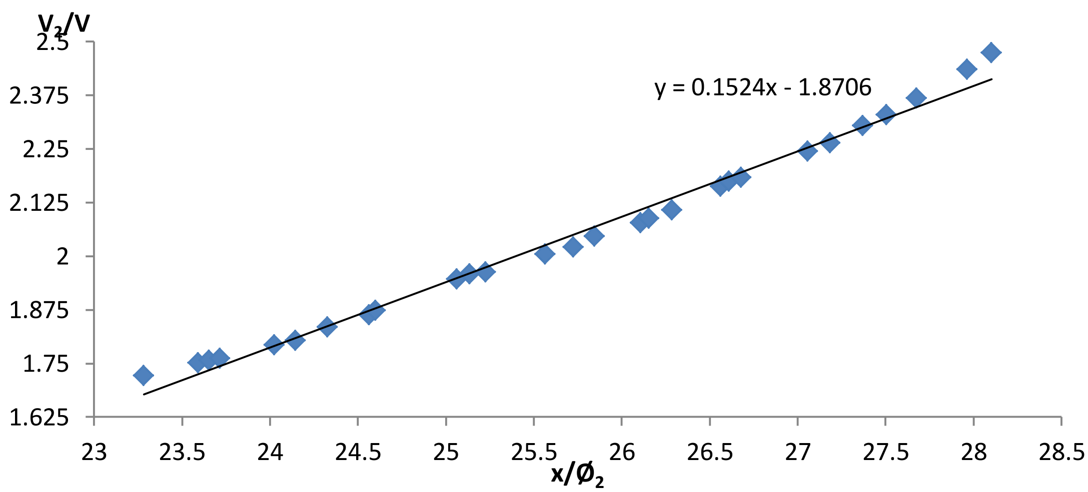

Figure D4. Normalized non-dimensional centreline velocity (V_2/V) along the normalized non-dimensional Axial Length ($x/Ø_2$), including the trend-line showing the K_{DEF} gradient

Appendix E – MC Model P_0 Comparison

Figure E1 displayed the respective P_0 curves for the Numerical and Analytical Models. The Numerical Model curve excluded the 3 SS Jet entries and the mixing stages along the intermediate lengths. The curve instead focused on the P_0 values of the intermediate Resultant Flow points; prior to each subsequent Jet entry. By excluding the P_0 values of the SS Jet entries and the respective intermediate mixing lengths (which housed high P_0 Jet cores), the P_0 axis scale could be reduced and refocused. The reduced P_0 axis readily identified the slow but inevitable increase in MC P_0 with each SS flow addition. The Analytical Model curve in Figure E1 reflected the slight, but permanent, MC P_0 boost with each SS Jet. The 1st Jet resulted in $P_{0\ MAIN}$ = 97510 Pa, the 2nd Jet $P_{0\ MAIN}$ = 97895 Pa, and finally the 3rd Jet $P_{0\ MAIN}$ = 98496 Pa. These boosts ultimately resulted in meeting the MC Out / WT In requirement of $P_{0\ WT\text{-}IN}$ = 98425 Pa (indicated by the vertical marker in Figure E1). Each boost of the Analytical Model curve occurred immediately with each Jet entry; and assumed complete mixing upon contact. Focusing on the Numerical Model curve in Figure E1, the P_0 at each of the points represented the intermediate 'settled' MC conditions. With each Jet entry, the MC P_0 permanently increased; from the Main Inlet P_0 = 83000 Pa to the eventual MC Out/ WT In $P_{0\ WT\text{-}IN}$ = 107633.50 Pa. After the 1st Jet Mix, the MC P_0 increased from 83000 Pa to 90006.25 Pa. This seemed like a significant boost to the MC P_0 from just a single SS Jet, but it was kept in mind that the Main flow P_0 up to that point was only drawing from the Main Inlet ($P_{0\ IN}$ = 83000 Pa). The 1st Jet flow contributed to the Main flow properties in a significant way; due to $\dot{m}$ comparison. After the 2nd Jet Mix, the MC P_0 = 99502.46 Pa was already higher than required by the Analytical Model MC Out/WT In ($P_{0\ WT\text{-}IN}$ = 98425 Pa). The cumulative Main flow surrounding the 2nd Jet had prevented the complete expansion of the Jet and, instead of extracting the Cooling potential, had inherited a higher P_0. This behaviour was repeated at the 3rd Jet as well, rising to $P_{0\ WT\text{-}IN}$ = 107633.50 Pa (at the vertical marker in Figure E1); much higher than what was required from the Analytical Model. The SS flow retained the higher P_0 due to incomplete expansion, and conveyed it to the Main Flow in the mixing process, rather than expending the $P_{0\ SS}$ to achieve a lower $T_{0\ MC}$.

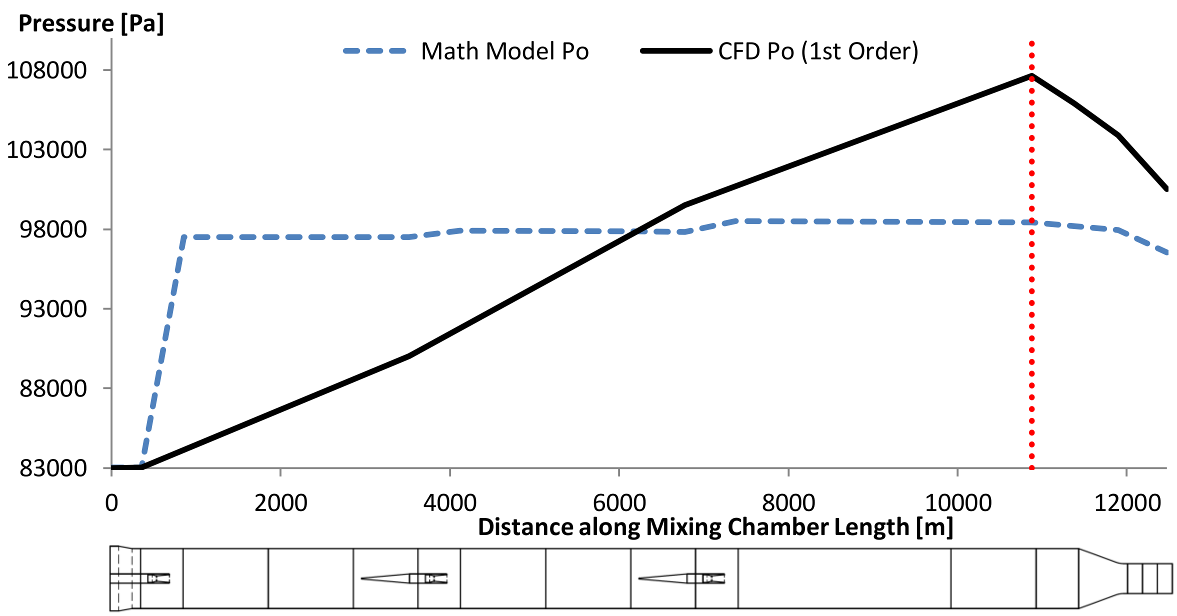

Figure E1. Collated P_0 plots (excluding Supersonic Jet entries) of Analytical and Numerical Models; depicting only the points where the flows have mixed (Intermediate Resultant Flows)